Surveillance and Broadcast Services Program

Systems Engineering
ADS-B Surface Detection Performance Risk Mitigation

Report on the Risk Mitigation Study Related to ADS-B Surface Detection Performance Issues in Support of Future ADS-B Surface Applications

Version 1.1

August 23, 2012

Approved By:________________________________ Date: 08/23/2012
Systems Engineering Lead, Surveillance and Broadcast Services, AJM

Table of Contents

List of Figures

List of Tables

1 Introduction

Recent advancements in surveillance techniques, satellite-based navigation technologies, avionics, and communication data links have combined to offer an opportunity to use Automatic Dependent Surveillance-Broadcast (ADS-B) as a surveillance source and to broadcast aeronautical information. Using these new ADS-B technologies, various ADS-B enabled operational applications have been developed which has led to the proposal to establish a Surveillance and Broadcast Services (SBS) program to support ADS-B operations throughout the National Airspace System (NAS).

ADS-B is an advanced surveillance technology that allows avionics to broadcast an aircraft's identification, position, altitude, velocity, and other information. Since the aircraft's position is normally derived from the Global Positioning System (GPS) and transmitted at least once per second, the broadcasted position information is more accurate than most current radar-based position information. Additionally, the avionics provides uniquely specific flight parameter information with the broadcast of its surveillance position. The greater positional accuracy and ability to provide aircraft-derived additional flight parameters, in addition to position data, defines ADS-B as enhanced surveillance. The accuracy and broadcast characteristics of ADS-B support numerous cockpit-based and air traffic control (ATC) applications. ADS-B-equipped aircraft with cockpit displays can receive ADS-B messages from other suitably-equipped aircraft within the reception range resulting in an air-to-air and airport surface surveillance capability. ADS-B surveillance broadcasts can also be received by ground-based transceivers to provide air-to-ground and airport surface surveillance information for air traffic services and other functions such as traffic flow management, fleet operations management, or security functions.

One such air-to-air application being used with ADS-B is SURF, which provides situational awareness of other traffic on the airport surface. Another application being considered for ADS-B is SURF IA which would provide pilots with indications and alerts for traffic operating on runways and taxiways. This SURF IA capability would enhance safety on the surface by providing alerts to pilots for imminent runway incursions and / or surface collisions.

1.1 Background

During FAA's development of the SURF-IA application requirements, capability demonstrations were conducted by Honeywell and ACSS. These capability demonstrations identified performance issues with test aircraft having ADS-B IN equipment being able to consistently detect other aircraft with ADS-B OUT that were operating on the surface movement area. Two potential causes of the poor detection performance were considered:

1. Obstructed Line of Sight between aircraft
2. Multipath or other interference affecting the detection of ADS-B signals.

A review of the data showed that in some cases targets did not have line of sight. This explains the poor detection performance for those targets. One possible mitigation for this issue is to rebroadcast data from targets on the movement area that do not have line of sight to targets with ADS-B IN capability. This mitigation requires the SBS infrastructure to be deployed at airports where this feature would be deployed. Airports that do not have SBS would be unable to see other targets that do not have line of sight on the surface. This may limit the usability of SURF IA at airports that have significant obstructions that affect line of sight visibility on the surface.

The more troubling issue identified from post analysis of SURF IA data was multipath effects degrading detection performance on the surface. The FAA Technical Center evaluated surface ADS-B data at Philadelphia International Airport from a dedicated test event on October 10, 2010 and determined that severe multipath was interfering with the incident ADS-B signals at multiple locations on the airport surface. In addition, the Technical Center evaluated targets of opportunity data from June 14, 2010 and September 1, 2010 that were collected from prior ADS-B test events. This data also indicated that multipath was impacting the ability of ADS-B IN capable aircraft to detect other ADS-B OUT aircraft operating on the airport surface. The multipath effect from the targets of opportunity data was not as severe as that observed in the dedicated testing of October 10, 2010. This difference is thought to relate to the placement of the ADS-B IN capable aircraft/test unit which was further away from reflecting structures on the airport during the test event. However, all data measurements from the PHL testing confirmed that the effects of surface multipath need to be addressed to optimize the benefits of ADS-B surface applications such as SURF and SURF IA.

As observed in the test results, the multipath signaling phenomenon effectively creates “blind spots” at which aircraft equipped with ADS-B OUT could not be seen with ADS-B IN capable systems. These “blind spots’ cannot be readily resolved through ADS-B retransmission in small known locations because complex airport structures with numerous hangars gates and terminals as well as the variety of aircraft operating at the airport will likely result in blind spots throughout the airport surface for some aircraft pairs.

SURF and SURF IA operation is highly dependent on good detection of aircraft operating on taxiways and runways. Areas of limited or no detection will limit the use of these surface applications. The inability to detect aircraft operating on the surface on an intermittent or consistent basis could render the application operationally unsuitable for airports that could gain the most benefit from a surface traffic alerting application.

1.2 Purpose and Scope

The ADS-B IN ARC chartered by the FAA to provide recommendations on ADS-B IN applications and rulemaking, endorsed the continued development of the SURF IA application in a letter to the FAA Administrator in November of 2010. The letter stated in part that “The ARC believes it is essential the FAA make it a priority to resolve the issues identified during the SURF–IA demonstration, such as line-of-sight interference and ADS–B drop-outs”.

Based upon the FAA work conducted on SURF IA to date and the ARC endorsement for continuing development of this application, the purpose of the "Risk Mitigation Study Relating to ADS-B Surface Detection Performance (ASDP) Issues" was as follows:

1. Fully Characterize Poor ASDP issues
    a. Further investigate the multipath issues observed during the SURF IA demonstrations to better characterize this effect and its impact on ADS-B performance.
    b. Determine line-of sight issues on airport surfaces and the impact to surface applications.
2. Determine mitigations that would improve detection performance on the surface such that SURF IA performance requirements would be met
    a. Line of sight mitigations due to multipath or other signaling phenomena
    b. Obstructed line of sight situations
3. Identify benefits and disadvantages of each mitigation
4. Model detection improvements as well as impacts to spectrum usage for each mitigation
5. Identify a recommended mitigation or set of mitigations to support FAA business case for SURF IA and other surface applications.

Since this risk is a technical risk to surface ADS-B applications, the mitigation approach is the responsibility of the Systems Engineering team on the SBS program. The SE team recommended to the SBS Leadership team that a study be conducted by SMEs in ADS-B datalinks, Multipath Effects, Spectrum limitations, Modeling / Simulation, Test and other engineering disciplines. This panel was comprised of the following groups:

1. Technical experts and systems engineers representing the FAA's SBS Program
2. MITRE Center for Advanced Aviation System Development
3. Massachusetts Institute of Technology/Lincoln Laboratories (MIT/LL)
4. Johns Hopkins University-Applied Physics Laboratory (JHU/APL)
5. William J. Hughes Technical Center (WJHTC)

This document describes the FAA's surface multipath evaluation, results, conclusions and recommendations for mitigating the Surface ADS-B Detection Performance risk that impacts current and future surface applications.

1.3 Characteristics of Surface Multipath

The propagation of RF messages when the transmitting and receiving antennas are on aircraft situated on the airport surface is much more difficult than when both aircraft are in flight. The message travels to the receiving antenna by three basic kinds of paths: the direct path, vertical bounce(s) off the horizontal ground, and horizontal bounce(s) off of nearly vertical surfaces such as buildings, signs, vehicles, and other aircraft (especially their tails). There can be paths containing both ground and vertical surfaces. For example, the path may be from the transmitting antenna to the ground to a building and on to the receiving antenna.

Models of such propagation to support analysis of multipath can be based on ray theory and/or Fresnel diffraction theory. In the Fresnel modeling the vertical reflector is treated as an aperture through which the unfolded reflection passes in a straight line toward the image of the receiver transposed across the plane containing the reflecting surface. The reflection can be modeled as specular or diffuse. The gain patterns of the transmit and receive antenna are included in the model. The result of the modeling supports the identification of the delays and relative powers of all the multipath reflections with respect to the desired direct reception, as a function of the geometry and structures of the environment under consideration.

In the case of 1090ES propagation between aircraft on the surface, considerable practical experience has been accumulated during development of the ASDE-X multilateration system and its predecessors the Cardion Cooperative Area Precision Tracking System (CAPTS) and the Airport Surface Target Identification System (ATIDS). The lessons are that ground bounces have very short delays (on the order of wavelengths) which constructively or destructively interfere with the direct signal. The net reception still retains the shape of the transmitted waveform, but amplified (up to 6 dB) or faded (by up to tens of dB). The horizontal bounces are usually in the tens to thousands of feet, and are experienced as delayed replicas of the transmitted signal overlaid on the direct reception. The effect is to distort the signal by stretching or narrowing the transmitted pulses, or inserting additional pulses or cancelling desired pulses. The reflector is usually a flat surface having a substantial reflection coefficient. The surfaces are on buildings, signs, vehicles, and other aircraft. Multiple reflections from several surfaces are not unusual.

The signal-to-multipath power ratio (SMR) is affected by the size of the surface in Fresnel zone units. Since the 1090 MHz wavelength is about one foot, even small nearby reflectors (such as a sign on the surface) can cause a substantial reflection. UAT signals have a similar wavelength with its operating frequency of 978 MHz.

Since both 1090-ES and UAT are approved ADS-B data links for use on the airport surface, the mitigation of multipath must encompass frequencies and modulation schemes for both of these signals.

2 Evaluation Plan

The evaluation plan for ASDP identified the approach and processes that the ASDP Study Team performed to meet its objective of determining appropriate mitigation strategies to ensure the ADS-B services will support beneficial surface applications such as SURF IA. The key areas employed in the approach to the ASDP issues risk mitigation were:

1. Characterized the ADS-B Surface Detection Performance Issues:
    a. Assessed the impact of aircraft to aircraft LOS Blockage at applicable ASDE-X airports for performing surface applications to determine whether mitigations are needed for this issue.
    b. Characterized multipath affects at other airports beyond PHL to help determine the full extent of this problem for surface applications.
2. Determined necessity of mitigations for surface LOS blockage: Identified whether mitigations for this issue are required for SURF IA or other surface applications.
3. Determined the mitigations for detection loss/degradation from multipath: Identified a set of viable mitigations that can reduce or eliminate the detection degradation experienced in surface applications due to multipath or signal fading.
4. Identified benefits and disadvantages for each mitigation: Considered items such as detection performance improvement, constraints on the operating environment (does it require non-ADS-B surface surveillance?), impacts to spectrum, impacts to aircraft, etc.
5. Analyzed surface detection performance improvements for each mitigation: Using models and simulation determined the detection improvement provided by various mitigation techniques.
6. Assessed spectrum usage impacts for any mitigation that requires additional spectral broadcasts:
    a. Determined the potential 1090-ES interference increase from these mitigations and the impacts to other 1090MHz spectrum users.
    b. Determined the ability of the mitigation to operate in future spectrum environments identified in prior SBS spectrum risk study.
    c. Determined potential impacts to UAT based ADS-B for each mitigation.
7. Validated modeling and simulation results for each alternative with bench test and/or real world testing: Used test equipment and test aircraft to verify that expected performance improvements are achieved.
8. Developed technical recommendations to SBS Leadership team for ASDP issues: Identified the recommended mitigation or mitigations and the basis for the recommendation. Included recommendations on additional analysis, such as cost / benefits analysis of applications such as SURF IA with the added costs of the mitigation set recommended.

The steps of this plan required a set of tools to support various activities for modeling multipath effects and/or determining the impact of certain mitigations on spectrum use. However, there is currently no known toolset to evaluate detection performance of various mitigations strategies in the presence of multipath. As part of this study, a set of analytical models that characterize signal detection performance in the presence of multipath were developed. The spectrum modeling tools previously employed on the Spectrum Risk Panel Work conducted by SBS were used for determining spectrum impacts of mitigations that require additional spectrum.

This report also identifies and describes the various tools and models that the Spectrum Risk Panel used to accomplish the activities defined in this document.

2.1 Details of ASDP Issues Mitigation Steps

This section provides further details on the steps that were conducted for this study.

2.2 Mitigation Strategies Evaluated

Based on the SURF IA demonstrations and the Technical Center assessment of the detection issues on the surface, an initial set of mitigation strategies was defined by the ASDP Study Team. The following sections identify the mitigations that were evaluated during the study.

2.2.1 Same Link Rebroadcast (SLR) of ADS-B

Rebroadcasting data from the ADS-B ground infrastructure on the same link on which it was received, provides a diverse signal feed for mitigating the impacts of multipath on the direct air-to-air signal feed. For this alternative, the SBS Ground Infrastructure will rebroadcast ADS-B messages to all aircraft clients operating on the surface with ADS-B IN. The rebroadcast operates similar to existing ADS-R/TIS-B transmissions wherein a client aircraft with ADS-B IN is provided target data transmitted from the radio best suited to be seen by the client. Since the intent is to support surface applications, it is assumed that the rebroadcast is made at low power, in order to minimize the impact to spectrum and airborne aircraft.

There are multiple benefits of this option. A key benefit of this approach is that it also addresses issues related to line of sight blockages so that aircraft with ADS-B IN can see targets in blind spots and around corners. No changes are anticipated on ADS-B IN avionics hardware for this mitigation. However, there may be software updates necessary to correlate direct and rebroadcasted messages to avoid ghost or split targets on aircraft display systems.

This option increases the spectrum utilization. There is a potentially unacceptable impact to 1090 MHz spectrum. All 1090-ES would be retransmitted for targets that already send 1090-ES messages from their avionics. There may also be a detrimental impact to the UAT 978 MHz spectrum due to the additional transmissions required to rebroadcast the UAT data. To mitigate the impacts to 1090 MHz and 978 MHz spectrum, algorithmic techniques need to be considered in utilizing this option including adjusting rebroadcast power levels and message transmit frequencies.

Possible disadvantages of this approach are that the ATSA applications could not be supported in an environment without an ADS-B ground infrastructure and that the additional latency involved might result in disqualifying some target aircraft for some surface applications.

A list of the Pros and Cons of this option are as follows:

Pros:

1. Does not require changes to avionics hardware.
2. Only minor changes needed in the ground infrastructure to support this capability

Cons:

1. May require aircraft to correlate direct versus rebroadcast messages to avoid shadows.
2. Potentially requires a significant increase in spectrum usage, particularly on 1090-ES, which may saturate the band and impact other users (ASDE-X, TCAS, and SSR).
3. May also experience multipath on the rebroadcast path that could limit detection.

2.2.2 Rebroadcast All Surface ADS-B on UAT

To eliminate any need for increasing1090 MHz utilization, this mitigation provides ADS-B data on UAT. The SBS Ground Infrastructure will be modified to rebroadcast ADS-B messages to all aircraft on UAT. This requires 1090-ES aircraft to equip with dual link receivers for surface applications. Regardless of whether ADS-B data is received from a 1090-ES aircraft or UAT aircraft, the SBS service would rebroadcast the ADS-B data over the UAT link. A client aircraft with ADS-B IN is provided target data transmitted from the UAT radio best suited to be seen by the client. Since the intent is to support surface applications, it is assumed that the rebroadcast will be made at low power, in order to minimize the impact to airborne aircraft. This modification does not cause additional transmission on 1090-ES but all 1090-ES aircraft would need to have dual reception capability. There may be a detrimental impact to the UAT 978 MHz spectrum due to the additional transmissions required to rebroadcast all the ADS-B data over this link, but the UAT data link is dedicated to ADS-B and not used by other NAS systems. Therefore, any impact is localized to ADS-B performance. A key benefit of this approach is that it also addresses issues related to line of sight blockages so that aircraft with ADS-B IN can see targets in blind spots and around corners. Possible disadvantages of this approach are that the ATSA applications could not be supported in an environment without an ADS-B ground infrastructure and that the additional latency involved might result in disqualifying some target aircraft for some surface applications. Modifications to the ground infrastructure as well as ADS-B IN aircraft avionics are required to support this capability.

The analysis necessary for this approach is as follows:

1. Determine required broadcast/rebroadcast rates.
2. Conduct an assessment of the impact to UAT spectrum from rebroadcasting UAT ADS-B messages for all aircraft transmitting ADS-B.
3. Model and simulate ADS-B reception performance in a retransmission environment for both UAT and 1090-ES aircraft. In model assume DME is on airport operating at frequency closest to 978MHz. JTIDS is not applicable to the surface so it doesn't need to be in performance model.

4. Determine if ATSA performance requirements can be met with the ADS-B Rebroadcast on UAT option.

Rebroadcasting messages received by the ADS-B ground infrastructure on the UAT link, provides a diverse signal feed for mitigating the impacts of multipath on the direct air-to-air signal feed. This option also provides the benefit of reducing the impacts to the current congested 1090MHz spectrum. While it increases the usage of UAT bandwidth, no additional data is transmitted over 1090MHz. Impacts on the UAT link still need to be assessed to determine if this option can be supported in dense traffic environments. Note that the spectrum impact of this approach on the UAT 978 MHz bandwidth is identical to that of SLR described in Section 2.2.1 above. Algorithmic techniques should also be considered to minimize spectrum impacts by adjusting rebroadcast power levels as well as message transmit frequencies. A list of the Pros and Cons of this option are as follows:

Pros:

1. No impact to 1090 MHz spectrum.
2. Only minor changes needed in the ground infrastructure to support this capability.
3. Provides both path and frequency diversity to mitigate affects of surface multipath.

Cons:

1. May require aircraft to correlate direct versus rebroadcast messages to avoid shadows.
2. Requires equipage with UAT receive and potentially dual receive equipage to support all ASD-B air-to-air applications.
3. Potentially requires a significant increase in UAT 978 MHz spectrum usage which could impact UAT Multilateration.

2.2.3 Enhanced ADS-B Reception Techniques

This option utilizes enhanced ADS-B reception techniques such as deconvolution and correlation of received signals with known components of the message to obtain interference resistant algorithms for ADS-B IN that provide better multipath rejection. This effort involved modeling and simulating performance capabilities of enhanced reception algorithms for ADS-B IN. It involved defining and evaluating algorithms within the receive chain of the avionics that could potentially reduce the effect of multipath fading as observed during SURF IA evaluations at PHL.

This option requires changes in the ADS-B IN avionics to implement algorithms that improve ADS-B reception performance. Aircraft choosing not to perform ATSA applications or equip with ADS-B IN are not affected by implementing enhanced reception processing algorithms. Changes would only be needed by operators desiring to perform surface applications such as SURF-IA. There would be no net affect on either UAT 978MHz or 1090MHz spectrum use for this option because it only affects the receiver.

A detailed list of Pros and Cons related to this option are as follows:

Pros:

- Supports single receiver implementations.
- No changes required in the ground-based infrastructure.
- There would be no increase in 978 MHz or 1090 MHz spectrum utilization.
- No costs would be incurred by aircraft that do not wish to utilize ground-ground 1090ES applications
- For avionics 1090ES receivers based on equipment that digitizes 1090ES messages early in the receive processing chain and performs most detection and decoding functions digitally, then it is possible that improved reception techniques would primarily take the form of software upgrades within the receiver.

Cons:

- Aircraft wishing to utilize ground-ground 1090ES applications at airports with high multipath environments would incur the costs of upgrading their 1090 ES receiver.
- In very severe multipath situations the improved techniques might be insufficient to provide the required reliability.

2.2.4 Diversity or Multi-Channel Reception

This alternative provides reception diversity to decode ADS-B messages least affected by multipath or mixing of receive signals from top and bottom antenna channels to reduce or eliminate multipath interference. Two methods of multi-channel reception were considered. Method #1 employed aircraft avionics receiving ADS-B from both the top and bottom antennas simultaneously using a separate receiver connected to each antenna. The second method employs a sectorized antenna on the aircraft with a receiver connected to each antenna sector.

This mitigation would only be necessary for ADS-B In equipped aircraft performing ATSA applications. There is no additional impact on spectrum use from this mitigation.

This option employs diversity combining techniques to improve reception performance. This alternative implemented the Maximal Ratio Combining (MRC) of two receivers at one or more of the following stages:

1. Performed combining prior to demodulation and decoding,
2. Performed combining at the output of the demodulators using soft decisions and / or hard decisions, and
3. Performed combining at the output of the decoders.

Maximal Ratio Combining involves coherently combining one or more channels, assigning higher weights to channels with high signal-to-noise ratios, and lower weights to channels with low signal-to-noise ratios. Signal combining can be optimized to maximize Signal to Noise ratio such that effects of multipath are mitigated. In addition, signal combining can be coupled with techniques such as Convolution or Correlation of a known preamble to reduce or eliminate multipath interference affects.

Specific Pros and Cons of the Diversity Combining technique are as follows:

Pros:

1. Does not impact spectrum utilization.
2. Does not require changes to ground infrastructure.
3. Only requires changes to aircraft participating in ADS-B In applications and may only be needed for aircraft intending to support surface applications.

Cons:

1. Requires changes to aircraft avionics reception path.
2. Increased cost of avionics receivers. Cost can be minimized by implementing post-detection combining, while costs would increase for a more optimal pre-detection combining. The performance improvement for each approach can be used in a cost/benefit analysis.
3. Reception performance impact is unknown without further analysis.

2.3 ASDP Study Metrics

Each mitigation options were evaluated based on the following criteria:

1. Detection improvement in a severe multipath environment.
2. Ability to meet ATSA / SURF IA detection performance and latency requirements.
    a. DO-289 provides a required update interval of 2 seconds (95%) for moving targets and 10 seconds (95%) for stopped targets.
    b. The maximum latency for ATSA applications is 3.0 seconds from measurement to glass.
3. Impacts to Aircraft Fleet and Aircraft subsystems
    a. New ADS-B receivers, processors, displays, etc.
    b. Aircraft applicability as to whether all aircraft are affected or only ADS-B IN capable aircraft
4. Impact on spectrum resources used by ADS-B and other NAS systems, both current and future.
5. Impact on NAS ground infrastructure including scope of changes to implement each option.
6. Technical Complexity to design, develop, implement.
7. Estimated schedule timeframe for implementation.

3 Activities and Results

3.1 Characterization of Multipath Environment

3.1.1 Field Measurements

Field measurements were conducted to support the risk mitigation study during various stages of the effort. The first data collection was initiated as a result of problems of track drops reported during field trials of the SURF-IA application. These trials were conducted at the SEA and PHL airports. Subsequently, a data collection at PHL was conducted to investigate the reported issues. One of the suspected causes of track continuity issues was destructive signal multipath, as operations on the surface have shown multipath is often experienced on L-band signals reducing reception probability. The initial test conducted at PHL on October 10, 2010 was to evaluate the existence and scope of such interference at the airport surface. This test utilized a King Air aircraft provided by Ohio University equipped with an ACSS Mode S transponder with 1090ES DO-260A version 1 broadcast capability to serve as the ADS-B OUT aircraft. The Technical Center van was equipped with a 1090ES receiver to serve as the ADS-B IN vehicle. The 1090ES receiver in the van was modified to allow recording of the log video signal for post-processing and detailed signal analysis. There were 7 test scenarios that were planned and executed that had the aircraft and/or van moving along various locations on the airport surface. During these tests there were mulitple instances of reduced or no reception for 30 seconds or more. Post-analysis of signal quality showed that mulitpath interference was the primary cause of the reception problems. Figure 1 shows a typical example of the multipath interferrence that was encountered.

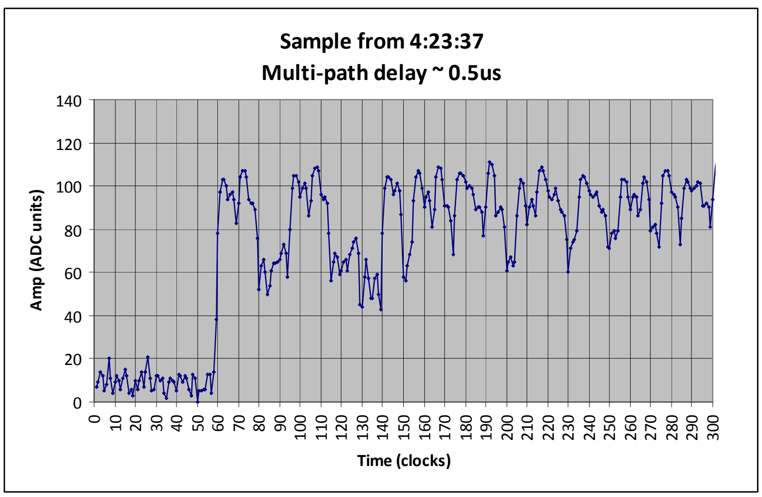

Figure 1: Multipath interference example from Philadelphia Tests on October 10, 2010

The above figure shows a segment of a 1090ES transmission where the reflected signal has ‘filled-in’ the spaces between the pulses. The preamble pulses that begin at about clock sample #60 no longer appear as 4 distinct pulses. Current decoding techniques did not successfully decode the signal in this example.

In addition to the controlled test described above, data from two previous tests to measure the 1090 MHz RF environment at the Philadelphia airport surface was analyzed to determine if surface targets of opportunity also showed the effects of multipath interference. These tests were conducted prior to the October surface multipath test in June 2010 and September 2010. This data showed some reception issues from multipath but was not as severe as with the dedicated test probably due to the location of the van farther from reflective surfaces.

Data was collected on January 24, 2011 to investigate multipath effects on UAT messages. This was a data collection opportunity as a result of tests conducted by another organization for a different purpose. Since it involved a UAT ADS-B equipped aircraft, it was decided to locate the test van at the airport and collect measurements to make use of the planned test. For most of the test, the aircraft was airborne performing low approaches, but it did land and taxi for a brief time. The van was equipped with a Garmin GDL-90 for recording UAT messages and the modified 1090 MHz receiver for recording and detailed analysis of 1090ES and Mode S signals. During the time the aircraft was taxiing there was a significant lapse (60 seconds) in reception of UAT messages. The van recording equipment only enables detailed signal analysis of 1090 MHz signals, so the 1090 MHz Mode S transmissions from the test aircraft were analyzed during the UAT lapse. It was concluded that there was apparent multipath interference that most likely impacted the reception of UAT as well. Although this test yielded a small data sample, it is reasonable to conclude that UAT signals are negatively affected by multipath interference.

Additional field measurements were conducted later in the study. After identification of multipath as a significant factor in poor reception performance on the surface, risk mitigation strategies included the development of receiver/decoder enhancements to overcome the effects of surface multipath interference. Additional field data collection efforts focused on collecting data to support the development of enhanced ADS-B reception techniques. These techniques relied on the use of I and Q data in the demodulation process. One technique relied on both top and bottom antenna receptions, so the measurement equipment had to provide diversity capability to simultaneously receive top and bottom antenna 1090 MHz signals. The recording equipment used for previous testing was modified to record I and Q data as well as log video. Two field data collection tests were conducted to record I and Q demodulated data specifically in the presence of multipath interference. The first data collection was at the FAA Technical Center/Atlantic City International Airport on December 5-8 2011. The second was conducted at the PHL airport on February 15, 2012. For both of these tests, a specially equipped test van was equipped as the ADS-B OUT source and a test aircraft equipped to receive on the top and bottom antennas was equipped with I and Q recording equipment as the ADS-B IN aircraft.

The test at Atlantic City consisted of positioning the van and the aircraft at various locations relative to the aircraft hangar building that was used as the signal reflection source. Experimentation determined that only the hangar doors located on the sides of the building were sufficient as a destructive multipath source. However, the ability to locate the van and aircraft was geographically constrained due to limited pavement and the location of other buildings. These tests yielded some I and Q samples with multipath interference but there were no samples where the signal received on both the top and bottom antennas of the aircraft was not decodable with current techniques.

A second test was conducted in Philadelphia with the goal of recording I and Q data samples in cases where there was destructive multipath preventing successful message decoding on the top and bottom antenna simultaneously. The aircraft and van were equipped the same as for the Atlantic City tests. Figure 2 shows an overview of the van locations and aircraft taxi routes used for the test.

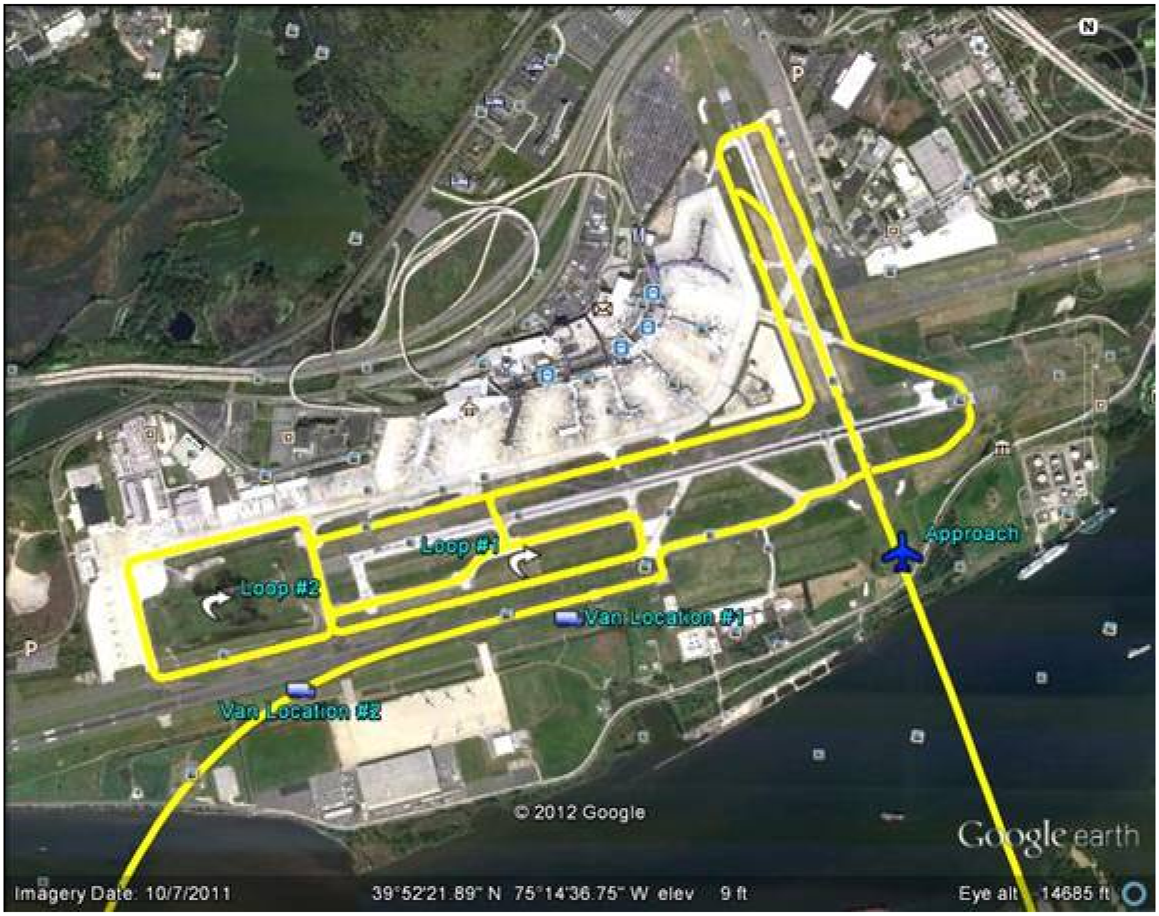

Figure 2: February 2012 Philadelphia Surface Multipath Field Test Aircraft Taxi Route

The test in Philadelphia yielded 14 1090ES I and Q samples where the message was not decoded on either the top or bottom antenna receiver/decoder chain with current enhanced decoding techniques. The data samples were provided to engineers at Massachusetts Institute of Technology/Lincoln Laboratories and Johns Hopkins University-Applied Physics Laboratory who were developing candidate enhanced reception techniques.

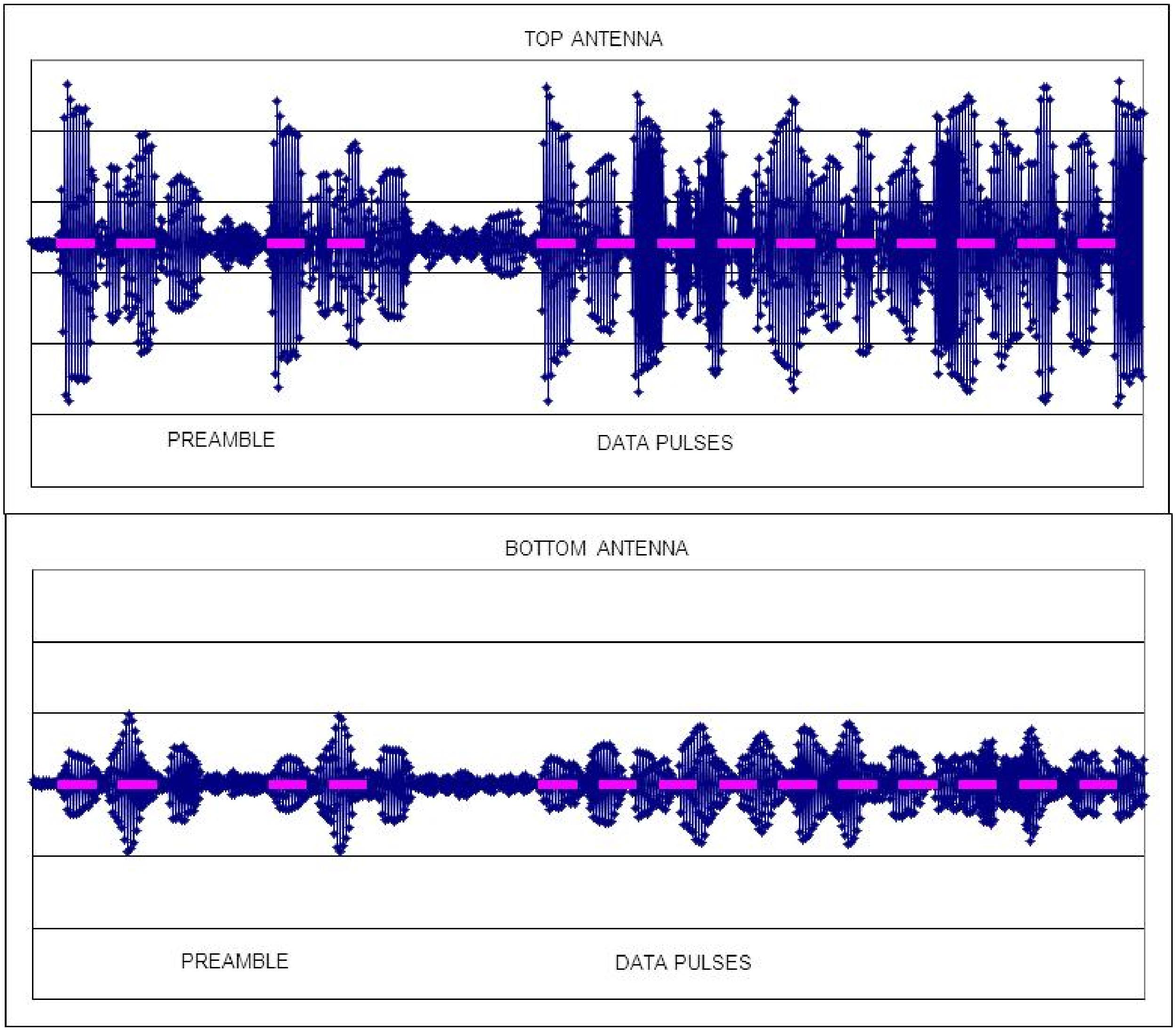

Figure 3: I and Q Data Sample

Figure 3 is a sample of I and Q data showing the preamble and the first 10 bits of a 1090ES recorded at the Philadelphia test. This extended squitter was not able to be decoded by the current enhanced decoder process. The two graphs show the top and bottom antenna data. The dark blue data points represent digital I and Q sampled data. Data was sampled at 80 MHz from a 20 MHz Intermediate Frequency signal. The pink dashes were added to the graph to show the nominal location of the preamble pulses and the left ('1') half (500 nanoseconds) of each data bit. The amplitude of the signal on the bottom antenna is significantly lower than the top antenna.

In both the Atlantic City and Philadelphia tests where the ADS-B IN aircraft was recording on both the top and bottom antennas, the data was analyzed to assess the benefit of diversity reception. In general, the top antenna showed a higher rate of message reception, but in some instances where there was reduced overall reception due to multipath or obstructions in the direct path, the bottom antenna contribution to the overall reception rate showed some benefit with diversity reception. This and other data analysis from any of the field tests can be found in the Technical Reports with detailed data and analysis from the associated test.

It should be noted that the severity and location of surface multipath depends on many factors. The number and types of reflectors at an airport are difficult to locate and the areas of potential multipath severity depends on the location of the transmitting aircraft, receiving aircraft and the distance to the reflector/reflectors. Measurements have shown that there is generally distortion of the signals on the surface due to multiple signal reflections. There are generally reflections from the underlying surface and this makes the surface a more difficult environment to operate. Surface to surface receptions benefit from the close proximity between aircraft which provides greater margin over MTL and most of these low level distortions do not reduce performance. However, there are many significant reflectors that are characterized by minimum attenuation of the reflected signals and based on the distances involved, especially delays of 200 nanoseconds or more, these reflections cannot be easily overcome by the receiver/decoder. There is significant variability in these types of reflectors and some of them only impact short distances that a moving aircraft would traverse. The variability of multipath is also influenced by the physical characteristics of the transmitting and receiving aircraft, location of the antennas and the height of the antenna above the surface all affect multipath. These variables make data collection and field measurements more difficult. Data collections cannot produce measurements for all combinations of the factors that influence multipath. However, the field measurements provide the potential to capture and analyze multipath opportunities. With controlled conditions, the measurements can provide data to support the development of potential solutions under consideration.

3.1.2 Modeling and Simulation

This section is intended to provide a better understanding of the link behavior in the airport surface environment, and based on this, generate empirical models of received 1090ES messages for use by the WJHTC in bench evaluations of the decoder capabilities of various receivers in multipath conditions.

3.1.2.1 Airport surface direct signal propagation loss

3.1.2.1.1 Propagation model and link budget factors

Most ADS-B coverage estimates are concerned with air-ground link characteristics. Peaks and nulls in elevation plane link coverage are due to vector addition of the ground reflected wave with the direct wave. In this case the path (or relative phase) difference between the direct and ground reflected waves is accurately described with an approximate model. On the other hand, a different approximation accurately models surface wave propagation loss between two antennas when both are at relatively low heights in comparison to the separation between them. An exact treatment of these factors is the basis for the exact model; contributing factors are discussed in the following.

Assume the transmitter and receiver antenna heights, a and h, are laterally separated by D as shown in Figure 4. The total received signal is the vector sum of the direct ray at slant range, R, and the reflected ray, Rr associated with the real antenna image an equal distance, h, below the surface. Elevation plane gains of the top and bottom antennas for the aircraft at height, a, are shown in Figure 5; note that the elevation angle for the top antenna is negative above the horizon.

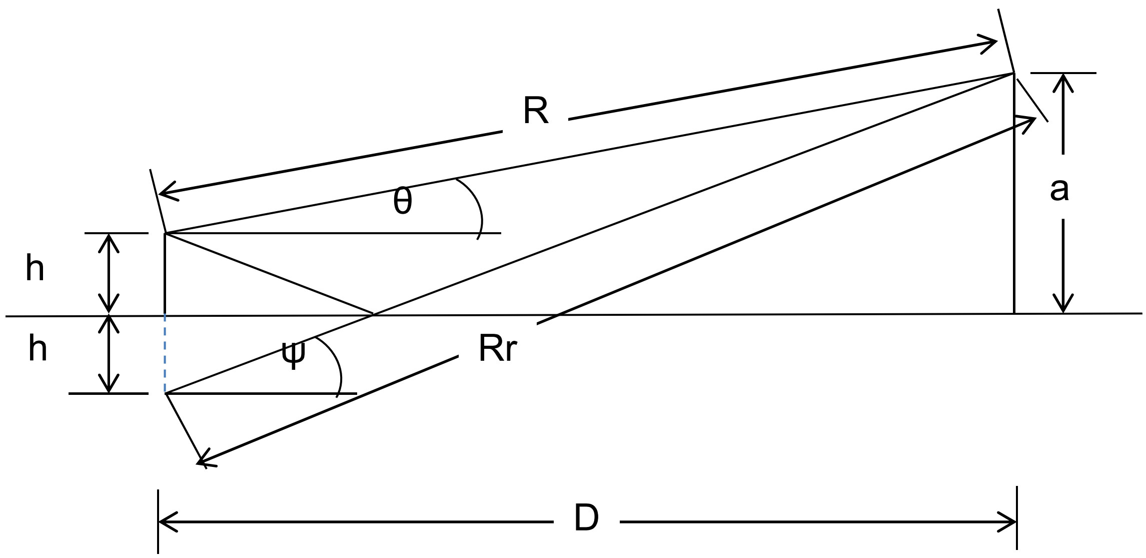

$D = R \cos\theta$, for small angles, $D \approx R$

For $R >> 2h$, $\psi \approx \theta$

Figure 4: Elevation plane multipath geometry

Gtd(0) = –0 Gbd(0) = –0

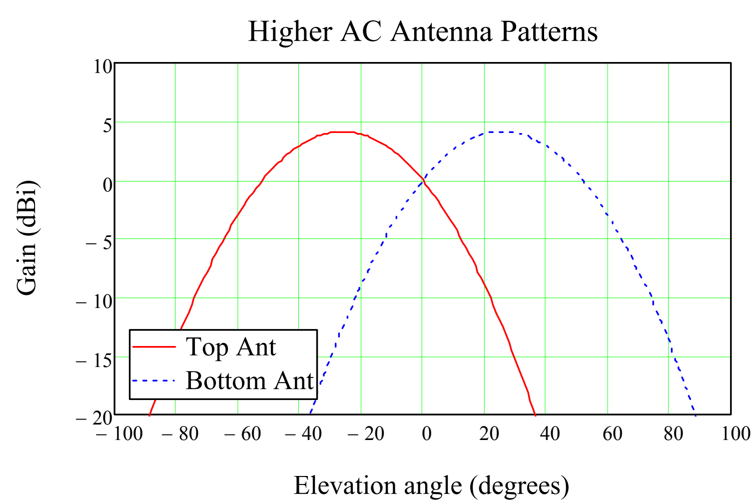

Assumed aircraft antenna patterns vs elevation angle for higher aircraft: top antenna solid, bottom antenna dashed (Note positive angle is down)

Figure 5: Top and bottom aircraft antenna patterns for higher aircraft

Figure 6 gives the top and bottom patterns for the aircraft at height, h, with their corresponding images for the reflected wave.

Ghtd(0) = –0

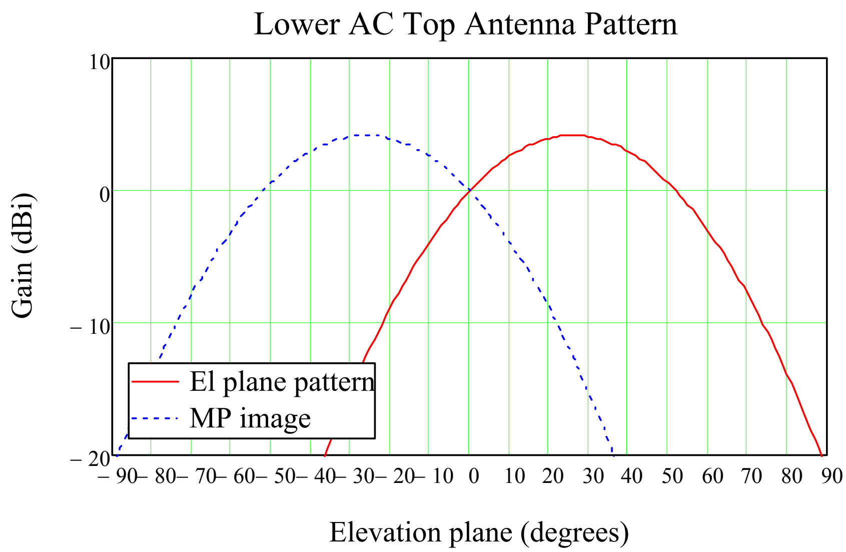

Assumed top antenna free space elevation plane pattern, and its image for multipath calculations (Note positive angle is up)

Ghbd(0) = –0

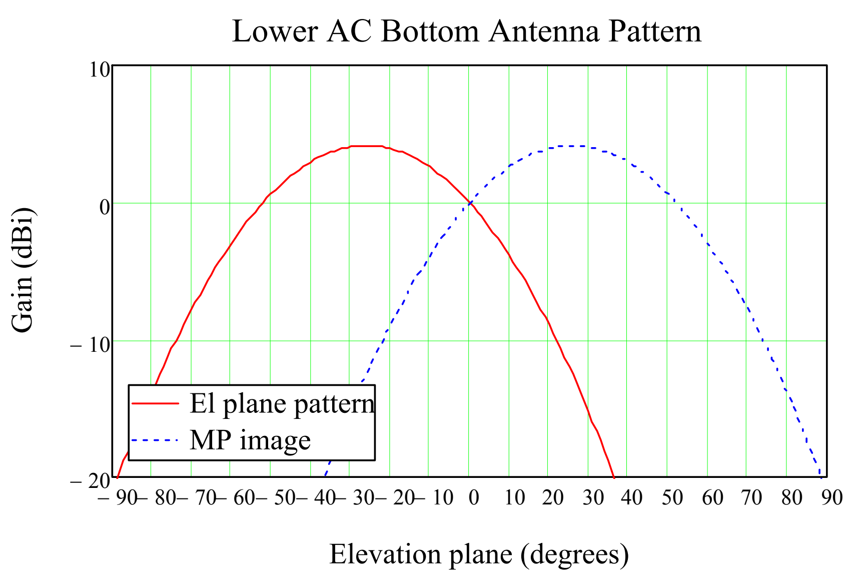

Assumed bottom antenna free space elevation plane pattern, and its image for multipath calculations (Note positive angle is up)

Figure 6: Lower aircraft antenna patterns and their surface reflection images

The magnitude of the reflected wave is determined by the coefficient of reflectivity given in Figure 7 for a smooth surface. As indicated, the vertically polarized ADS-B wave has a 180 degree phase shift on reflection at low elevation angles.

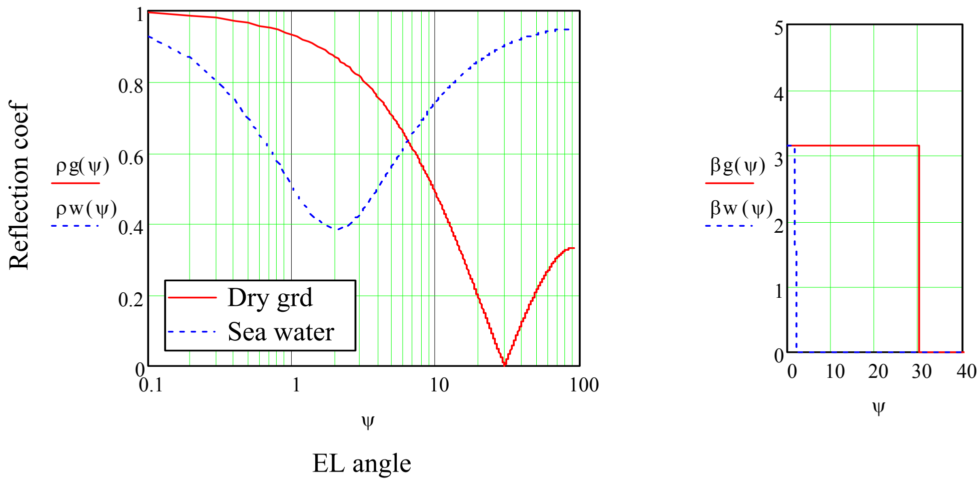

Reflection coefficient for smooth earth (solid) and water (dashed) vs grazing angle.

$F = 1.09 \times 10^3$ $\lambda = 0.903$ $\delta = 0.1$

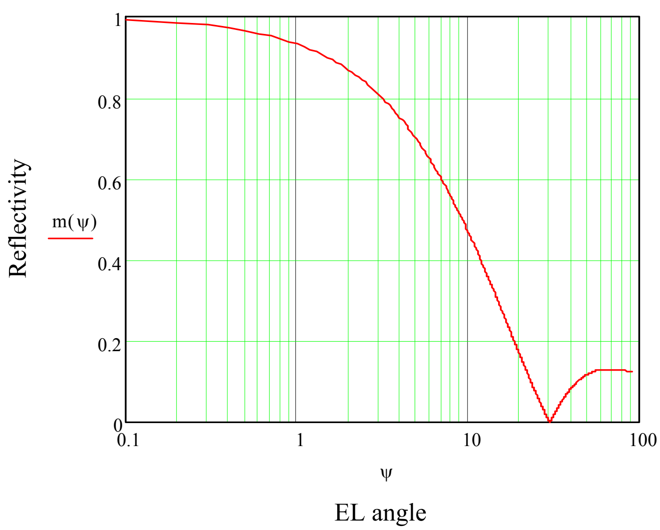

Rough surface reflection coefficient,m, vs grazing angle for wavelength, λ, and mean surface roughness height, δ:

Figure 7: Vertical polarization coefficient of reflection with assumed surface roughness factor

Effects of surface height variations are given in the lower part of the figure for an assumed standard deviation of 0.1 feet. Scattering loss due to this roughness is most noticeable at higher elevation angles.

Details are not given here, but the aggregate effect of the pair wise combination of top and bottom antenna gains, the surface reflectivity, and the exact direct-reflected wave propagation path differences are shown in Figure 8 for antenna heights of h = 15 feet, and a = 200 feet. Although these effects are significant at higher elevation angles (see right hand scale), no measureable difference is found in the first lobe, or at angles below about 2 degrees in this case.

$a = 200 \quad h = 15 \quad \delta = 0.1 \quad \lambda = 0.9$

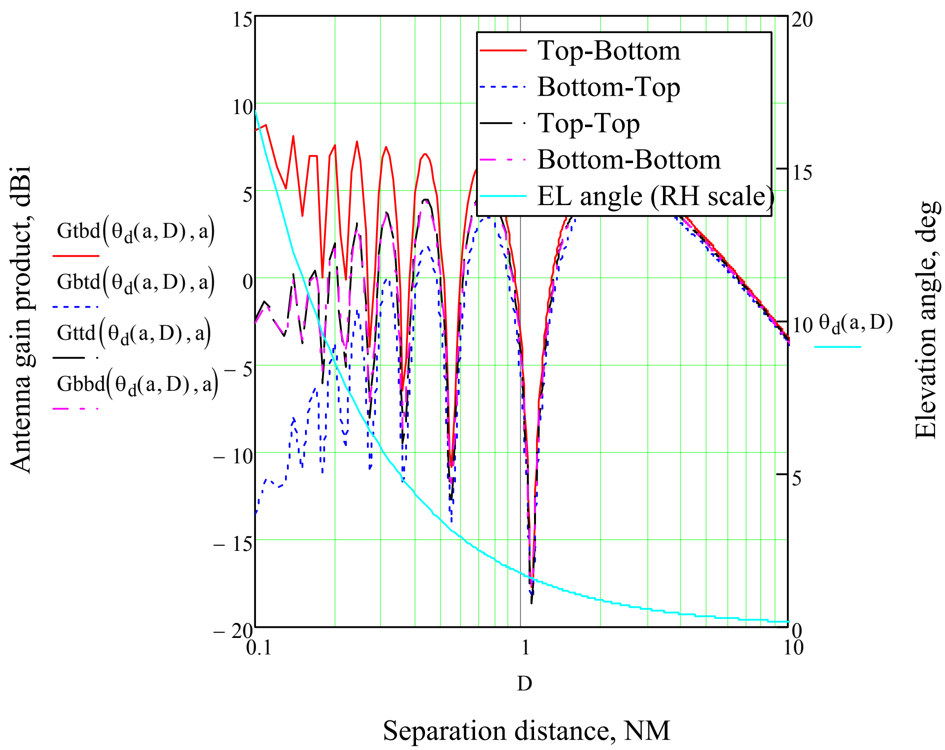

Product of aircraft-aircraft antenna gains vs distance,D, in multipath environment for indicated parameters. Elevation angle: read right hand scale.

Figure 8: Illustration of transmit-receive antenna pair gain products for constant height aircraft

3.1.2.1.2 Examples of expected received signal levels on airport surface

The above examination indicates that a simplified propagation model can accurately represent expected link behavior at low elevation angles. However, the exact model is used in the following examples in order to be sure that this low angle limitation is not violated in any of the geometries considered. ADS-B 1090ES link parameters for the assessment and assumed antenna heights for large and small aircraft are listed in Table 1.

Table 1: Link parameters and assumptions for aircraft to aircraft pair wise coverage examples

Link and antenna height assumptions
Large and small aircraft transmit power at antenna terminals is 125 watts
Large and small aircraft receiver MTL = -79 dBm at antenna terminals
Large aircraft antenna height assumptions
Top antenna height is 25 – 30 ft
Bottom antenna height is 5-8 ft
Small aircraft antenna height assumptions
Top antenna height is 8 – 10 ft
Bottom antenna height is 1.5 - 2 ft
No azimuth fade margin considered

With this assumed 51 dBm power at the transmit antenna, the received signal level as a function of the aircraft-aircraft separation (NM) on the airport surface for various pair wise combinations of large and small aircraft, and top and bottom antennas follows in Figure 9 through Figure 16. The received signal level based on the usually assumed free space propagation loss model and 0 dBi antenna gains is also shown in each figure for reference. The signal-to-noise based limit of link connectivity is indicated by the receiver MTL = -79 dBm (90% detection probability) measured at the receive antenna.

These results may generally be treated as optimistic since:

Signal fades associated with antenna gain nulls due aircraft structural blocking at certain aspect angles may be significant and are not included in these results.

There is no margin for transmit power variations over the aircraft population due to excessive feed line loss and equipment ageing.

Any receiver decoder limitation due to co-channel interference will also limit actual reception capability. It is beyond the scope of this study, but this could impose a noticeable range limitation since the lower signal level received on the higher propagation loss surface mode must compete with fruit replies received in the lower loss free space mode.

F = 1090 Pw = 125 Ptd = 51 Ld = 0 Gbd(0) = –0 Gtd(0) = –0 MTL = –79

h = 25 at = 30 ab = 5 δ = 0.1

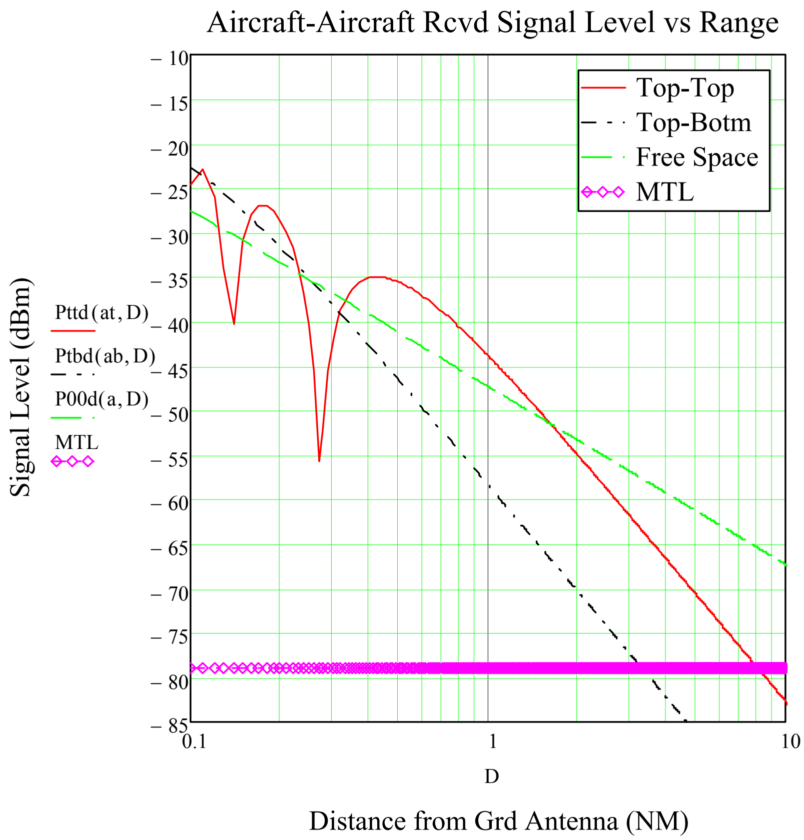

Received signal level (dBm) vs range (NM) for aircraft-aircraft link and indicated parameters.
Dashed free-space is for 0 dBi aircraft antenna gains.

Figure 9: Large aircraft top Tx antenna height, h = 25 ft; Large AC Rx antenna heights, at = 30 ft top, and ab = 5 ft bottom

F = 1090 Pw = 125 Ptd = 51 Ld = 0 Gbd(0) = −0 Gtd(0) = −0 MTL = −79

h = 6 at = 30 ab = 5 δ = 0.1

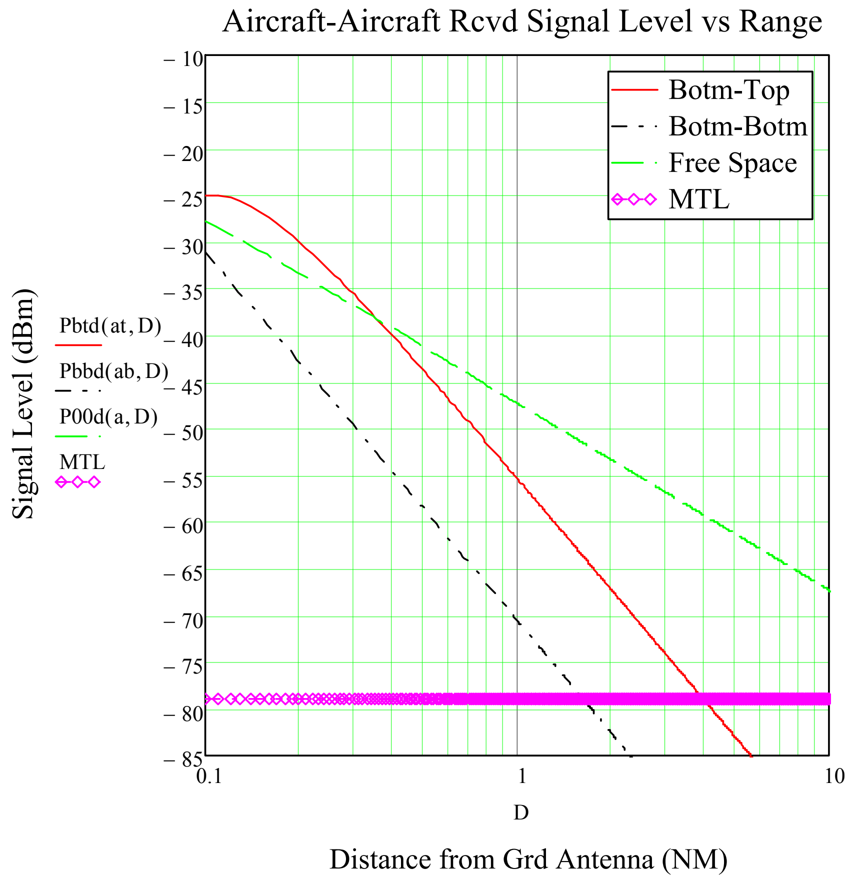

Received signal level (dBm) vs range (NM) for aircraft-aircraft link and indicated parameters.
Dashed free-space is for 0 dBi aircraft antenna gains.

Figure 10: Large aircraft bottom antenna reference height, h = 6 ft; Large AC Rx heights, at = 30 ft top, ab = 5 ft bottom

F = 1090 Pw = 125 Ptd = 51 Ld = 0 Gbd(0) = −0 Gtd(0) = −0 MTL = −79

h = 25 at = 7 ab = 2 δ = 0.1

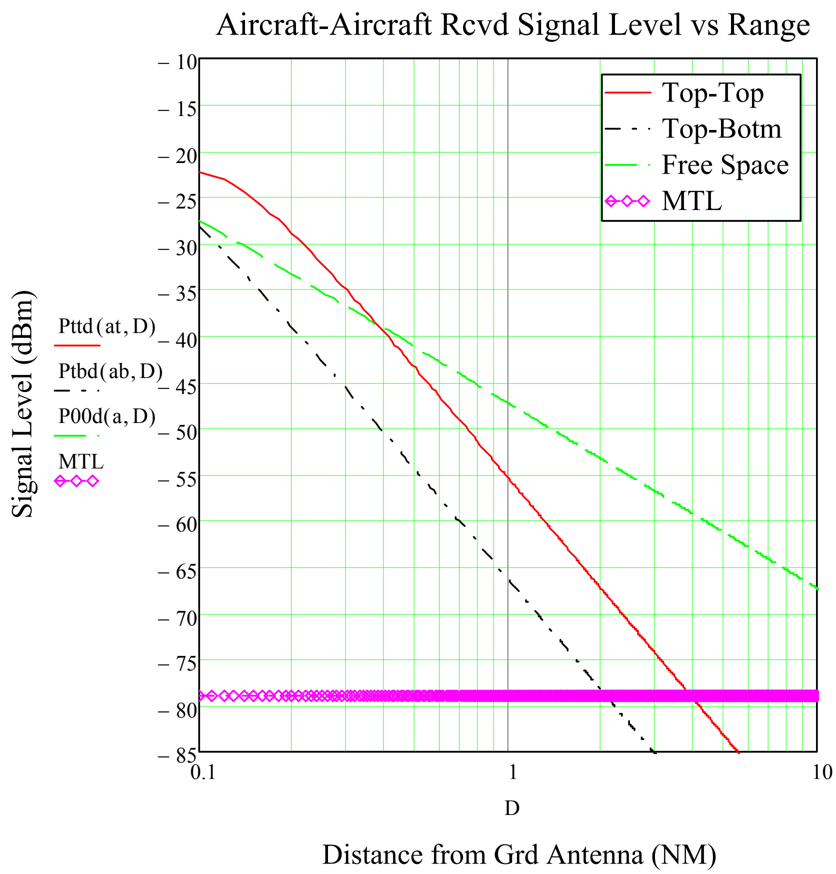

Received signal level (dBm) vs range (NM) for aircraft-aircraft link and indicated parameters.
Dashed free-space is for 0 dBi aircraft antenna gains.

Figure 11: Large aircraft top Tx antenna height, h = 25 ft; Small AC Rx antenna heights, at = 7 ft top, and ab = 2 ft bottom

F = 1090 Pw = 125 Ptd = 51 Ld = 0 Gbd(0) = −0 Gtd(0) = −0 MTL = −79

h = 6 at = 7 ab = 2 δ = 0.1

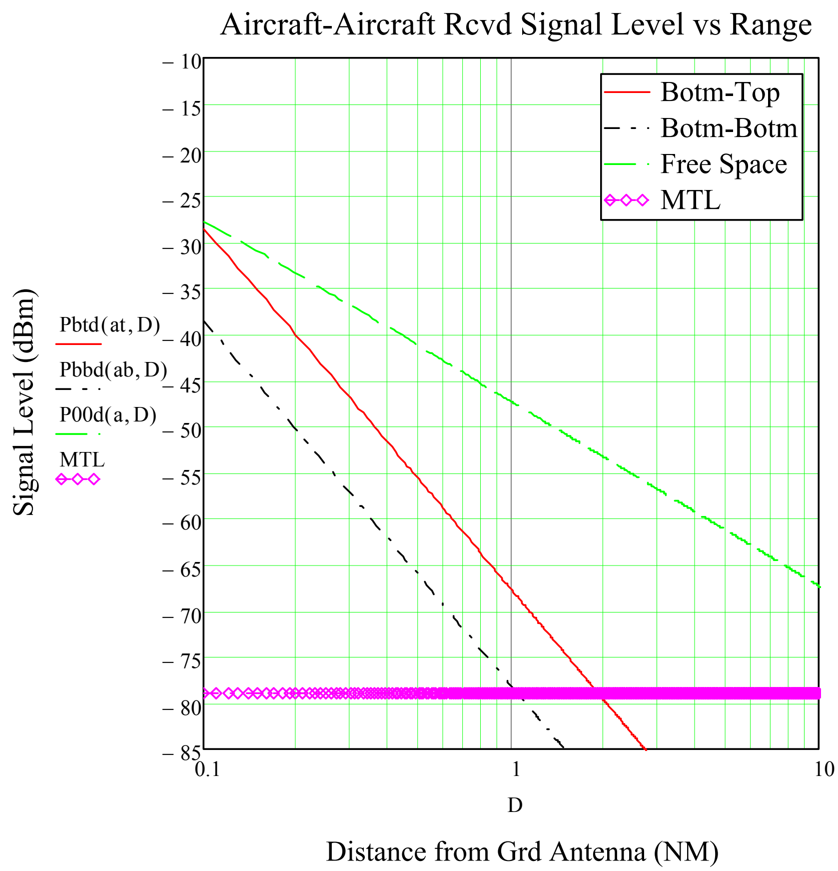

Received signal level (dBm) vs range (NM) for aircraft-aircraft link and indicated parameters.
Dashed free-space is for 0 dBi aircraft antenna gains.

Figure 12: Large aircraft bottom Tx antenna height, h = 6 ft; Small AC Rx antenna heights, at = 7 ft top, and ab = 2 ft bottom

F = 1090 Pw = 125 Ptd = 51 Ld = 0 Gbd(0) = –0 Gtd(0) = –0 MTL = –79

h = 8 at = 30 ab = 5 δ = 0.1

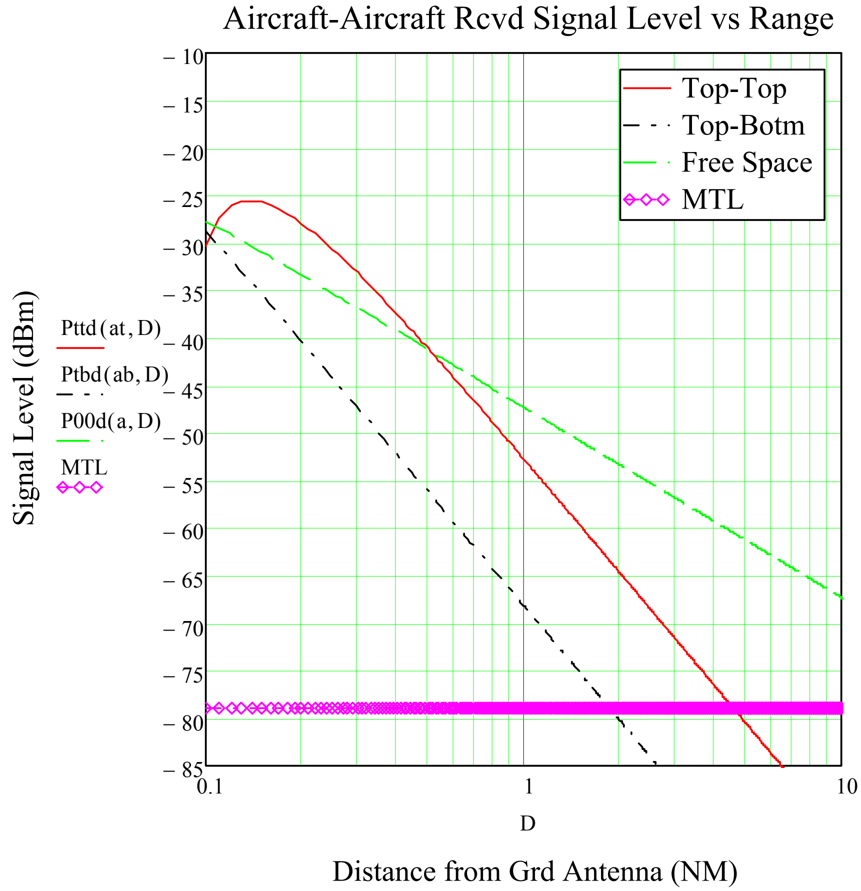

Received signal level (dBm) vs range (NM) for aircraft-aircraft link and indicated parameters.
Dashed free-space is for 0 dBi aircraft antenna gains.

Figure 13: Small aircraft top antenna reference height, h = 8 ft; Large AC Rx heights, at = 30 ft top, ab = 5 ft bottom

F = 1090 Pw = 125 Ptd = 51 Ld = 0 Gbd(0) = −0 Gtd(0) = −0 MTL = −79

h = 2 at = 30 ab = 5 δ = 0.1

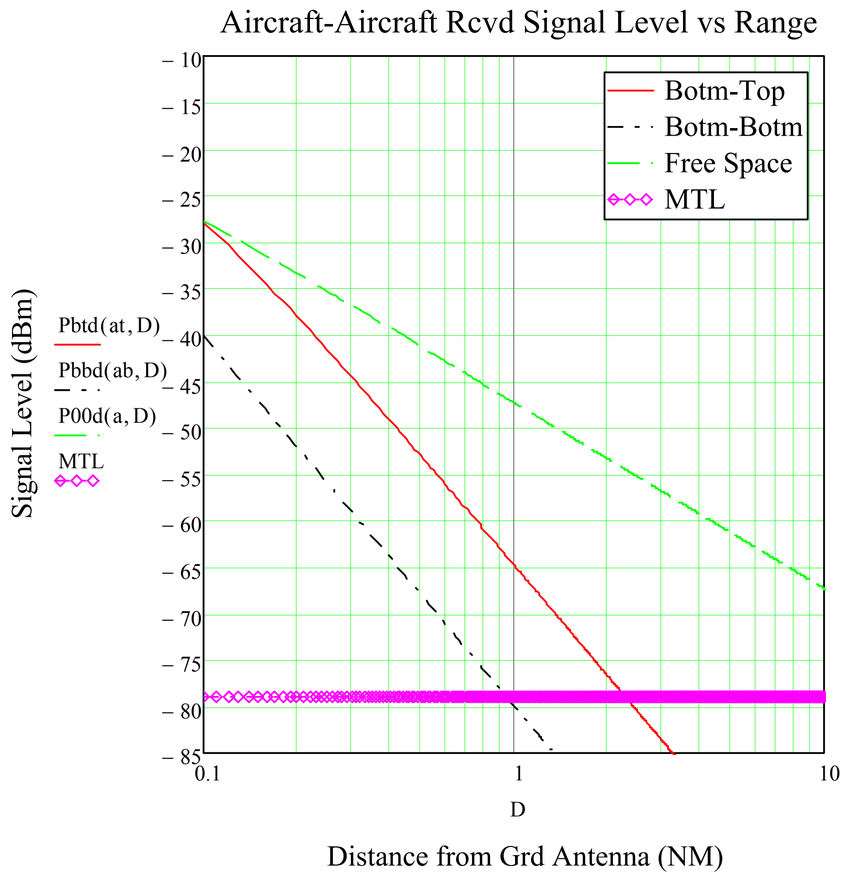

Received signal level (dBm) vs range (NM) for aircraft-aircraft link and indicated parameters.
Dashed free-space is for 0 dBi aircraft antenna gains.

Figure 14: Small aircraft bottom antenna reference height, h = 2 ft; Large AC Rx heights, at = 30 ft top, ab = 5 ft bottom

F = 1090 Pw = 125 Ptd = 51 Ld = 0 Gbd(0) = −0 Gtd(0) = −0 MTL = −79

h = 8 at = 7 ab = 2 δ = 0.1

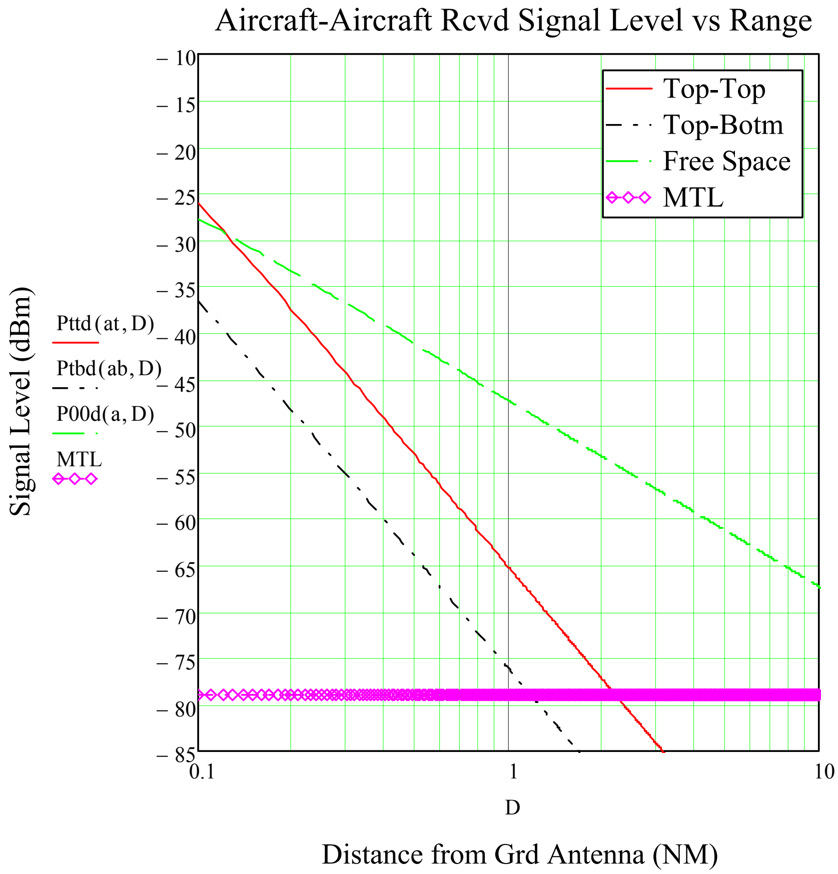

Received signal level (dBm) vs range (NM) for aircraft-aircraft link and indicated parameters.
Dashed free-space is for 0 dBi aircraft antenna gains.

Figure 15: Small aircraft top antenna reference height, h = 8 ft; Small AC Rx heights, at = 7 ft top, ab = 2 ft bottom

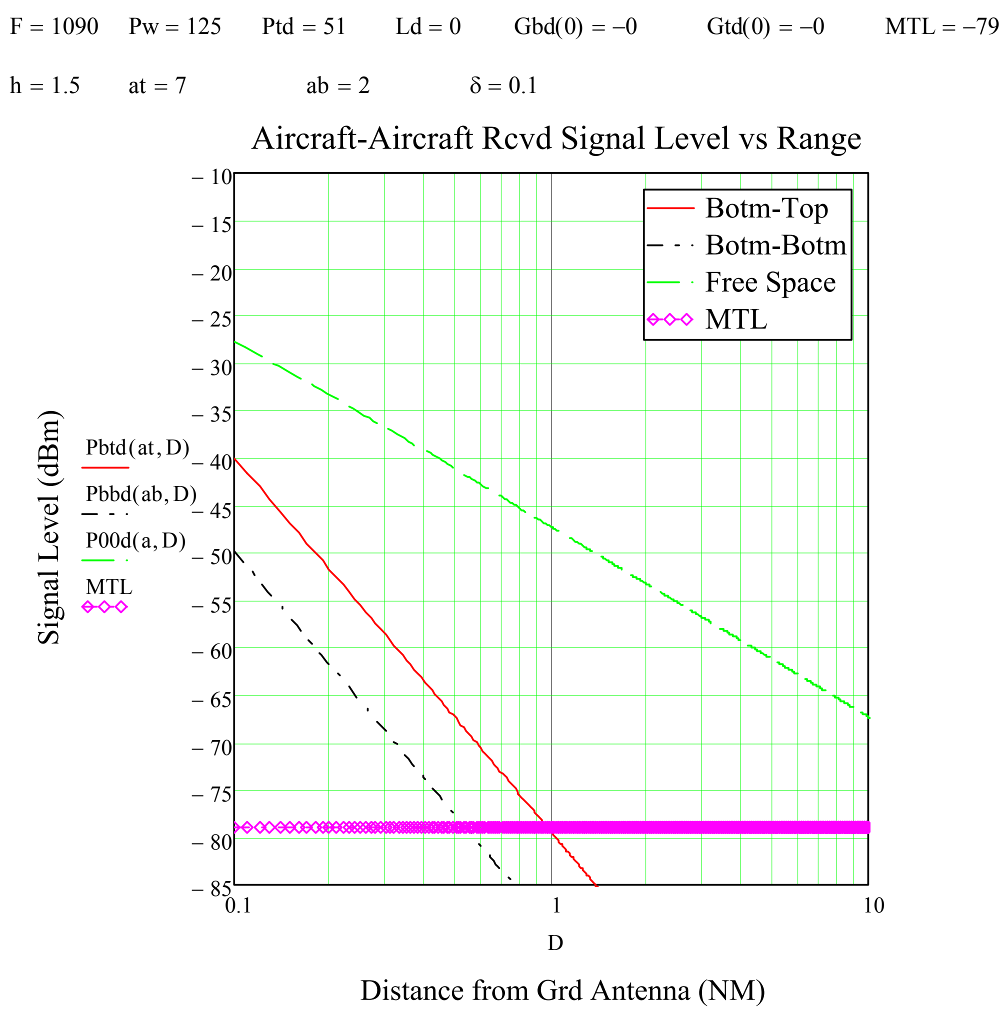

Received signal level (dBm) vs range (NM) for aircraft-aircraft link and indicated parameters.
Dashed free-space is for 0 dBi aircraft antenna gains.

Figure 16: Small aircraft bottom antenna reference height, h = 1.5 ft; Small AC Rx heights, at = 7 ft top, ab = 2 ft bottom

These surface aircraft-aircraft MTL range results are summarized in Table 2 below.

Table 2: Interactive Large and Small aircraft MTL ranges (NM) on airport surface

Rx Tx	Lg AC Top	Lg AC Btm	Sm AC Top	Sm AC Btm
Lg AC Top	8	3	4	2
Lg AC Btm	4	1.5	2	1
Sm AC Top	4	2	2	1
Sm AC Btm	2	1	1	0.5

How do these results compare with operational needs? Desired aircraft-to-aircraft coverage on the airport surface depends upon the airport configuration and supported ADS-B applications, but based on an informal examination of representative airport maps, reasonable guidance seems to be:

- Desired surface to surface operational coverage
  - Maximum coverage for a large airport is nominally about 2 NM
  - Maximum coverage for a small airport is nominally about 1 NM
- Minimum Surface Applications MOPS (DO xxx) required coverage for an aircraft at the runway threshold to an aircraft on final approach is 3 NM

With this interpretation of the above surface coverage results, most limitations are associated with potential use of bottom mounted aircraft antennas.

Support vehicles moving in the active area of the airport also transmit ADS-B position data. With a power limitation of 16 watts, their coverage range is shown in Figure 17. Single antenna equipage is permitted for lower capability ADS-B users; the visibility of such a bottom mounted antenna aircraft to an aircraft on final approach is indicated in Figure 18.

Table 3 summaries these direct received signal results.

F = 1090 Pw = 16 Ptd = 42 Ld = 0 Gbd(0) = −0 Gtd(0) = −0 MTL = −79

h = 5 at = 25 ab = 2 δ = 0.1

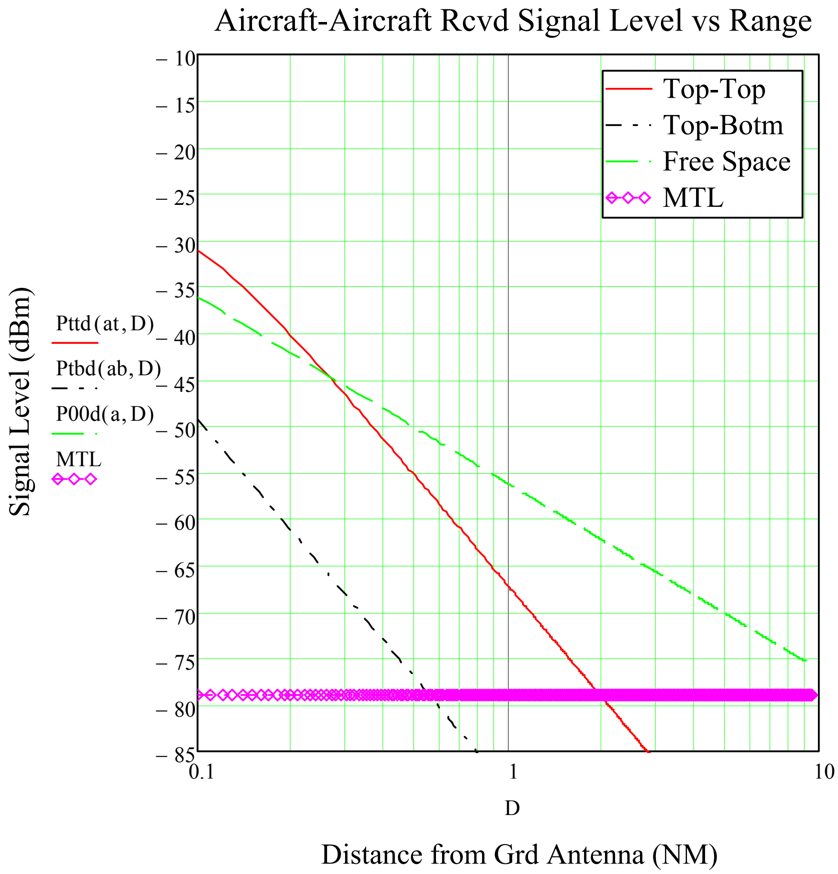

Received signal level (dBm) vs range (NM) for aircraft-aircraft link and indicated parameters.
Dashed free-space is for 0 dBi aircraft antenna gains.

Figure 17: Airport vehicle Tx ht = 5 ft, Large AC Top Rx ht = 25 ft, Small AC bottom Rx ht = 2 ft

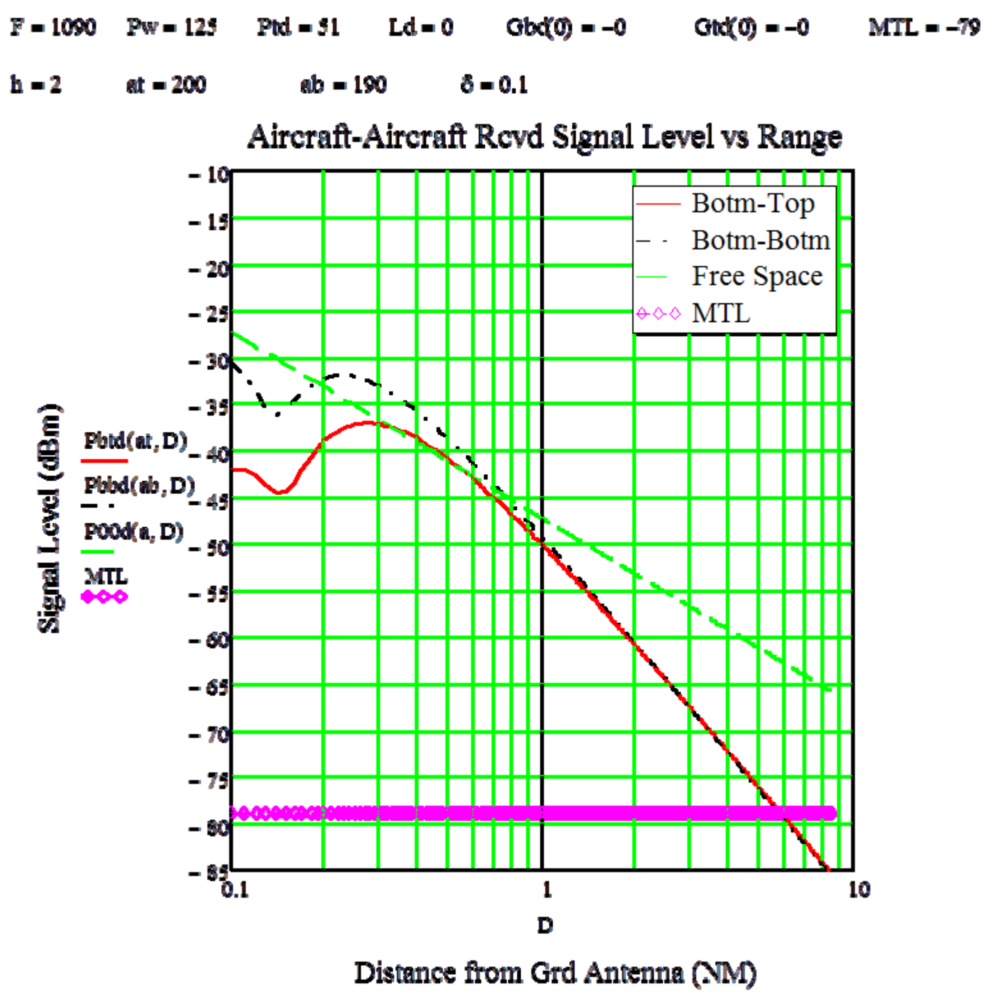

Received signal level (dBm) vs range (NM) for aircraft-aircraft link and indicated parameters. Dashed free-space is for 0 dBi aircraft antenna gains.

Figure 18: Small aircraft bottom antenna reference height, h = 1.5 ft at runway threshold; approach AC Rx heights, at = 200 ft, ab = 190 ft

Table 3: Airport surface link budget results summary

- **Surface propagation loss is substantially greater than free-space loss**
- **Large-large aircraft meet nominal large airport coverage for T-T and T-B antenna pairs (B-B is marginal)**
- **Small-small and small-large aircraft meet nominal small airport coverage for T-T and T-B antenna pairs (B-B is marginal)**
- **Small-large aircraft meet nominal large airport coverage for T-T with marginal B-T (B-B is limited)**
- **Airport vehicle MTL range from 0.5 NM for small AC bottom antenna to 2 NM for large AC top antenna**
- **Bottom antenna on small aircraft at runway THD meets final approach coverage needs**

3.1.2.1.3 Blocking obstruction loss

Signal loss when the direct path line-of-sight is obstructed by a building or humped runway can be estimated with the knife-edge diffraction model. The Fresnel zone model considers a shadowing height, H, above the propagation path and separated from one end of the link by D1, and at a distance, D2 from the other end. Details are given in Table 4 and the application is illustrated for assumed values Ha = 50, antenna height, a = 25, D1 = 1000, and D2 = 5078. All dimensions are in feet. From these values a diffraction parameter, ve = 2.4, is calculated and used to enter the diffraction loss curve of Figure 19. The resulting blocking or shadowing loss is shown to be G = -21.2 dB. This loss is added to the unobstructed LOS path loss. Inspection of the expression for ve shows that a different relative separation for an obstruction of the same height will produce a different loss.

Table 4: Shadowing loss model for blocking obstruction

Signal loss due to horizon blockage by obstacle of height, Ha, above antenna:

Knife-edge ht relative to grd antenna, Ha, at distance, D1, with aircraft altitude, a, at distance, D1+D2, then effective knife-edge ht is H:

$Ha := 50 \qquad a := 25 \qquad D1 := 1000 \qquad D2 := 5076 \qquad \frac{D1 + D2}{6076} = 1$

$H := Ha - \frac{a \cdot D1}{D1 + D2} \qquad H = 45.885$

Fresnel zone assesment of knife-edge difraction loss for long horizontal obstacle of ht, H, above the propagation path, D1+D2:

Obstruction geometry parameters:

Step 1- Determine geometry: $Ha = 50 \quad a = 25 \quad D1 = 1 \times 10^3 \quad D2 = 5.076 \times 10^3 \quad H = 45.885$

Step 2- CalculateFresnel Diffraction Parameter, v: $\lambda = 0.903 \qquad ve := H \cdot \sqrt{2 \cdot \frac{D1 + D2}{\lambda \cdot D1 \cdot D2}} \qquad ve = 2.363$

Lee approximation to Fresnel integral: $v := -3, -2.9 .. 7$

$Go := 0 \qquad G1(v) := 20 \cdot \log(0.5 - 0.62 \cdot v) \qquad G2(v) := 20 \cdot \log(0.5 \cdot \exp(-0.95 \cdot v))$

$G3(v) := 20 \cdot \log\left[0.4 - \sqrt{0.1184 - (0.38 - 0.1 \cdot v)^2}\right] \qquad G4(v) := 20 \cdot \log\left(\frac{0.225}{v}\right)$

$G3(v) := \text{if}(1 < v \le 2.4, G3(v), G4(v)) \qquad G2(v) := \text{if}(0 < v \le 1, G2(v), G3(v))$

$G1(v) := \text{if}(-1 < v \le 0, G1(v), G2(v)) \qquad G(v) := \text{if}(v \le -1, Go, G1(v))$

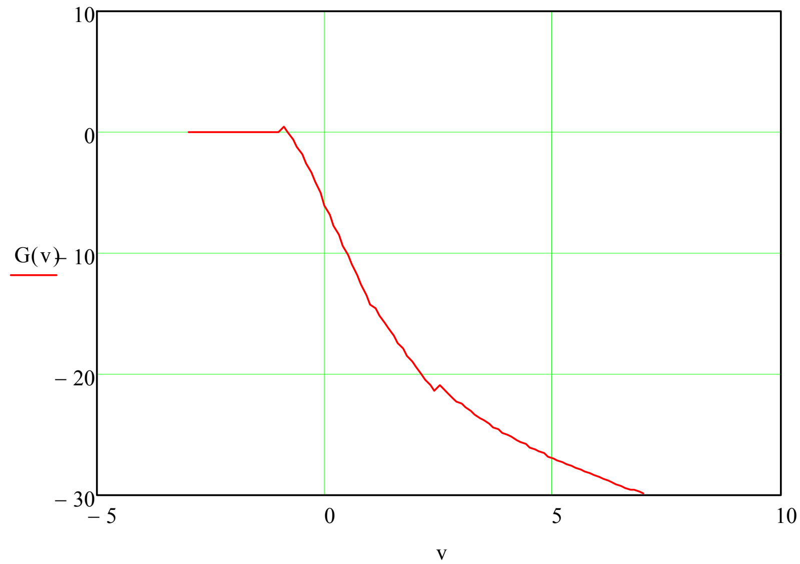

Knife-edge diffraction gain (dB) vs Fresnel diffraction parameter, v

Step 3- Read diffraction loss, G(ve), from curve $ve = 2.363$ $G(ve) = -21.2$ dB

Figure 19: Shadowing loss model for blocking obstruction

3.1.2.1.4 Surface wave limiting case propagation model

Simplifications to the exact propagation model are appropriate under many surface-surface geometries as suggested in most of the examples treated so far. This surface mode model is compared with free space propagation loss below.

Exact propagation model with antenna gain patterns and reflection coefficient

$$Ext(a, D) := Gttd\left(\theta_d(a, D), a\right) - \left[37.5 + \left(20 \cdot \log(R(a, D)) + 20 \cdot \log\left(\frac{984}{\lambda}\right)\right)\right] + Ptd$$

Normalized conditions with Ga = Gg = 0 dBi and 180 deg surface reflection

Surface limiting case model

$$SUL(R) := 10 \cdot \log\left[\frac{h^2 \cdot at^2}{(R \cdot 6076)^4}\right] + Ptd$$

Free space model (no reflection)

$$FSL(R) := 10 \cdot \log\left[\left(\frac{\lambda}{4 \cdot \pi \cdot R \cdot 6076}\right)^2\right] + Ptd$$

Some comparisons of the surface and exact propagation loss models follow in Figure 20 through Figure 22. Free space loss is again shown for reference. Good agreement between the exact and surface models is indicated for separations of at least one NM with the exact model tending more towards free space loss at closer ranges, or higher elevation angles. With these results, the following treatment of horizontal multipath on the airport surface uses the surface mode model for direct and multipath estimates where a direct separation greater than one NM is the assumed baseline.

h = 25 at = 7 λ = 0.903 D := 0.1, 0.12.. 10 R := 0.1, 0.2.. 10

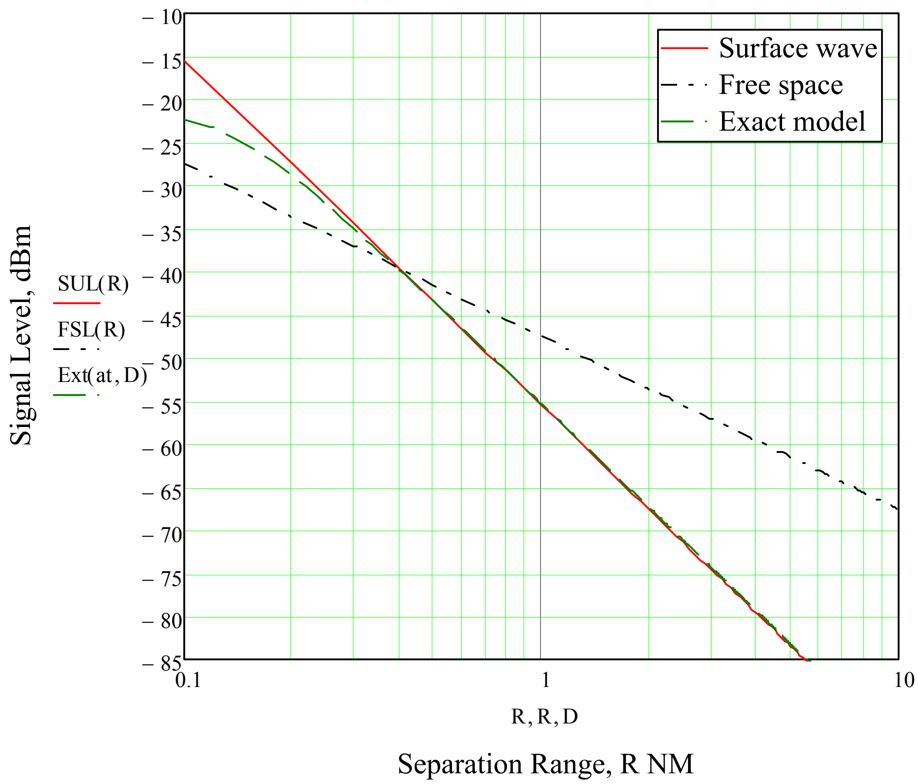

Figure 20: Surface wave propagation model relative to free space loss and with exact loss model for h = 25 ft, at = 7 ft for aircraft configuration of Figure 11

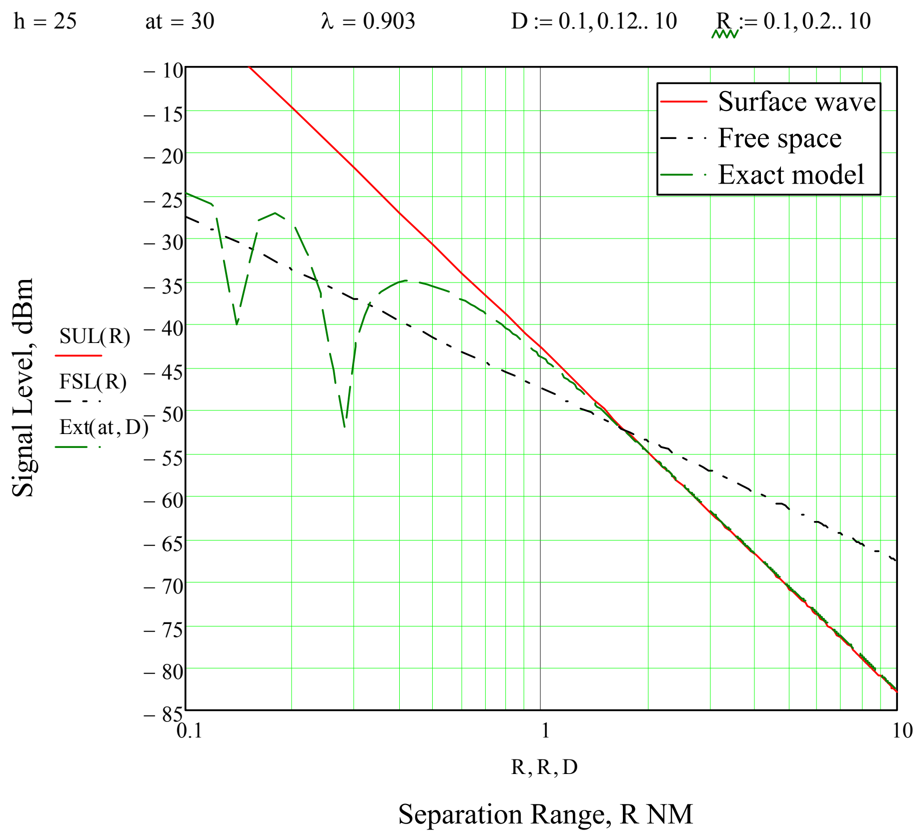

Figure 21: Surface wave propagation model relative to free space loss and with exact loss model for h = 25 ft, at = 30 ft for aircraft configuration of Figure 9

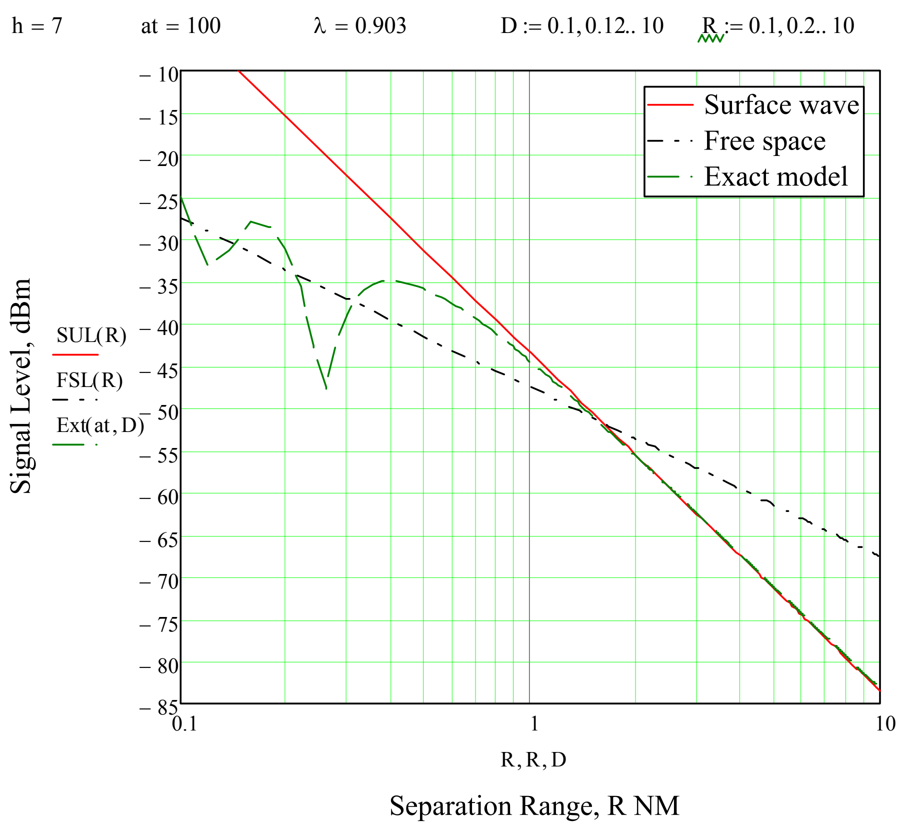

Figure 22: Surface wave propagation model relative to free space loss and with exact loss model for h = 7 ft, at a range = 100 ft

3.1.2.2 Horizontal multipath characteristics on the airport surface

3.1.2.2.1 Horizontal multipath geometry

Geometry for horizontal multipath examinations is illustrated in Figure 23. The transmitter and receiver are separated by Do with their positions, xs and xr, the focal points of a constant path difference, r1 + r2, ellipse. A horizontal multipath reflector is shown at point, P, on the ellipse. Azimuth gains for the aircraft antennas at xs, xr, are assumed to be omni-directional. Angles from the direct path baseline to the reflector are α and β with the multipath scattering angle, γ.

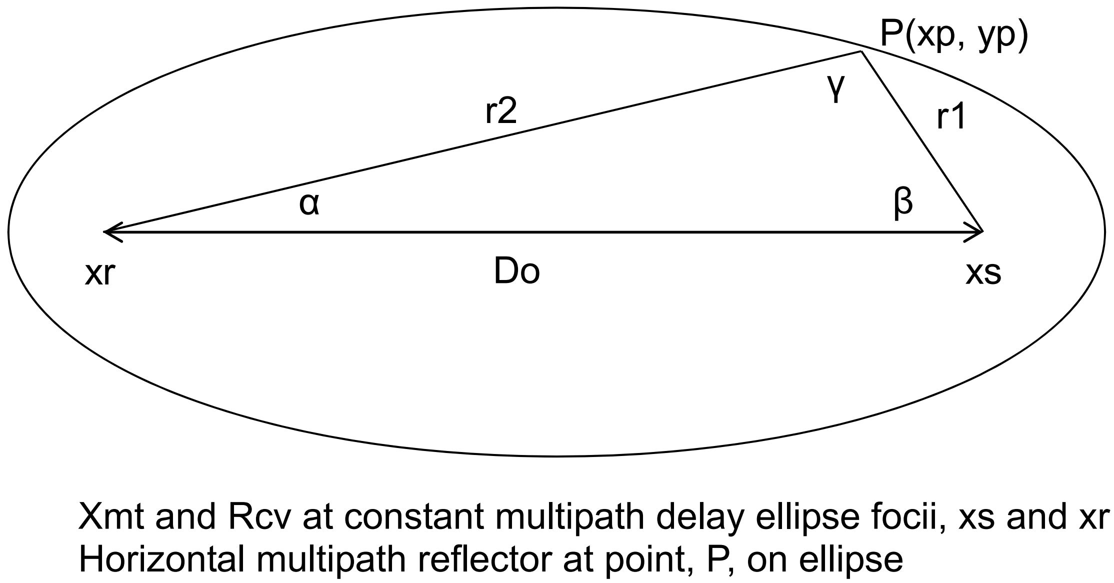

Figure 23: Horizontal multipath geometry

Derivation of the constant delay ellipse is shown below.

Constant delay multipath ellipse for Xmt-Rvr separation, Do, and delay, t $\tau := 1.5$ us

Velocity, c = 984 ft/μs, then MP path delay for t μs is: $c := 984 \quad \Delta(\tau) := \tau \cdot c \quad \Delta(\tau) = 1476$ ft

Do = Xmt-Rvr separation in ft $Do := 7400$ ft

Equation of constant delay ellipse with Tmt and Rcv at focal points F1(xs,ys) and F2(xr,yr)

$$xs := \frac{Do}{2} \qquad ys := 0 \qquad xr := \frac{-Do}{2} \qquad yr := 0$$

$$a(\tau) := \frac{Do + \Delta(\tau)}{2} \qquad b(\tau) := \frac{\sqrt{2 \cdot \Delta(\tau) \cdot Do + \Delta(\tau)^2}}{2} \qquad y(x,\tau) := b(\tau) \cdot \sqrt{1 - \left(\frac{x}{a(\tau)}\right)^2}$$

Distance to scatter at pt(x,y) on ellipse $r1(x,y) := \sqrt{(x - xs)^2 + y^2} \quad r2(x,y) := \sqrt{(x - xr)^2 + y^2}$

Resulting constant delay contours for path difference delays of 0.5 usec, 1.0 usec, and 1.5 usec are illustrated in Figure 24 for an assumed separation of Do = 7400 feet. Note that the x and y axis are not to scale.

$Do = 7.4 \times 10^3 \quad xs = 3.7 \times 10^3 \quad xr = -3.7 \times 10^3 \qquad \Delta(0.5) = 492 \qquad \Delta(1.0) = 984 \qquad \Delta(0.25) = 246$

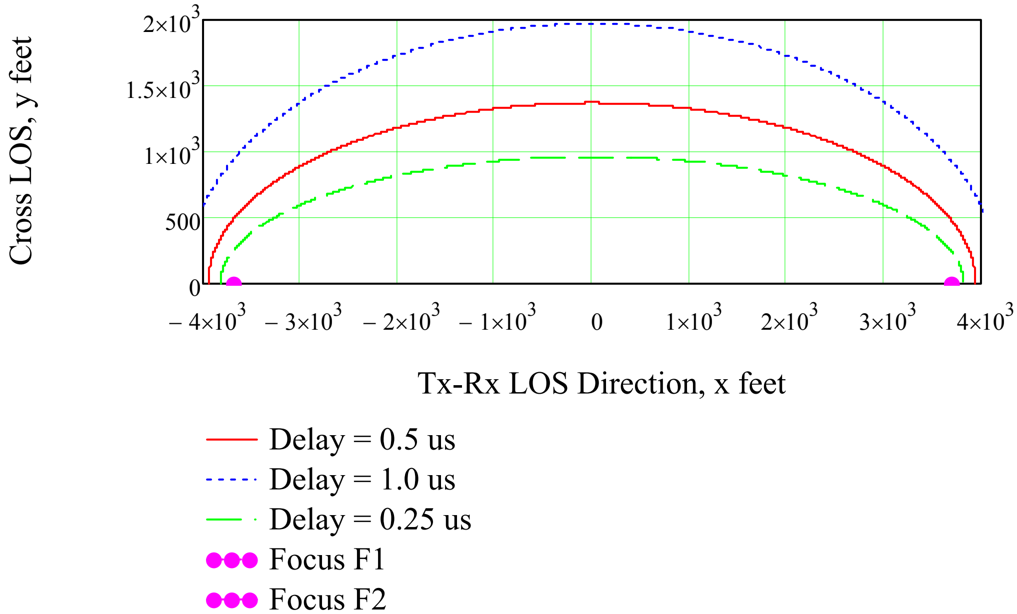

Figure 24: Examples of horizontal multipath geometry for above transmit-receive separation parameters and three constant delay elliptical contours

Any reflection point on one of these contours produces the same relative multipath delay as any other point on that ellipse. Inter-relationships among the parameters of interest are derived below with an example given for a delay of 1.5 usec and a reflection point at P(xp,yp). The following examples assume the angle measured from a transmitter on the LOS baseline at the focal point, xs, to this point of reflection is β = 150 degrees. Any multipath scattering from this point then appears at an angle, α = 2.8 degrees from the LOS baseline for a receiver at the other focal point, xr. The subtended angle of bi-static reflection is γ = 27 degrees, and a specular reflector at that point must have a normal angle close to φN = 16.5 degrees (the normal to the elliptical contour at this point) to produce multipath at xr.

For parameters: $Do = 7400$ $xs = 3700$ $xr = -3700$ $\tau = 1.5$ $\Delta(\tau) = 1476$

Select reflector point on ellipse at xp $xp := 4380$ Then $yp := y(xp, \tau)$ $yp = 394.911$

$r1(xp, yp) = 786.355$ $r2(xp, yp) = 8089.6$ $r1(xp, yp) + r2(xp, yp) = 8876$ $Do + \Delta(\tau) = 8876$

For point at: $xp = 4380$ $yp = 394.9$ $Xt := xp - xs$ $Xr := xp - xr$

$Xt = 680$ $Xr = 8080$

Baseline-Tx angle to P $\beta(xp, yp) := 180 - \text{atan2}(Xt, yp) \cdot \frac{180}{\pi}$ $\beta(xp, yp) = 149.9$ deg

Baseline-Rx angle to P $\alpha(xp, yp) := \text{atan2}(Xr, yp) \cdot \frac{180}{\pi}$ $\alpha(xp, yp) = 2.8$ deg

Scatter included angle $\gamma(xp, yp) := 180 - (\beta(xp, yp) + \alpha(xp, yp))$ $\gamma(xp, yp) = 27.3$ deg

Specular reflector normal angle $\phi N(xp, yp) := \alpha(xp, yp) + \frac{\gamma(xp, yp)}{2}$ $\phi N(xp, yp) = 16.5$ deg

As a check, note that the normal angle to ellipse tangent at pt(xp,yp) derivecd from the slope is:

$$Slp(x) := \frac{-b(\tau) \cdot x}{a(\tau)^2 \cdot \sqrt{1 - \left(\frac{x}{a(\tau)}\right)^2}} \quad Slp(xp) = -3.382 \quad \phi Ne(x) := \text{atan}(Slp(x)) \cdot \frac{180}{\pi} + 90 \quad \phi Ne(xp) = 16.5$$

3.1.2.2.2 Surface propagation model and signal-to-multipath calculations

Section 3.1.2.2 reviewed the geometric factors related to horizontal multipath; the directly received signal level and reflected multipath signal levels for this geometry when the surface propagation mode losses are applied are examined in this section. The surface mode approximation to the exact loss model used in section 2 is given below as SUL, along with the free space loss model, FSL, usually employed for received signal level estimates.

Path loss calculations follow for freq in MHz: $F := 1090$ $\lambda := \frac{984}{F}$ $\lambda = 0.903$ feet

Free space loss: $FSL(R) := 10 \cdot \log\left[\left(\frac{\lambda}{4 \cdot \pi \cdot R}\right)^2\right]$

Surface wave loss, SUL, for direct signal with elevation plane low angle multipath for heights, a and h feet; and El plane MP loss

Select antenna hts in feet: $a := 30$ $h := 25$

For surface separation, R cos ? = D, and R = D approx. $R := Do$ $R = 7400$ ft

EL plane MP signal with phase reversal below Brewster angle. $SUL(R) := 10 \cdot \log\left[\frac{a^2 \cdot h^2}{(R)^4}\right]$

Back scatter cross-sections, or multipath reflectivity estimates for several potential objects are described below. It should be noted, however, that the reflectivity varies greatly for complex objects such as buildings with setback configurations and corners, as well as for specific aircraft and aspect angles. Also, as indicated above, the bi-static reflectivity of even a flat vertical surface depends sharply on the relative azimuth orientation of the surface and the subtended bi-static angle.

Horizontal multipath source has a bi-static cross-section, s, at P(xp,yp), with a resulting signal-MP ratio G. Example radar back scatter sources are:

Vertical cylinder ht, hc, radius, ar $hc := 30$ $ar := 10$ $\rho := 0.9$

$$\sigma_c := 2 \cdot \pi \cdot \frac{hc^2 \cdot ar}{\lambda} \cdot \rho \qquad \sigma_c = 5.638 \times 10^4 \text{ sq-ft}$$

Flat plate with area, A (normal incidence) $\sigma_a(A) := 4 \cdot \pi \left(\frac{A}{\lambda} \right)^2$ $A := 300$ $\sigma_a(A) = 1.388 \times 10^6$ sq-ft

Note bi-static cross-section depends on relative geometry of Tx-Rx

Large aircraft cross-section = 1000 sq-m $\sigma_{ac} := 10^3 \cdot 3.28^2$ $\sigma_{ac} = 1.076 \times 10^4$ sq-ft

Link margin calculations for the surface and free space propagation modes are given below along with the associated signal-to-multipath ratios in dB. Since the bi-static cross-section is so dependent upon specific considerations, the following multipath sensitivity examination assumes a fixed bi-static cross-section of $\sigma s = 10^5$ square feet as shown.

Link margin parameters: Tmt pwr, dBm $Pt := 51$

Antenna gain, dBi $Gt := 0$ $Gr := 0$ Rcvr MTL, dBm $MTL := -79$

Rcvd signal level for different propagation modes

Free space mode $PrF(R) := Pt + Gt + Gr + FSL(R)$

Surface wave mode $PrS(R) := Pt + Gt + Gr + SUL(R)$

Select reflector bi-static x-section (sq-ft) $\sigma_s := 10^5$ sq-ft

Surface propagation mode signal-multipath ratio for reflector ht, hp: $hp := 40$ ft

$\sigma_s = 1 \times 10^5$ sq ft $h = 25$ ft $a = 30$ ft $\tau = 1.5$ usec $Do = 7400$ feet

Signal/MP ratio surface wave mode $\Gamma su(xp, yp, hp) := 10 \cdot \log\left[\frac{1}{\sigma_s} \cdot \left(\frac{r1(xp, yp) \cdot r2(xp, yp)}{Do \cdot hp}\right)^4\right]$

Rcvd sig level $PrS(Do) = -46.3$ dBm **Sig MP ratio** $\Gamma su(xp, yp, hp) = 3.3$ dB

Free space propagation signal-multipath ratio $\sigma_s = 1 \times 10^5$ $\tau = 1.5$ $Do = 7400$

Signal/MP ratio free space (no surface reflection)

$\Gamma fs(xp, yp) := 10 \cdot \log\left[\frac{4 \cdot \pi}{\sigma_s} \cdot \left(\frac{r1(xp, yp) \cdot r2(xp, yp)}{Do}\right)^2\right]$ $\Gamma fs(xp, yp) = 19.7$ dB

Rcvd sig level $PrF(Do) = -49.3$ dBm **Sig MP ratio** $\Gamma fs(xp, yp) = 19.7$ dB

Direct signal free space and surface mode propragation loss difference

$\Delta FS(Do) := PrF(Do) - PrS(Do)$ $\Delta FS(Do) = -3$

3.1.2.2.3 Surface propagation horizontal multipath sensitivity

Review of the surface mode received signal level expression shows that it is a function of the transmit and receive antenna height, h and a. Similarly, the surface mode signal-to-multipath ratio depends on the reflector height, hp. The corresponding free space mode equations do not include these factors. Sensitivity of the directly received signal level to antenna heights was the subject of section 2 above. Sensitivity of the surface mode signal-to-multipath ratio (S/MP) to the reflecting object height follows. Again, the free space mode behavior is included for reference.

Figure 25 compares the S/MP for reflector heights, hp = 10 feet and hp = 40 feet, as a function of three assumed reflector locations on the constant delay ellipse for τ = 0.5 usec. The plot points correspond to xp = 0 (the mid-point between xs and xr), a point where β = 90 degrees, and point even closer to xs located by β = 150 degrees. The assumed bi-static cross-section is constant for all cases and again Do = 7400 feet. Notice the results are very sensitive to the reflector height and proximity to the focal point (or location of either the transmitter or receiver). Notice that a high reflector produces a much lower S/MP than that expected from the free space model.

$\tau 5 = 0.5$ usec $hp1 = 10$ ft $hp4 = 40$ ft $\sigma_s = 1 \times 10^5$ sq ft

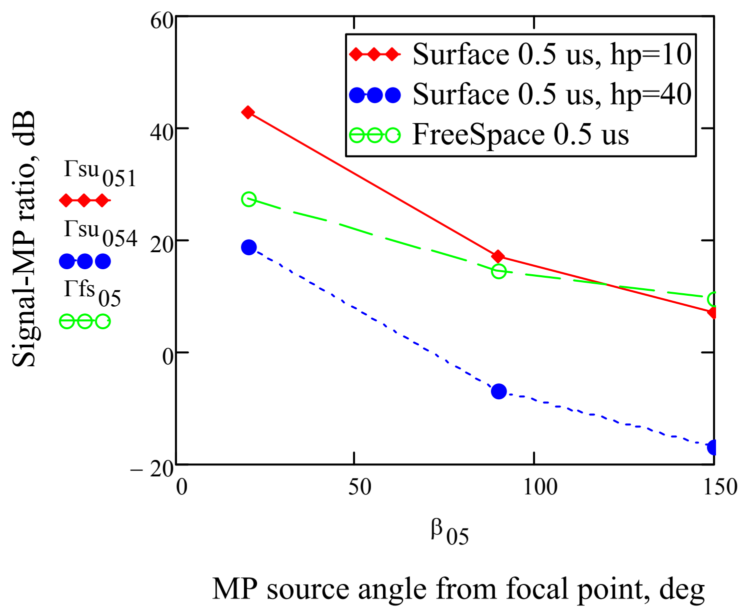

Figure 25: Signal-to-multipath ratio for a 0.5 usec delay and reflector heights, hp = 10 and 40 feet

The same sort of variation is shown in Figure 26 for the hp = 40 feet case, but with an increase in relative time delay to τ = 1.0 usec. The time delay is further increased to τ = 1.5 usec in Figure 27. The corresponding free space mode results are shown in each case for reference. In all cases the surface mode S/MP results are much lower than those expected from the free space model.

The results for hp = 40 with increasing relative time delay (increased distance to the reflector) are directly compared in Figure 28. As would be expected, the S/MP decreases as total reflected path length decreases (smaller relative time delays), and it decreases as the reflector moves closer to either the transmitter or the receiver.

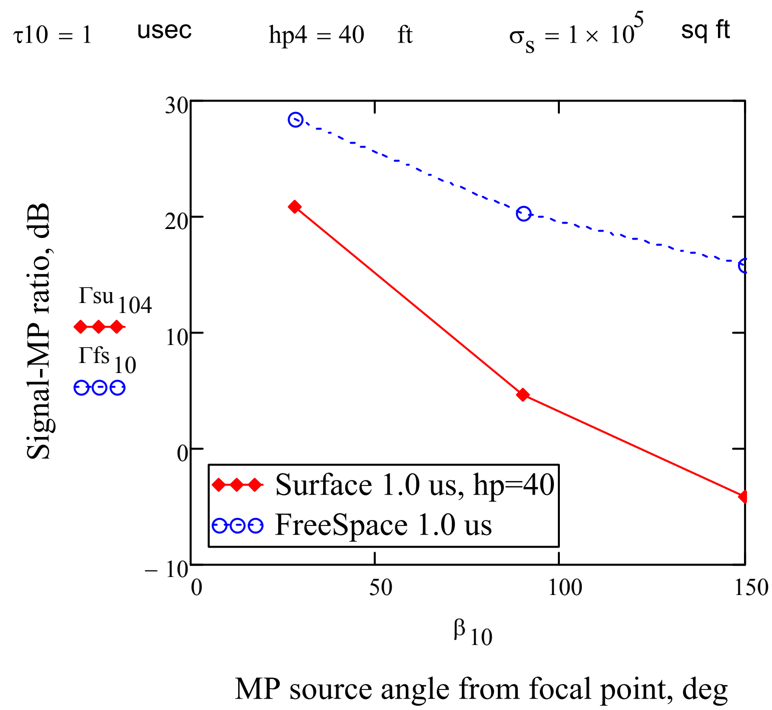

Figure 26: Signal-to-multipath ratio for a 1.0 usec delay and reflector heights, hp = 40 feet

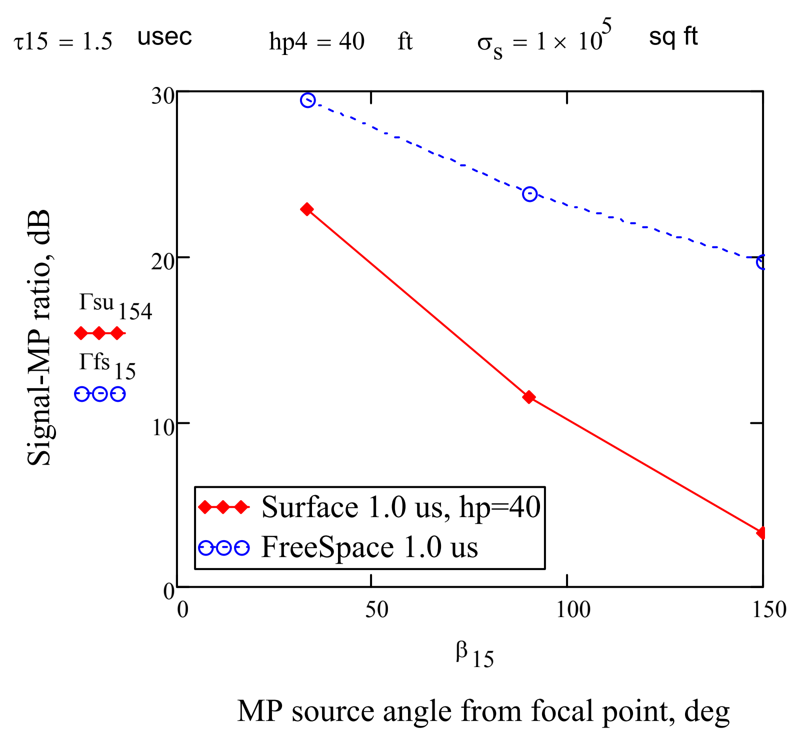

Figure 27: Signal-to-multipath ratio for a 1.5 usec delay and fixed reflector height, hp = 40 feet, compared with free space estimate

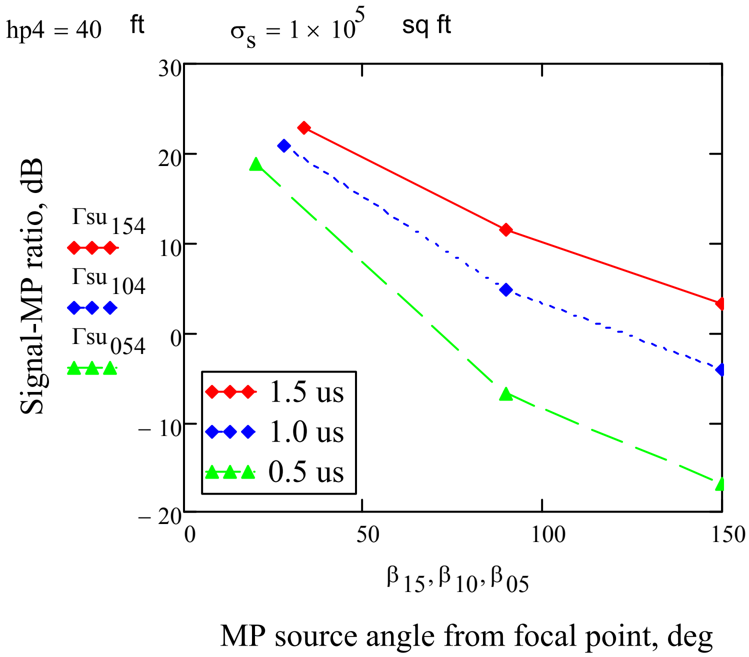

Figure 28: Signal-to-multipath ratio for different relative delays and a fixed reflector height, hp = 40 feet

3.1.2.3 ADS-B 1090ES received messages with horizontal multipath overlaps

3.1.2.3.1 The detected message sampled waveform model

Bench testing of receiver decoder capability when the desired signal has overlapped multipath with relatively long delay times could involve rather sophisticated test equipment. This bench test equipment need is avoided by analytically creating digitized replicas of the detected 1090ES message after it has been combined with the vector sum of any combination of multipath produced overlaps. Creation of this desired bench test input is described here. The sampling rate is 80 MHz, and the pass band filter shape factor is matched to WJHTC measured received pulse shapes. The Mathcad program generating the basic 1090ES pulse is in Figure 29 and the resulting pulse is shown in Figure 30.

The following model is in time units of usec. The sample rate is in units of MHz

Sample rate $s := 80$ MHz $\iota := \frac{1}{s}$ $\iota = 0.013$ usec $t := -0.5, -0.5 + \iota .. 1$

Chip width $w := 0.5$ usec Pulse length $tb := 2 \cdot w$ usec

Rectangular pulse function $p(t) := \Phi(t) - \Phi(t - w)$

Filter shape factor $wo := 12$ $\sigma := \frac{w}{wo}$ $\sigma = 0.042$ usec

Gaussian filter transform function $FF(t) := \frac{1}{\sqrt{2 \cdot \pi \cdot \sigma^2}} \cdot \exp\left(\frac{-t^2}{2 \cdot \sigma^2}\right)$

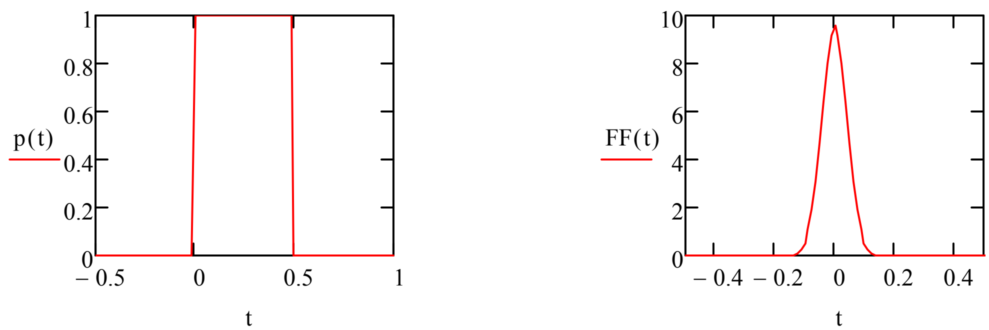

Figure 29: Basic 1090ES rectangular chip width and pulse shaping function

Convolve rectangular pulse with Gausian filter for shaped pulse $pf(t) := \int_{-\infty}^{\infty} p(\zeta) \cdot FF(\zeta - t)\, d\zeta$

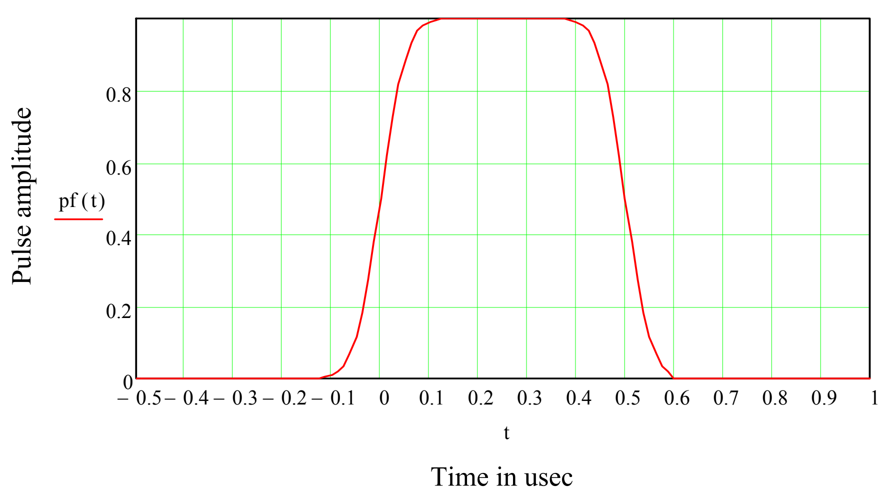

Figure 30: Basic 1090ES pulse shape

Pulses in the binary one or zero coded chip positions are shown in Figure 31.

$$pf(t) := \int_{-\infty}^{\infty} p(\zeta)\cdot FF(\zeta - t)\, d\zeta \qquad pp(t) := \Phi(t + w) - \Phi(t - 2\cdot w) \qquad t := -0.5, -0.5 + \iota .. 2$$

$$s1(t,n) := pf(t - n)\cdot pp(t - n) \qquad s0(t,n) := s1(t, n + w) \qquad n := 0$$

$$n = 0 \quad s = 80 \quad w = 0.5 \quad wo = 12$$

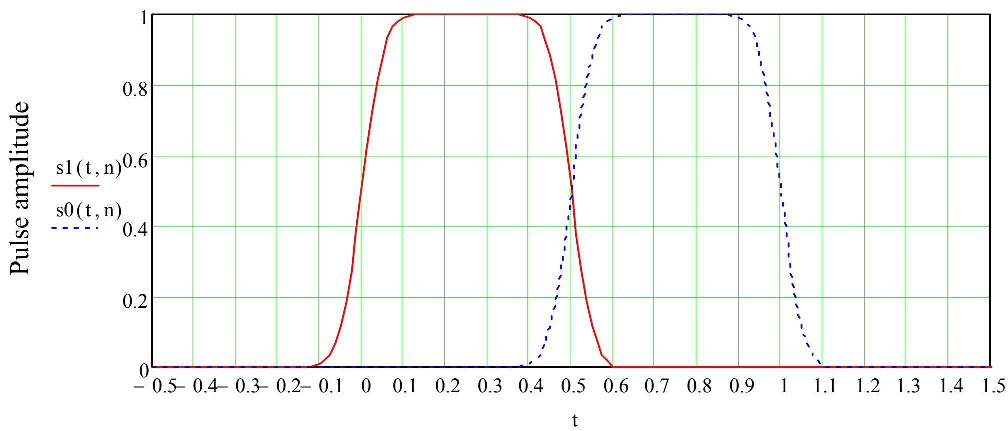

Figure 31: Pulses for chip positions one and zero

The 1090ES message four bit preamble is in Figure 32.

Synch preamble $\quad Syn(t) := s1(t,0) + s1(t,1) + s0(t,3) + s0(t,4)$

$$s = 80 \quad w = 0.5 \quad wo = 12$$

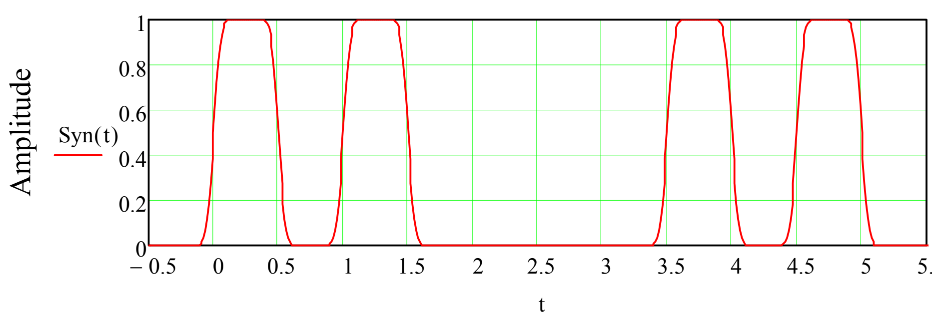

Figure 32: 1090ES message preamble pulse pattern

3.1.2.3.2 Modeled message waveform with horizontal multipath overlap examples

The program simulating the 112 bit 1090ES message with a random distribution of one and zero encoded bits is given below as Smb. The total preamble plus this payload message is Sm. A delayed multipath replica of this message reduced in amplitude by a factor, Mr, at relative phase, γ, is combined as C.

Synch preamble length in usec $dpl := 8$ usec

Modulation sequence,A(n), for random bit message payload $N := Nm \quad N = 112$

$$A := \begin{array}{|l} \text{for } n \in 1..N \\ \quad \begin{array}{|l} b_n \leftarrow rnd(1) \\ A_n \leftarrow if(b_n < 0.5, 0, 1) \end{array} \\ \text{return } A \end{array} \qquad n := 1..N \qquad A(n) := A_n$$

Random message payload bit pattern $Smb(t) := \sum_{n=0}^{N} if(A(n) > 0.5, s1(t,n), s0(t,n))$

Combined synch and payload $Sm(t) := if(t \le dpl, Syn(t), Smb(t)) \qquad t := -0.5, -0.5 + \iota .. Nm + 5$

Detected amplitude plot of total message with end tail $Sm(t) := if(t > Nm + 1, 0, Sm(t))$

Message envelope in dB $SmdB(t) := 20 \cdot \log(Sm(t))$

Multipath delay $\tau := 1.4$ amplitude $Mr := 0.5$ phase $\gamma := 0$

Composite MP signal $C(t, \tau, Mr) := Sm(t) + Mr \cdot Sm(t - \tau) \qquad CdB(t, \tau, Mr) := 20 \cdot \log(C(t, \tau, Mr))$

Figure 33 shows the clear message in the top of the figure and the resulting overlapped composite message below for an assumed delay of τ = 1.4 usec. Only the first part of the message is shown to preserve chip resolution in the figure. Notice the more complex appearance of the waveform due to amplitude additions when the delayed pulse overlaps the direct message pulse, and filled chip positions when the basic message chip position is empty.

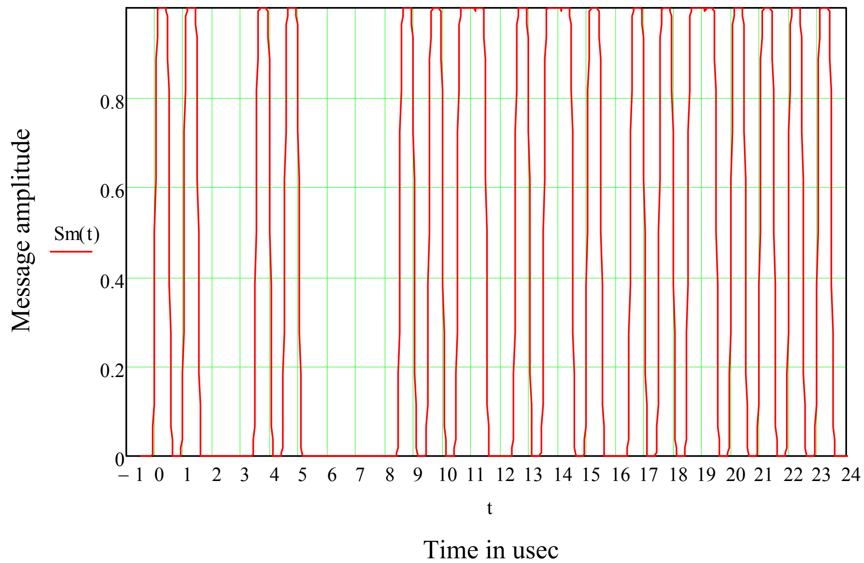

τ = 1.4 usec Mr = 0.5 γ = 0

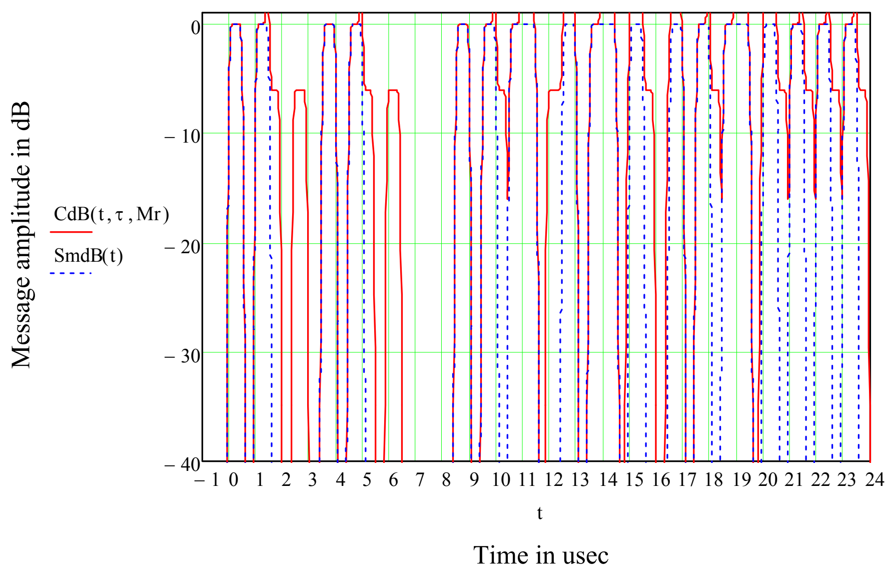

Figure 33: Illustration of first part of 1090ES message with random ones and zeros bits (top), and an example of the same message with an assumed multipath overlap

The time delay is related to path difference next, and the total relative phase including any phase shift on reflection is then given.

For overlapping messages with delay, t us; relative amplitude, M dB; freq off-set, df Hz; and relative phase, f radians

Multipath message envelope delayed by t us $Sd(t,\tau) := Sm(t-\tau)$

For vector addition of RF signals at F MHz: $F := 1090$ MHz

Wavelength (ft) $\lambda := \frac{983.569}{F}$ $\lambda = 0.902$ ft

Propagation velocity $c := 983.569$ ft / usec

A path difference of delta feet produces a time difference in usec given by $\tau(\Delta) := \frac{\Delta}{c}$

Time delay for path delay of one wavelength, or 2p radians $\tau o := \frac{\lambda}{c}$ $\tau o = 9.174\times 10^{-4}$ u sec

Total phase shift of delayed MP $\alpha o(\tau) := 2\cdot\pi\cdot\frac{\tau}{\tau o}$ $\alpha o(\tau o) = 6.283$ rad

Assumed relative phase for phase shift on reflection and differential path delay, ?

Relative phase shift of delayed signal $\alpha(\tau,\gamma) := \alpha o(\tau) + \gamma$

The composite waveform with any Doppler shift is given by D.

If rcvr, xmtr, or reflector are moving at radial velocity, vk kts:

Doppler shift $vk := 100$ kt $v := vk\cdot 1.7$ $v = 170$ ft per sec $\delta f := \frac{v}{\lambda}$ $\delta f = 188.4$ Hz

Relative phase of delayed MP with Doppler $\phi(t,\delta f,\tau,\gamma) := 2\cdot\pi\cdot\delta f\cdot t + \alpha(\tau,\gamma)$ $i := \sqrt{-1}$

Amplitude of delayed message at M dB relative power $Am(M) := 10^{\frac{M}{20}}$

Vector of multipath delayed message $D(t,\tau,M,\gamma) := Sm(t-\tau)\cdot Am(M)\cdot e^{i\cdot\gamma}$

$C(t,\tau,M) := Sm(t) + M\cdot Sm(t-\tau)$ $CdB(t,\tau,M) := 20\cdot\log(C(t,\tau,M))$

Two limiting case examples of vector addition of the multipath message with the direct message are shown in Figure 34 and Figure 35. In both case the time delay is 1 usec, or one bit length, and the reflected amplitude is equal to the direct message amplitude. The assumed phase shift is zero in Figure 34 so the composite amplitude is 6 dB higher when bits overlap, and no-energy bit positions are filled by the overlap. The assumed phase shift is 180 degrees in Figure 35 so the composite amplitude is zero when bits overlap, and again the no-energy bit positions are filled. Since the 1090ES wavelength is less than one foot, the composite message features can be very sensitive to the multipath geometry.

For relative phase effects examination, assume single overlap parameters

$M1 := 0$ $\delta f1 := 10.5$ $\tau 1 := 1.0$ $\gamma 1 := 0$

Total MP delays $Ds(t,\tau,M,\gamma) := D(t,\tau,M,\gamma)$

Vector resultant message plus MP $Ssm(t,\tau,M,\gamma) := Sm(t) + Ds(t,\tau,M,\gamma)$

Amplitude of resultant envelope $Asm(t,\tau,M,\gamma) := |Ssm(t,\tau,M,\gamma)|$

Envelope of resultant in dB $SsM(t,\tau,M,\gamma) := 20 \cdot \log(|Ssm(t,\tau,M,\gamma)|)$

Multipath level $M1 = 0$ Multipath delay $\tau 1 = 1$

assumed phase shift $\gamma 1 = 0$ Doppler $\delta f1 = 10.5$

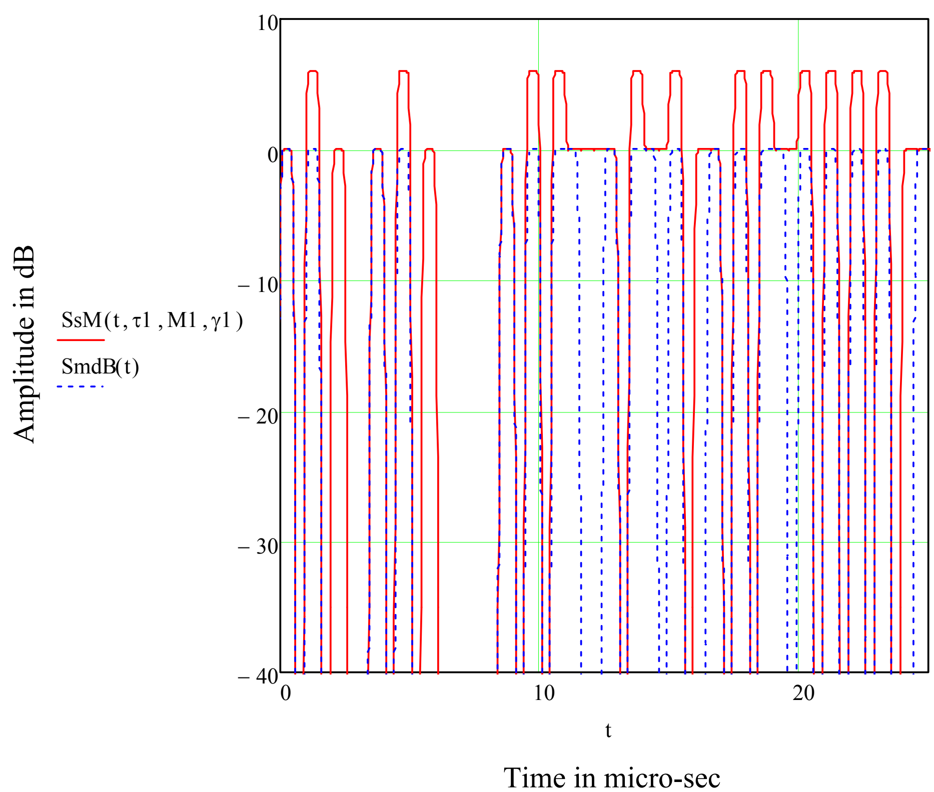

Figure 34: Message with equal amplitude overlap delayed by 1 usec and at zero degrees relative phase angle

Multipath level $M1 = 0$ Multipath delay $\tau1 = 1$

assumed phase shift $\gamma1 = 3.142$ Doppler $\delta f1 = 10.5$

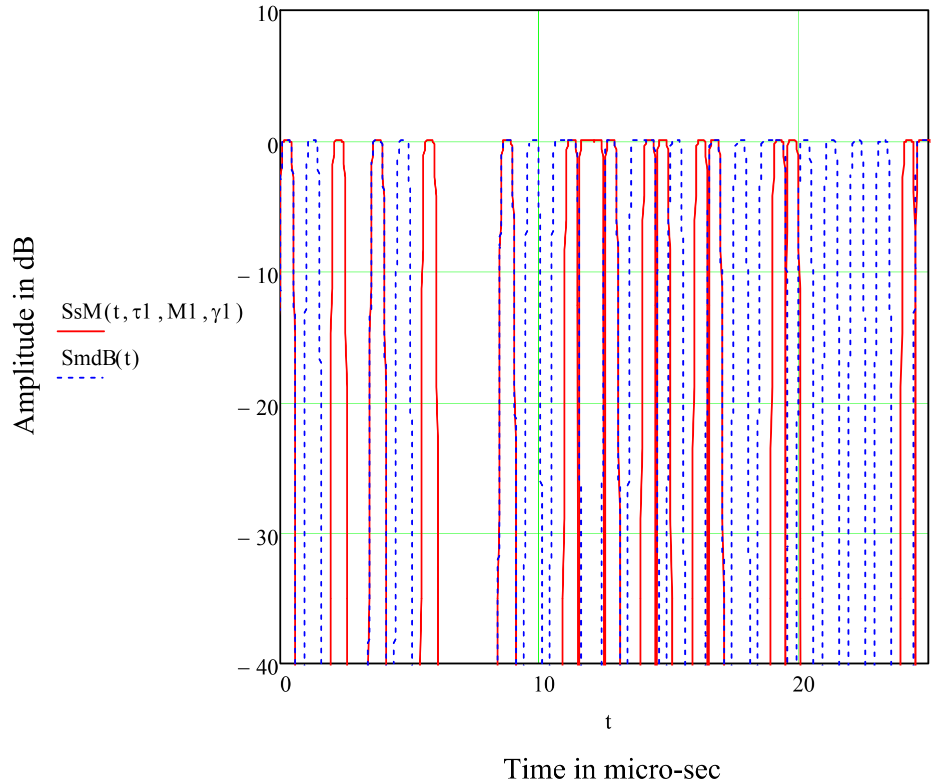

Figure 35: Message with equal amplitude overlap delayed by 1 usec and at 180 degrees relative phase angle

Any scenario of multipath reflectors can be represented in this way, and in theory, any measured composite message detected envelope can be modeled with this tool set. This is illustrated below for a composite message waveform recorded by the WJHTC and shown in Figure 36. Amplitude is logged as the A-to-D converter value. With a receiver MTL = -83 dBm and a 10 dB SNR for 90% decode probability, the receiver noise level is about -93 dBm. For 3 ADCs/dB, the resulting SNR is about 33 dB. With this SNR = 33 dB and -93 dBm noise level, the received signal level is estimated to be about -60 dBm.

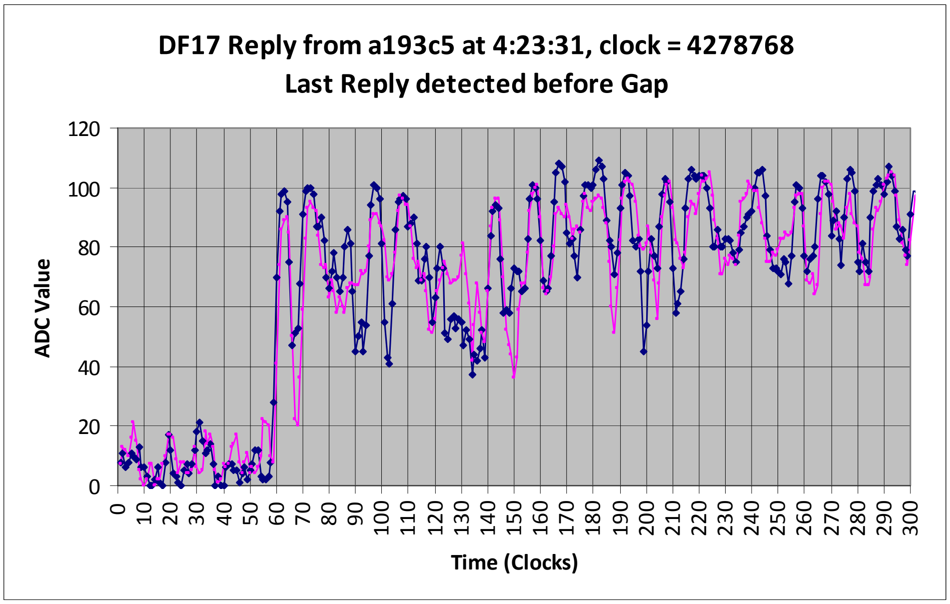

Figure 36: Log video of PHL scenario 6 message with MP overlaps

An empirical approximation to this envelope is based on the following:

To describe a complex overlap case, assume following MP overlap parameters:

Put $m := 4$

$M_1 := -6$ $\tau_1 := 1.4$ $\gamma_1 := \frac{\pi}{2}$ $\delta f_1 := 0$

$M_2 := -12$ $\tau_2 := 2.4$ $\gamma_2 := \pi$ $\delta f_2 := 0$

$M_3 := -18$ $\tau_3 := 0.5$ $\gamma_3 := \frac{\pi}{2}$ $\delta f_3 := 100$

$M_4 := -20$ $\tau_4 := 2.75$ $\gamma_4 := 0$ $\delta f_4 := 500$

Total MP delays $$Dt(t,\tau,M,\gamma) := \sum_{j=1}^{m} D\left(t,\tau_j,M_j,\gamma_j\right)$$

Vector resultant message plus MP $Srm(t,\tau,M,\gamma) := Sm(t) + Dt(t,\tau,M,\gamma)$

Amplitude of resultant envelope $Arm(t,\tau,M,\gamma) := |Srm(t,\tau,M,\gamma)|$

Envelope of resultant in dB $SpM(t,\tau,M,\gamma) := 20\cdot\log(|Srm(t,\tau,M,\gamma)|)$

Composite MP delay in dB $Mt(t,\tau,M,\gamma) := 20\cdot\log(|Dt(t,\tau,M,\gamma)|)$

Figure 37 shows the result and the compound multipath waveform providing this result.

Sample rate $s = 80$ MHz

$$M = \begin{pmatrix} 0 \\ -6 \\ -12 \\ -18 \\ -20 \end{pmatrix} \quad \tau = \begin{pmatrix} 0 \\ 1.4 \\ 2.4 \\ 0.5 \\ 2.75 \end{pmatrix} \quad \gamma = \begin{pmatrix} 0 \\ 1.571 \\ 3.142 \\ 1.571 \\ 0 \end{pmatrix} \quad \delta f = \begin{pmatrix} 0 \\ 0 \\ 0 \\ 100 \\ 500 \end{pmatrix}$$

Signal plus multipath in dB

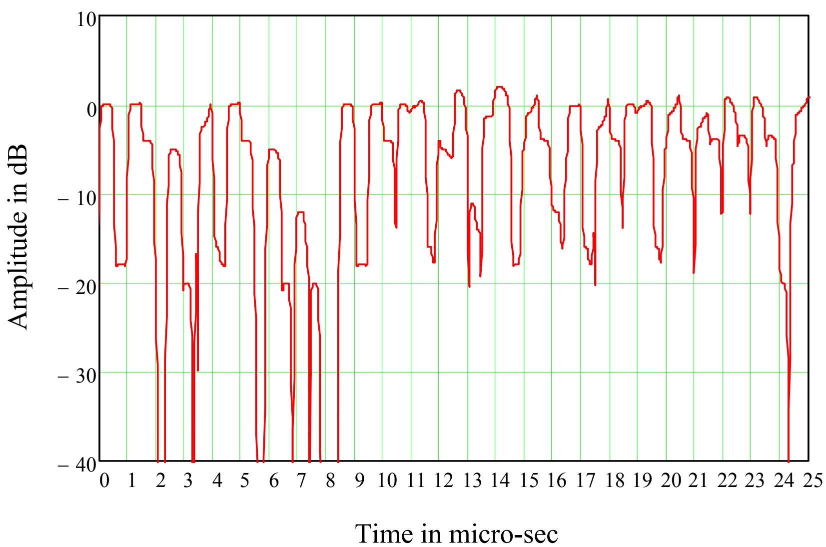

Multipath composite in dB

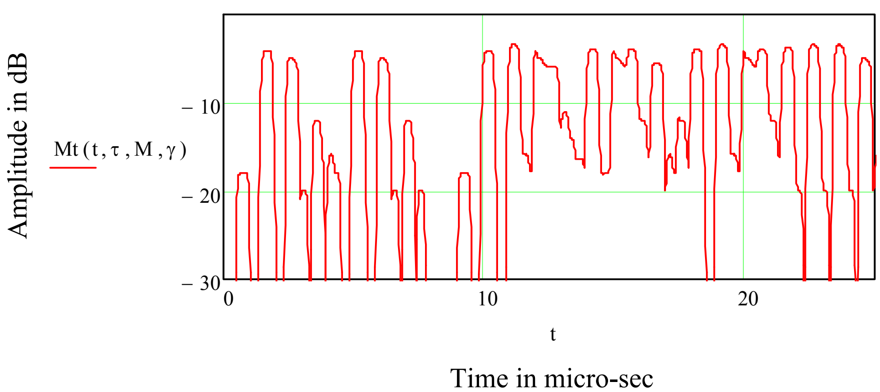

Figure 37: Empirical fit to multiple multipath overlaps measured in PHL scenario 6 (top), and composite of the overlap multipath waveform (bottom)

3.1.2.4 Comparison of theoretical and measured data

Aircraft top and bottom antenna signal levels received from the test van (considered an aircraft top antenna at a height, h = 11.5 feet, in the following discussion) were recorded in recent airport surface tests. The test configuration geometry and power level parameters were used in the exact model to produce the results shown below.

Comparison of these results with test results from the WJHTC report on PHL measurements shows excellent agreement. In Figure 38 notice the exact model for the signal strength of the Top to Bottom configuration is over 20 dB below that expected from the free space propagation loss model at 1.4 NM, and that for the Top to Top antenna configuration is 10 dB below free-space at this range. This matches the measured data from the WJHTC field tests that is shown in Figure 39.

F = 1090 Pw = 160 Ptd = 52 Ld = 0 Gbd(0) = –0 Gtd(0) = –0 MTL = –79

h = 11.5 at = 14.5 ab = 5 δ = 0.1

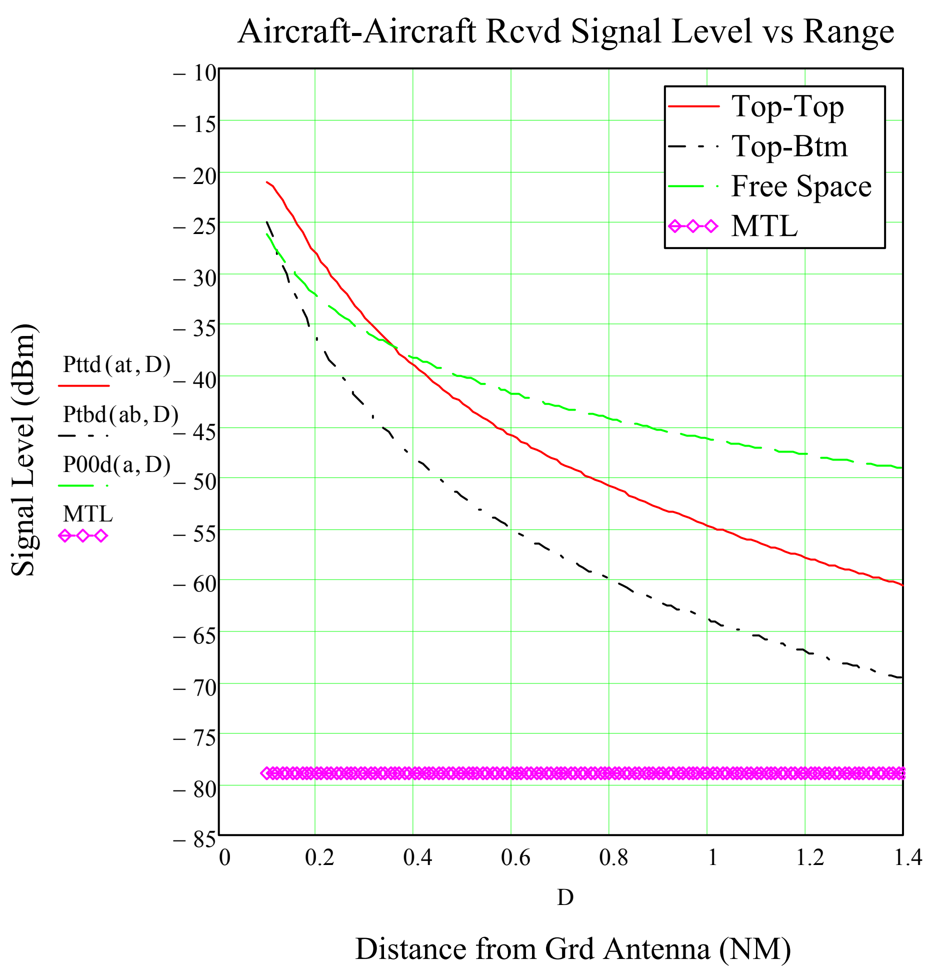

Received signal level (dBm) vs range (NM) for aircraft-aircraft link and indicated parameters. Dashed free-space is for 0 dBi aircraft antenna gains.

Figure 38: Theoretical Signal strength on surface for top-bottom aircraft antennas to test van

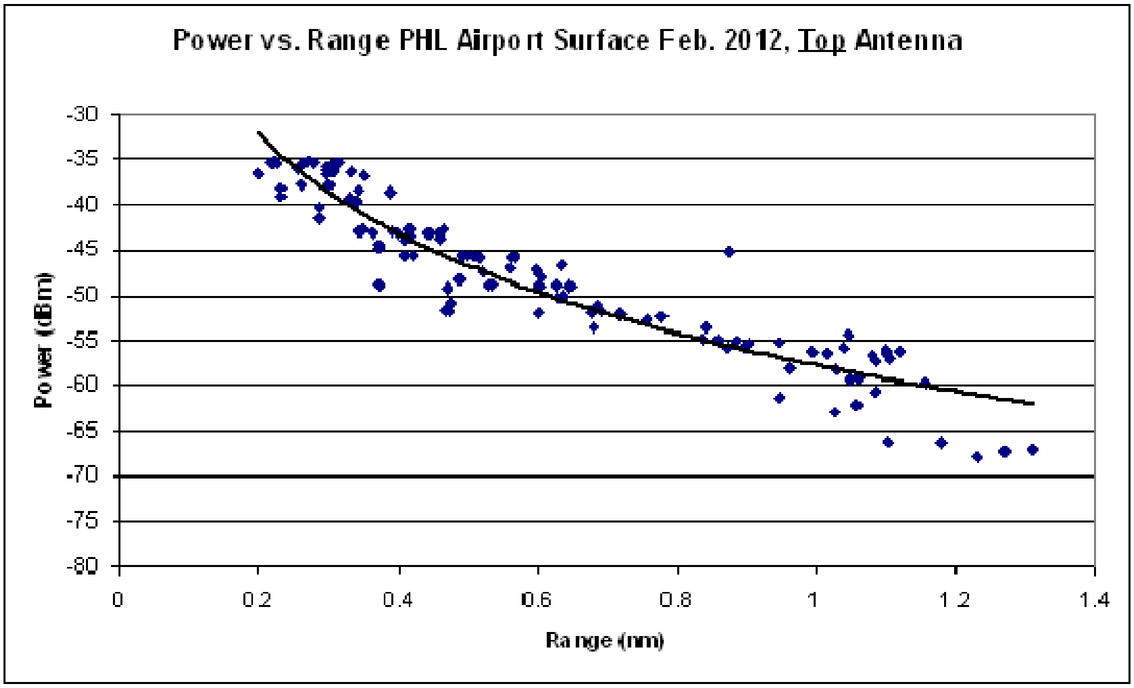

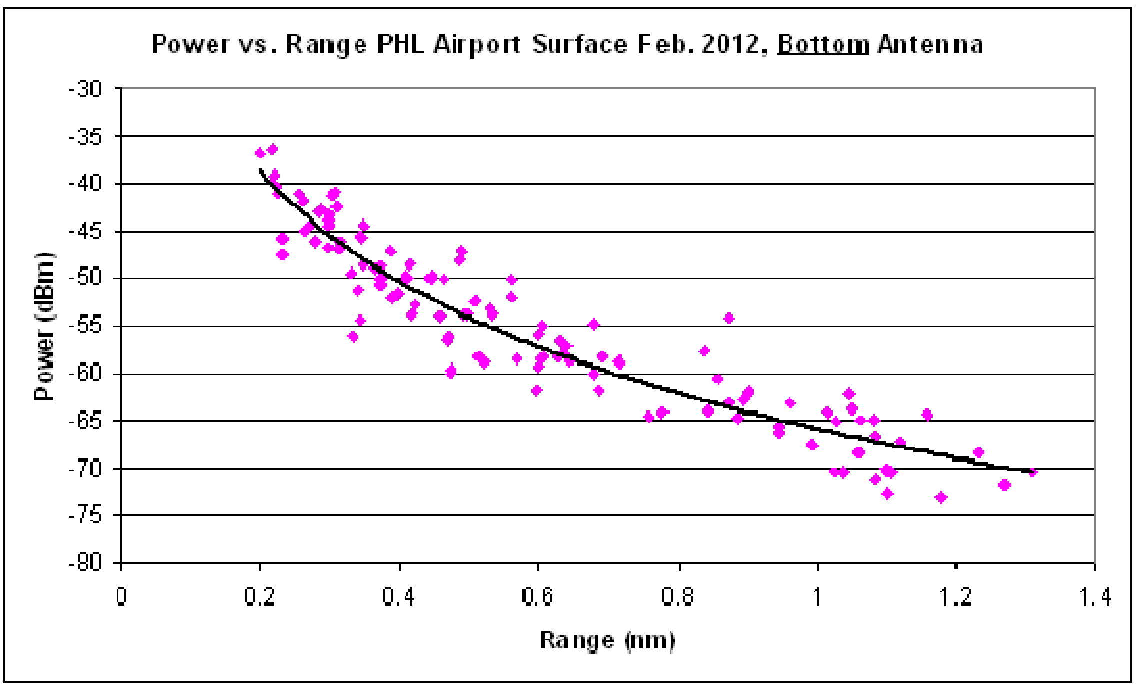

Figure 39: Field Measurements of Power vs. Range on Aircraft Top and Bottom Antenna

3.1.2.5 Summary of Modeling and simulation results

The exact elevation plane reflection model yields airport surface propagation losses significantly greater than those expected on the basis of the usual free space loss model. The simple surface mode propagation loss model is a close approximation to the exact loss model for all but the closest aircraft to aircraft separations with nominal antenna heights. This direct path signal loss is strongly dependent on transmit and receive antenna heights with bottom to bottom aircraft antenna losses typically 10-15 dB below top to top combinations. Available measured signal strength data agree closely with these modeled results. The diffraction loss with any blocking obstruction is dependent on the relative separations of the obstruction and the aircraft, but may be on the order of tens of dB.

Directly received aircraft to aircraft signal levels for large aircraft top to top antennas, however, should still meet expected operational coverage requirements for large airports. Similarly, top to top antennas on small aircraft seem to meet small airport coverage needs. Suitability of combinations of top to bottom, or bottom to bottom coverage may depend upon specific configurations of airports and aircraft of interest.

The higher surface mode propagation loss has a noticeable effect on the S/MP produced by horizontal multipath on the airport surface. As with the comparative effect of the direct surface mode loss, horizontal reflectors on the airport surface degrade the resulting S/MP much more than that expected on the basis of the free space loss model. Specific results are sensitive to size, orientation, height, and proximity of the reflector to either transmit or receive antenna. Direct link fading increases the possibility of horizontal multipath corruption of the message.

The digitally sampled 1090ES message described here affords a flexible way to empirically model measured received messages in multipath conditions for bench test evaluations of receiver decoder performance. The approach is particularly useful for sensitivity examinations.

3.2 Same Link Rebroadcast (SLR) of ADS-B Evaluation

Same link rebroadcast of ADS-B transmissions on the airport surface are examined in this section. Possible improvements in link performance with rebroadcast are: higher received signal levels by use of a relay antenna on the airport surface to off-set the high surface mode aircraft-aircraft propagation loss, and de-correlation of message overlaps due to horizontal multipath or fades due to obstacle shadowing loss relative to the direct link experience.

3.2.1 Performance Improvement Assessment

Expected signal levels provided to surface aircraft by the rebroadcast is examined in the following section. After that, the additional co-channel interference seen by airborne units due to these repeated transmissions is estimated.

3.2.1.1 Airport surface rebroadcast model

Direct and reflected path angular relationships for surface repeater to surface aircraft signal level calculations are shown in Figure 40. Notice that positive elevation angles, θ, from the aircraft antenna at a height, h, correspond to positive lookdown angles from the higher repeater antenna at height, ar. Repeater look-up angles above the horizon are then negative angles in this reference system.

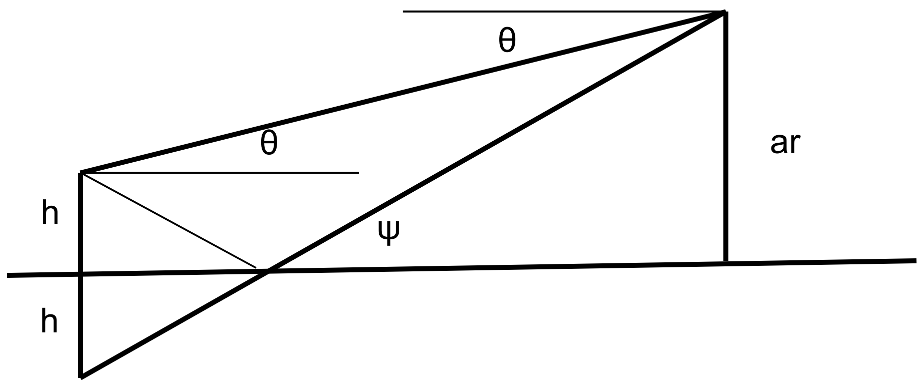

Figure 40: Angular relationships for surface repeater geometry

Two antenna types are modeled for the surface rebroadcast performance assessment: the existing ITT installed dB Systems model 5100A DME antenna, and an assumed single vertical dipole repeater. Both are omni-directional in the horizontal plane. The DME elevation plane antenna pattern is tilted at -4.1 degrees to reduce gain in the elevation plane multi-path look-down direction, and has gain shaping to assure reception of aircraft at higher elevation angles. Since this pattern tilt and shaping is just the opposite from that ideally desired for look-down coverage on the airport surface, and has undesired high gain in the ground-air direction where rebroadcasts contribute to the co-channel interference level, the single dipole is assumed as an alternate repeater intended to mitigate both these problems.

Rebroadcast performance is assessed in terms of the relayed signal level as a function of distance from the repeater antenna when the rebroadcast signal is at the same power level as the basic surface aircraft to surface aircraft transmission over the same distance. Since the link is reciprocal, this is also a measure of reception of the initial transmission from the originating aircraft to the repeater receiver. We assume that all aircraft have a top mounted antenna in order to limit the number of combinations of cases considered. The top mounted aircraft antenna and the two assumed repeater antenna patterns are shown in the surface operation reference coordinate system in Figure 41 along with their gains (in dBi) and beam-widths in degrees.

DME Antenna $Ggod(\theta gp) = 9$ $\theta 3 = 9$ $\theta gp = 4.1$

Dipole Antenna $GRd(\theta pR) = 2.1$ $\theta R = 70$ $\theta pR = 0$ $\phi R = 360$

Top AC Antenna $Gtd(\theta pt) = 4.2$ $\theta pt = 26$

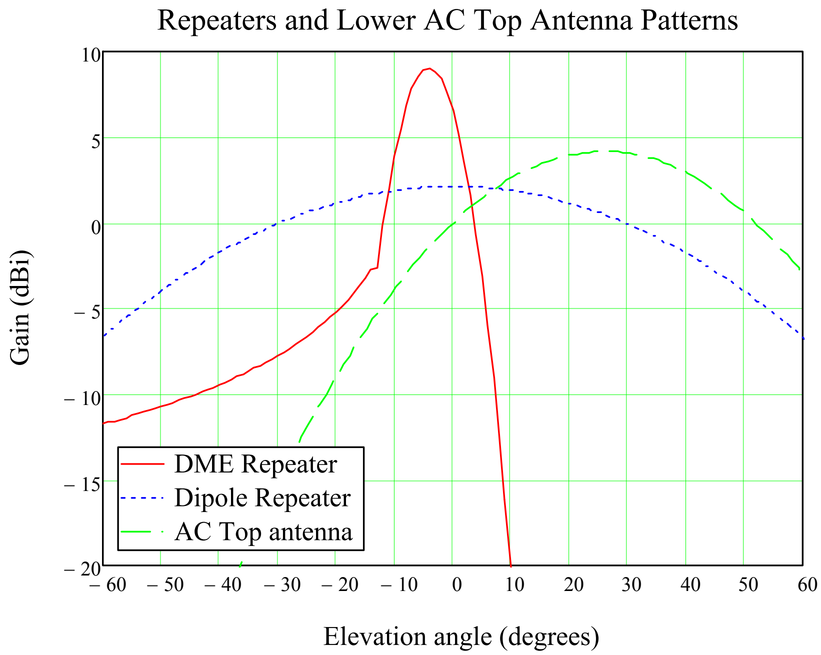

Assumed antenna patterns vs repeater-surface elevation angle for surface reference system (Note positive angle is down for repeater height, ar > AC height, h)

Figure 41: Antenna patterns for surface operation

3.2.1.2 Surface rebroadcast assessment results

The exact propagation loss model and parameters for aircraft-aircraft signal level evaluations described in section 3.1.2.1.1 are assumed for the following rebroadcast assessment. The repeater's transmitter power level and receiver sensitivity are the same as those assumed for aircraft operation. Repeater heights of ar = 47 feet and ar = 66 feet are examined; these are the heights of the ITT installed DME antennas on the PHL airport surface. Performance of each repeater type and height is compared with different combinations of aircraft top antenna heights. Large aircraft antenna heights of 25 feet or 30 feet are assumed; small aircraft top mounted antenna heights of 8 feet or 10 feet are considered.

Although the aircraft-to-repeater and the repeater-to-aircraft links are bi-directional with our reciprocity assumptions, the following discussion is in terms of the down-link repeater-to-aircraft signal levels. These received signal levels for the DME and Dipole repeaters as a function of separation distance, D NM, are shown in Figure 42 for message relays to a small aircraft antenna at a height, h = 8 feet, from repeater heights, ar = 47 feet. The direct small aircraft-to-small aircraft link (for heights h = 8 feet and a = 10 feet) is shown for comparison. In this case the DME repeater link is almost 20 dB higher than the direct link for the same separation; the Dipole repeater link margin is about 15 dB.

$F = 1090$ $Pw = 125$ $Ptd = 51$ $PRd = 51$ $\lambda = 0.9$ $MTL = -79$

DME Antenna $Ggod(\theta gp) = 9$ $\theta 3 = 9$ $\theta gp = 4.1$ Top AC Antenna $Gtd(-\theta pb) = 4.2$

Dipole Antenna $GRd(\theta pR) = 2.1$ $\theta R = 70$ $\theta pR = 0$ $\phi R = 360$

$a = 10$ $h = 8$ $ar = 47$ $\delta = 0.1$ $Ggod(0) = 6.6$ $GRd(0) = 2.1$ $Gtd(0) = -0$

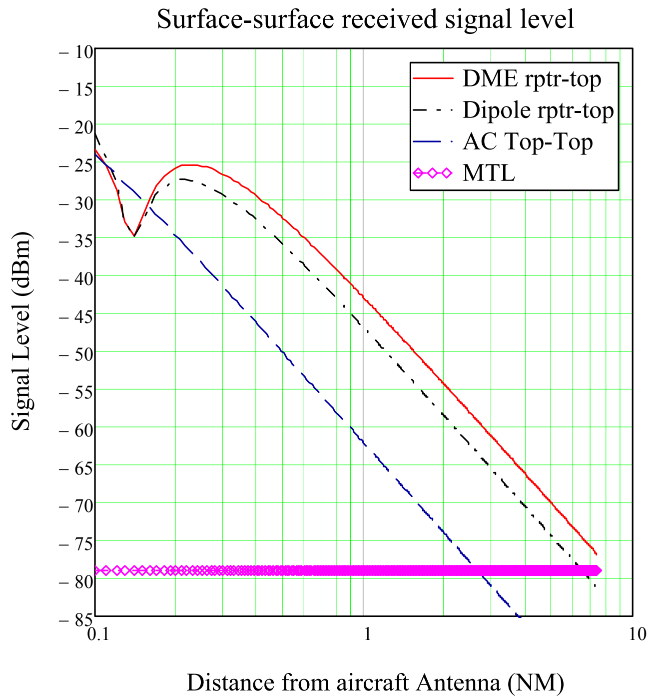

Received signal level (dBm) vs surface distance (NM) for aircraft-aircraft, aircraft to DME repeater, and aircraft to Dipole repeater

Figure 42: Rebroadcast signal levels for DME and Dipole antennas at height, ar = 47 feet to aircraft top antenna height, h = 8 feet. Aircraft-aircraft top antennas at heights, h = 8 feet and a = 10 feet shown for comparison.

Figure 43 is a similar plot for the higher assumed repeater height of ar = 66 feet combined with the small aircraft case. Comparison of the signal levels for these two cases at a nominal distance of D = 1 NM shows the higher repeater height has no effect on the dipole performance, but improves the DME relayed signal level by about 3 dB due to the slope of the gain cut-off angle dependence.

DME Antenna $Ggod(\theta gp) = 9$ $\theta 3 = 9$ $\theta gp = 4.1$ Top AC Antenna $Gtd(-\theta pb) = 4.2$

Dipole Antenna $GRd(\theta pR) = 2.1$ $\theta R = 70$ $\theta pR = 0$ $\phi R = 360$

$a = 10$ $h = 8$ $ar = 66$ $\delta = 0.1$ $Ggod(0) = 6.6$ $GRd(0) = 2.1$ $Gtd(0) = -0$

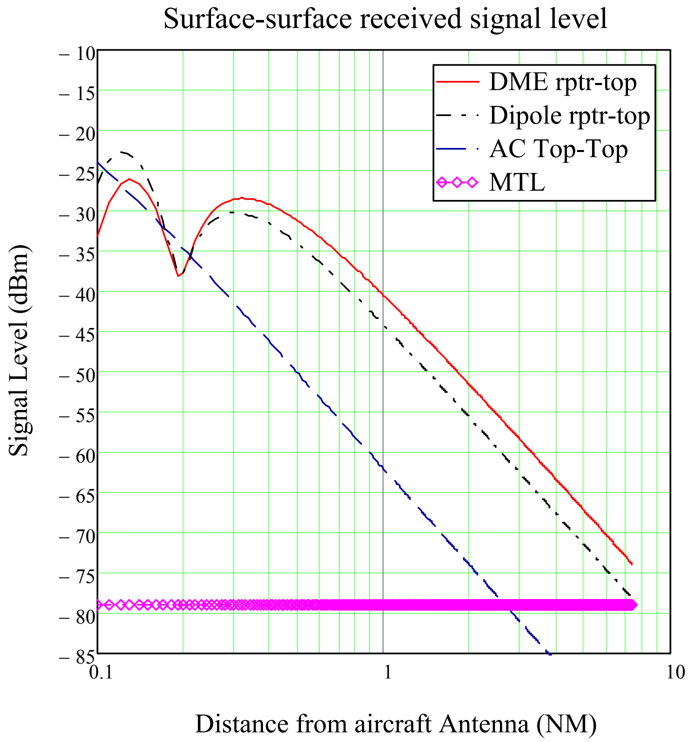

Received signal level (dBm) vs surface distance (NM) for aircraft-aircraft, aircraft to DME repeater, and aircraft to Dipole repeater

Figure 43: Rebroadcast signal levels for DME and Dipole antennas at height, ar = 66 feet to aircraft top antenna height, h = 8 feet. Aircraft-aircraft top antennas at heights, h = 8 feet and a = 10 feet shown for comparison.

Rebroadcast signal strengths for alternate relay antennas at a height of 66 feet are shown in Figure 44 in comparison to the direct link reference for a large aircraft (a = 30 feet) to small aircraft (h = 8 feet) surface to surface pair.

F = 1090 Pw = 125 Ptd = 51 PRd = 51 λ = 0.9 MTL = −79

DME Antenna Ggod(θgp) = 9 θ3 = 9 θgp = 4.1 Top AC Antenna Gtd(−θpb) = 4.2

Dipole Antenna GRd(θpR) = 2.1 θR = 70 θpR = 0 ϕR = 360

a = 30 h = 8 ar = 66 δ = 0.1 Ggod(0) = 6.6 GRd(0) = 2.1 Gtd(0) = −0

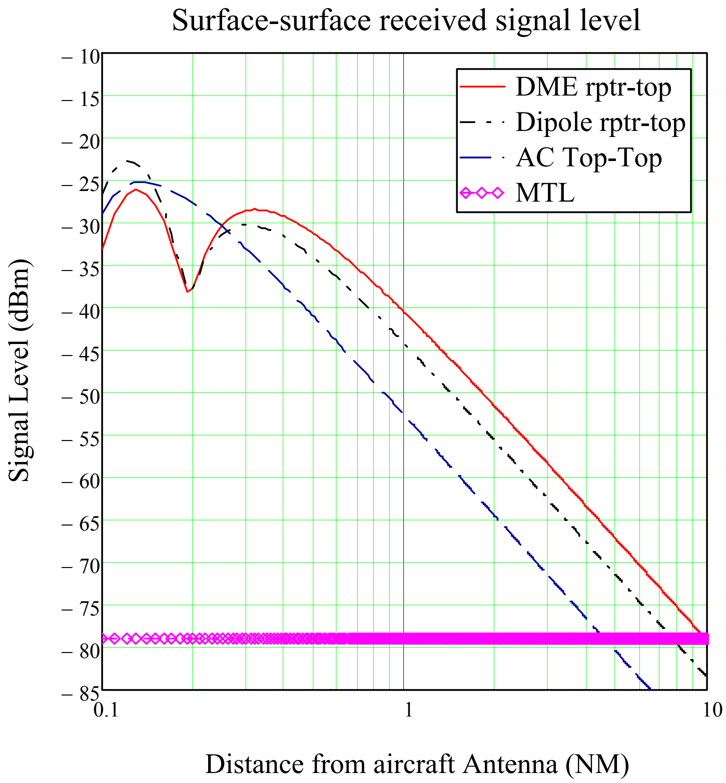

Received signal level (dBm) vs surface distance (NM) for aircraft-aircraft, aircraft to DME repeater, and aircraft to Dipole repeater

Figure 44: Rebroadcast signal levels for DME and Dipole antennas at height, ar = 66 feet to aircraft top antenna height, h = 8 feet. Aircraft-aircraft top antennas at heights, h = 8 feet and a = 30 feet shown for comparison.

The same dependence is shown in Figure 45 for a large aircraft to large aircraft pair. The null structure occurring at shorter distances is due to the higher aircraft top antenna heights but the minima in these instances are still well above the receiver MTL.

F = 1090 Pw = 125 Ptd = 51 PRd = 51 λ = 0.9 MTL = −79

DME Antenna Ggod(θgp) = 9 θ3 = 9 θgp = 4.1 Top AC Antenna Gtd(−θpb) = 4.2

Dipole Antenna GRd(θpR) = 2.1 θR = 70 θpR = 0 ϕR = 360

a = 30 h = 25 ar = 66 δ = 0.1 Ggod(0) = 6.6 GRd(0) = 2.1 Gtd(0) = −0

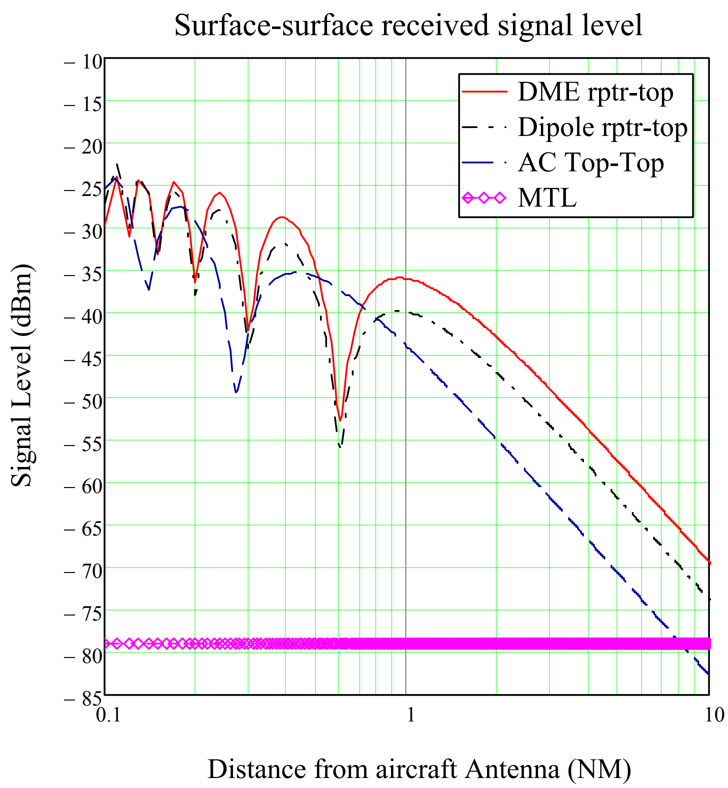

Received signal level (dBm) vs surface distance (NM) for aircraft-aircraft, aircraft to DME repeater, and aircraft to Dipole repeater

Figure 45: Rebroadcast signal levels for DME and Dipole antennas at height, ar = 66 feet to aircraft top antenna height, h = 25 feet. Aircraft-aircraft top antennas at heights, h = 25 feet and a = 30 feet shown for comparison.

The last two rebroadcast examples are for surface vehicles; Figure 46 is for a 1090ES equipped vehicle, and Figure 47 is for a UAT equipped vehicle. Alternate repeaters are at a height of 47 feet, and the assumed vehicle height is 5 feet in both. The 1090ES transmit power is 16 w and the UAT transmit power is 8 w. The direct link reference in both figures is the surface vehicle to small aircraft height of 8 feet. Comparison of the two figures shows the MTL limited range for UAT for these assumptions is twice the 1090ES range.

F = 1090 Pw = 16 Ptd = 42 PRd = 42 $\lambda = 0.9$ MTL = −79

DME Antenna $Ggod(\theta gp) = 9$ $\theta 3 = 9$ $\theta gp = 4.1$ Top AC Antenna $Gtd(-\theta pb) = 4.2$

Dipole Antenna $GRd(\theta pR) = 2.1$ $\theta R = 70$ $\theta pR = 0$ $\phi R = 360$

a = 8 h = 5 ar = 47 $\delta = 0.1$ Ggod(0) = 6.6 GRd(0) = 2.1 Gtd(0) = −0

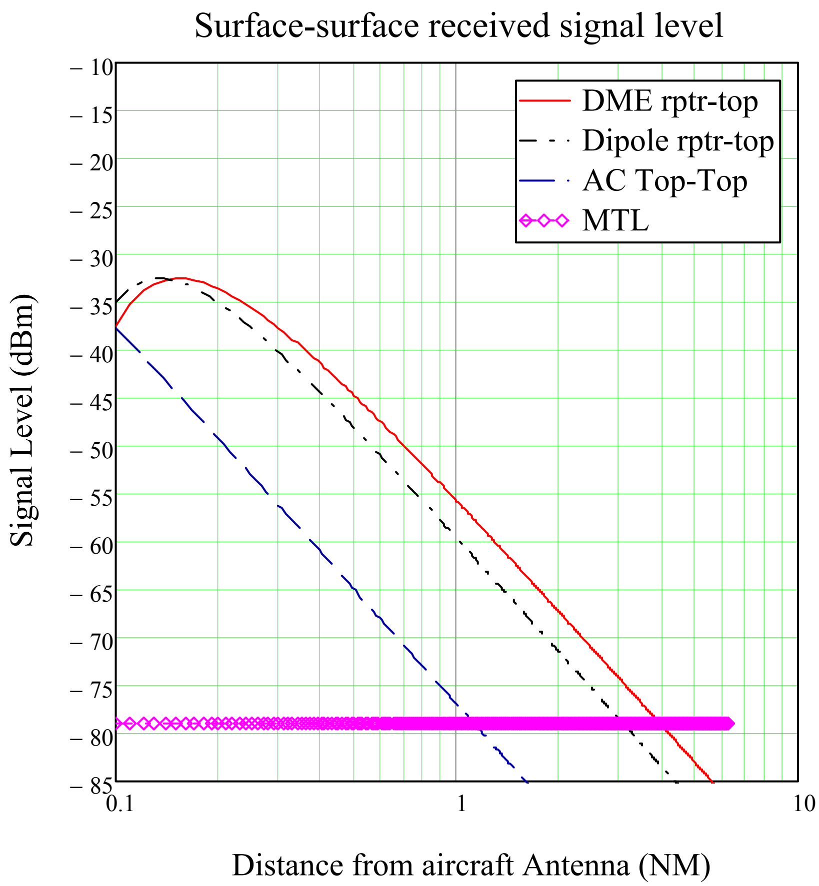

Figure 46: Rebroadcast 1090ES signal levels for DME and Dipole antennas at height, ar = 47 feet to surface vehicle antenna height, h = 5 feet. Surface vehicle-aircraft top antenna at heights, h = 5 feet and a = 8 feet shown for comparison.

F = 978 Pw = 8 Ptd = 39 PRd = 39 λ = 1 MTL = −93

DME Antenna Ggod(θgp) = 8.6 θ3 = 10.1 θgp = 4.6 Top AC Antenna Gtd(−θpb) = 4.2

Dipole Antenna GRd(θpR) = 2.1 θR = 70 θpR = 0 ϕR = 360

a = 8 h = 5 ar = 47 δ = 0.1 Ggod(0) = 6.1 GRd(0) = 2.1 Gtd(0) = −0

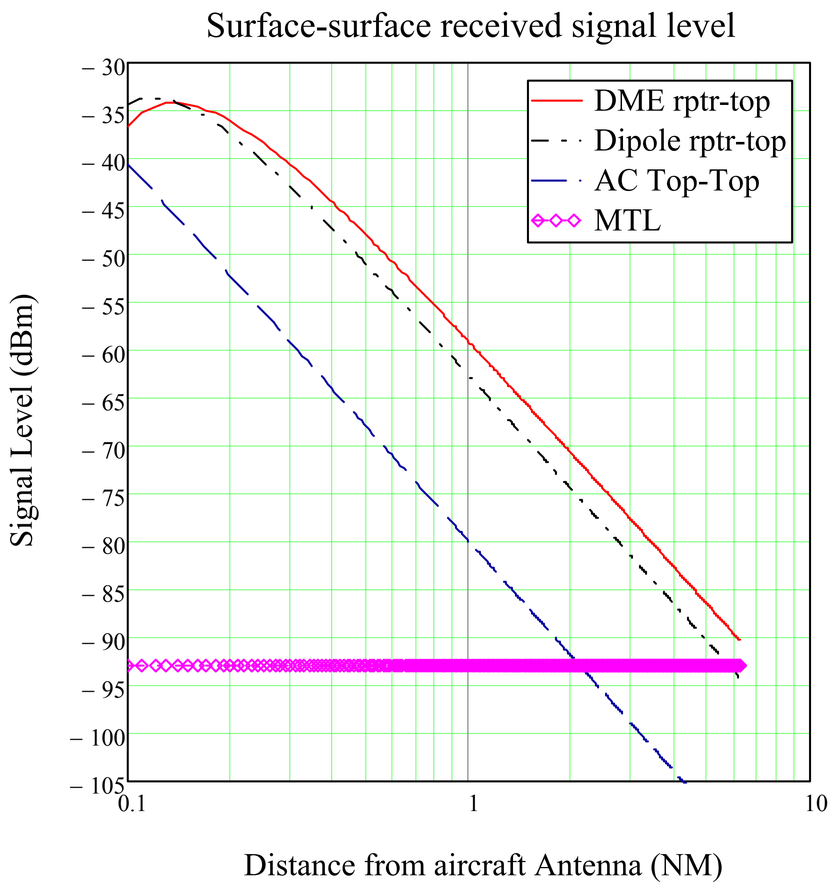

Figure 47: Rebroadcast UAT signal levels for DME and Dipole antennas at height, ar = 47 feet to surface vehicle antenna height, h = 5 feet. Surface vehicle-aircraft top antenna at heights, h = 5 feet and a = 8 feet shown for comparison.

As previously mentioned, the exact propagation model has been used in all these examples. Figure 48 compares the results for this exact model for an assumed DME height of 47 feet and top antenna height of 8 feet with those obtained with the simpler free space and surface mode models and antenna gains of 0 dBi. Other than the higher DME gain off-set, the simpler surface mode model is in close agreement with the exact model. This result should be useful in any future examinations of surface to surface operations.

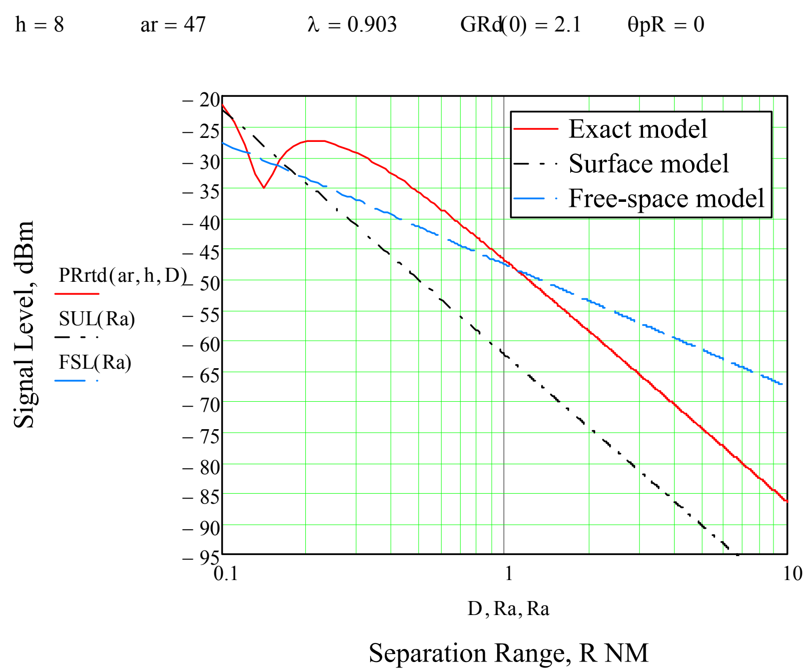

Comparison of exact with approximate propagation models

Figure 48: Exact model rebroadcast signal levels for DME antenna at height, ar = 47 feet to aircraft top antenna height, h = 8 feet compared with surface and free-space models with 0 dBi antenna gains.

3.2.2 Spectrum impact assessment

3.2.2.1 Analysis of Spectrum Impacts of SLR

An evaluation of an estimated worst case airport surface scenario was done to determine the number of messages to re-broadcast for each of the two data links. These results were then compared to the number of messages that would be sent out by the ground infrastructure for ADS-R alone. TIS-B messages were not considered, as it was assumed that all aircraft would be equipped with ADS-B.

A worst case surface scenario was determined by using an estimate of a maximum at an airport today and scaling it up to reflect future growth, resulting in the following:

- 100 1090 ES-equipped aircraft on the movement area
- 40 1090 ES-equipped aircraft at the gate (off the movement area)
- 20 UAT-equipped aircraft anywhere (UAT transmission rate is independent)
- 25 vehicles (equipped with ADS-B and transmitting)
- 15 airborne 1090 ES-equipped aircraft in the SV (below 3000 feet and within 5 miles)

This scenario encompasses 200 ADS-B active transmitters and is used for estimating the re-broadcast rates for both 1090 ES and UAT.

3.2.2.1.1 1090 ES SLR Impacts

The following ES messages are transmitted on the surface:

- Moving A/V
  - Position – 2/s
  - Aircraft ID – 0.2/s
  - Operational Status – 1.25/s (worst case)
  - Aircraft Status – 0.2/s (this does not have to be re-broadcast, as the only information is Mode A code, which is not needed by other aircraft)
- Stationary A/V
  - Position – 0.2/s
  - Aircraft ID – 0.1/s
  - Operational Status – 0.2/s
  - Aircraft Status – 0.2/s (this does not have to be re-broadcast, as the only information is Mode A code, which is not needed by other aircraft)
- Airborne Aircraft in Surface SV
  - Position – 2/s
  - Velocity – 2/s
  - Aircraft ID – 0.2/s
  - Operational Status – 1.25/s (worst case)
  - Aircraft Status – 0.2/s (this does not have to be re-broadcast, as the only information is Mode A code, which is not needed by other aircraft)

The total average number of 1090 ES messages transmitted by an A/V on the airport surface is 3.45/s (worst case) for a moving A/V on the surface and 0.5 for a stationary A/V. For airborne aircraft in the service volume, the number is 5.45/s. We assume that all of these messages are received by the ground infrastructure.

Table 5 below summarizes the total transmissions that would be made by a ground transmitter re-broadcasting every 1090 ES message from each A/V in the Surface SV.

Table 5: SLR Transmissions anticipated for Surface Traffic

A/V Type	Number	Squitters/Second	Total
Moving on Surface	100	3.45	345
Stationary on Surface	40	0.5	20
Airborne	15	5.45	81.75
Moving Vehicles	13	3.45	44.85
Stationary Vehicles	12	0.5	6.0

The surface moving aircraft in the scenario thus transmit 345 squitters/second (3.45*100), while the stationary aircraft transmit 20 squitters/second 0.5*40), for a total of 365 squitters to be re-broadcast each second. The airborne aircraft add around another 82/s (5.45*15). If we assume that the vehicles are also equipped with 1090 ES and that half of them are stationary, then the vehicles add around 51 (13*3.45+12*0.5) more squitters/second and the total number of 1090 ES messages that are transmitted by all of the A/Vs in the scenario is around 500/second.

If we assume that all of these are re-broadcast, then the consequences are the following:

- This number of 1090 ES transmissions would exceed the duty cycle limitation of 6 % cited in the SBS Air Interface Control Document.
- It also would violate the FAA Spectrum requirement that no aircraft be exposed to more than 1000 ADS-B transmissions per second, when taken in conjunction with the original aircraft transmissions.
- Currently, the only 1090 ES ADS-B transmissions the ground transmitter is required to make are for ADS-R for the 20 UAT equipped aircraft, which amounts to 80 transmissions per second (10*4). Therefore, for the worst case scenario, implementing the re-broadcast of all 1090 ES to resolve the multipath issue would mean increasing the number of transmissions by the ground from 80/s to around 580/s.
- Airborne traffic should be received without increased surface attenuation or horizontal multi-path problems and not require rebroadcast. However, reducing the rebroadcast of these squitters does not substantially improve the spectrum congestion as these messages are only 16 percent of the total rebroadcast count for this scenario.

Now we attempt to reduce the transmissions to the point where the two-second surface position update requirement can still be met. A simple implementation strategy for this involves eliminating one position re-transmission per moving A/V per second, or 128 messages less each second. This still leaves one position transmission per second, which should be sufficient to meet the two second requirement. Under this assumption, the total number of 1090 ES messages that are re-transmitted would be reduced to around 370/s. This number would meet the duty cycle requirement, would not violate the 1,000/s spectrum limitation (barely), but would still increase the 1090 ES ground transmissions from 80 UAT ADS-R transmissions to 450 total per second.

3.2.2.1.2 UAT SLR Impacts

Using the same worst case scenario, the effect on UAT of re-broadcasting all UAT messages transmitted by UAT-equipped aircraft/vehicles is analyzed in this section.

UAT-equipped A/Vs transmit UAT messages at a once per second rate, so the re-broadcast of UAT messages on the surface would amount to 20/s for the twenty UAT aircraft in the Surface SV. This number would be in addition to the ADS-R transmissions over UAT that are currently required for the 1090 ES A/Vs in the SV.

The ADS-R transmission load in this scenario is two UAT messages per 1090 ES aircraft per second (from the SBS Air Interface Control Document), or 2*180 = 360/s. Adding the 20/s for re-broadcast results in a total load of 380/s. This number results in a duty cycle of around 13%, just over the 12.5% cited in the SBS Air Interface Control Document. If the ADS-R function does not transmit two UAT messages per second for stationary 1090 ES A/Vs, then this number is reduced somewhat, but is still near the duty cycle limit. However, if the ADS-R function transmits only one UAT message per second for all 1090 ES aircraft, then the total UAT transmission rate from the ground is 200 per second, which meets the duty cycle limitation.

3.2.2.2 Ground repeater interference model

The disadvantage of surface rebroadcast is that any radiation at elevation angles above the horizon contributes to the co-channel interference exposure of airborne receivers within detection range of the repeater. This potential for undesired airborne reception of rebroadcast messages is now evaluated for the alternate repeater antenna choices. Direct and reflected path angular relationships for ground to air signal level calculations are shown in Figure 49. Notice that positive elevation angles, θ, from the lower ground repeater site at a height, ar, correspond to positive lookdown angles from the higher airborne aircraft at altitude, A.

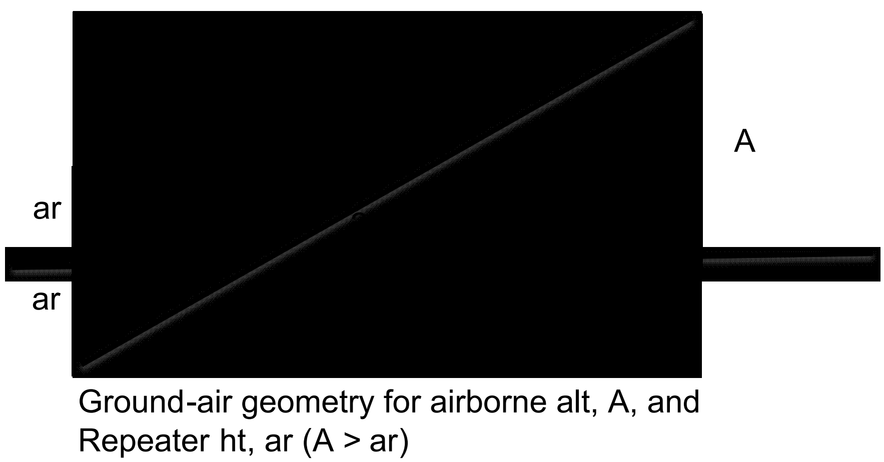

Figure 49: Angular relationships for ground-air geometry

The relevant repeater and bottom mounted airborne aircraft antenna elevation plane patterns used in these ground-air calculations are shown in this reference coordinate system in Figure 50. Although the aircraft antenna is mislabeled in the figure as a top antenna for model convenience, its orientation is correct for our interests.

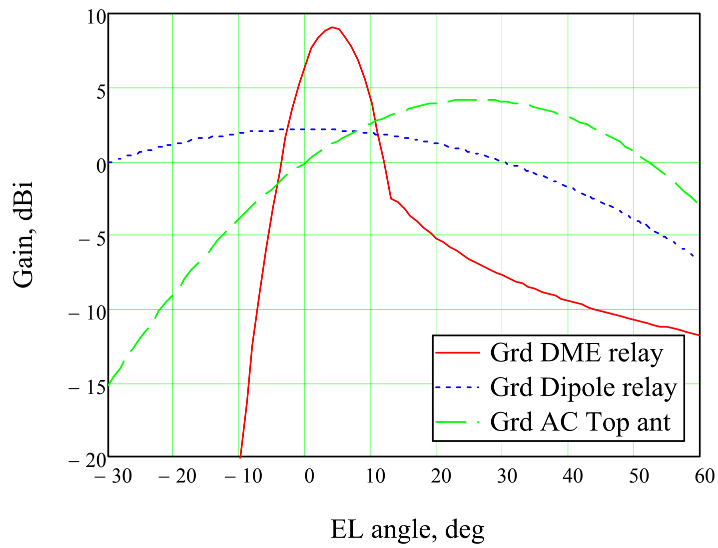

Antenna gains for ground-air signal level calculation (Positive angle up for ar < A)

Figure 50: Antenna patterns for ground-air operation

The question now is how to represent the interference potential of the ground rebroadcast in the most useful way for general evaluation of the issue. Here we employ previous measurements of traffic distributions with altitude summarized in Figure 51. Details are given in the figure, but the results are that the measured maximum altitude is 50,000 feet, the mean (or most likely) altitude is 10,400 feet, and the median altitude is 7,700 feet. Received signal levels at each of these altitudes are shown in the following as a function of distance from the surface repeater under the assumption that the altitude distribution is constant with distance from the airport located repeater.

Altitude distribution of traffic over area of interest given by p(h) where h is altitude in feet/1000. Analytic fit to data from MITRE MTR 95W0000100, STARS System Loads Analysis (and independently measured by WJHTC):

Traffic density fit in altitude For ZNY, put $a := 0.09$ $ph(h) := a \cdot e^{-a \cdot h}$

Cumulative traffic in altitude with LOS limit is then $F(h) := \int_0^h ph(h)\,dh$

Max traffic altitude from fit $hm := 50$ $F(hm) = 0.989$

$$\int_0^h a \cdot e^{-a \cdot h}\,dh \rightarrow \int_0^h 0.09 e^{-0.09 \cdot h}\,dh \rightarrow -1.0 e^{-0.09 \cdot h} + 1.0$$

For flat earth all in view $F(h) := 1 - e^{-a \cdot h}$ Median alt $ho := 7.7$ $F(ho) = 0.5$

Mean or expected altitude $ha := \int_0^{hm} ph(h) \cdot h\,dh$ $ha = 10.4$ $F(ha) = 0.609$

$a = 0.09$ $hm = 50$ $h := 0, 1 .. hm$

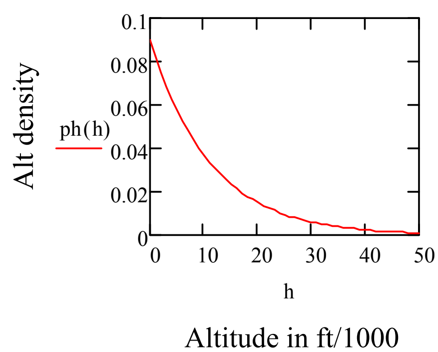

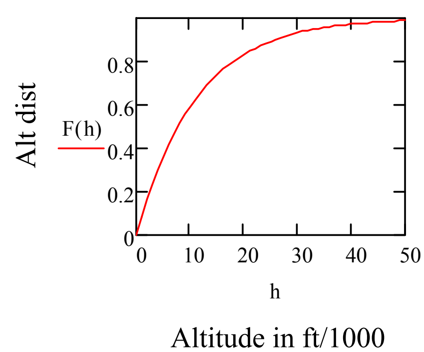

Figure 51: Traffic distribution with altitude

3.2.2.3 Airborne receiver interference level results

Transmit power level and antenna gains are identical with the surface cases already presented – just the coordinate system has changed to represent the ground air geometry of interest now. As with the surface rebroadcast evaluation, both repeater antenna types are compared with the surface aircraft top mounted antenna direct signal level. The plots are shown in terms of the 4/3 earth line of sight limited distance for the selected altitude. Sensitivity of rebroadcast produced interference to the surface repeater height and top mounted aircraft antenna height is illustrated at each probe altitude choice in the following two series of plots. The first series, Figure 52 at 10,400 feet, Figure 53 at 7,700 feet, and Figure 54 at an altitude of 50,000feet , is for the alternate repeater antenna height of ar = 66 feet, and an aircraft antenna height of 30 feet. The second series, Figure 55, Figure 56, and Figure 57, is for the same set of altitudes but for the repeater height of 47 feet and an aircraft height of 10 feet.

F = 1090 Pw = 125 Ptd = 51 PRd = 51 AC Altitude A = 10400 Repeater ht ar = 66

DME Repeater Ggod(θgp) = 9 θ3 = 9 θgp = 4.1 Surface AC ht a = 30

Dipole Repeater GRd(θpR) = 2.1 θR = 70 θpR = 0 ϕR = 360 D := 1, 1.1.. LOS

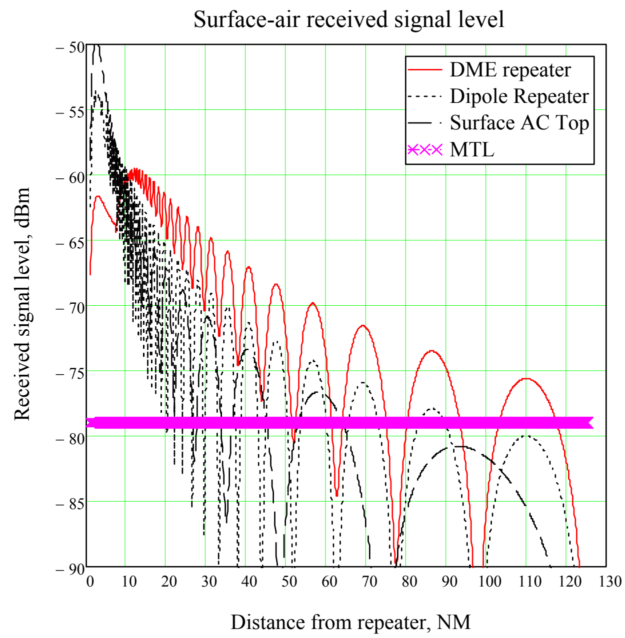

Airborne bottom antenna received signal level from DME and Dipole surface repeater antennas, and from surface aircraft top antenna

Figure 52: Airborne received interference levels from DME repeater, Dipole repeater, and surface aircraft direct. Repeater heights, ar = 66 feet, surface aircraft top antenna height, a = 30 feet, and airborne receiver altitude, A = 10,400 feet.

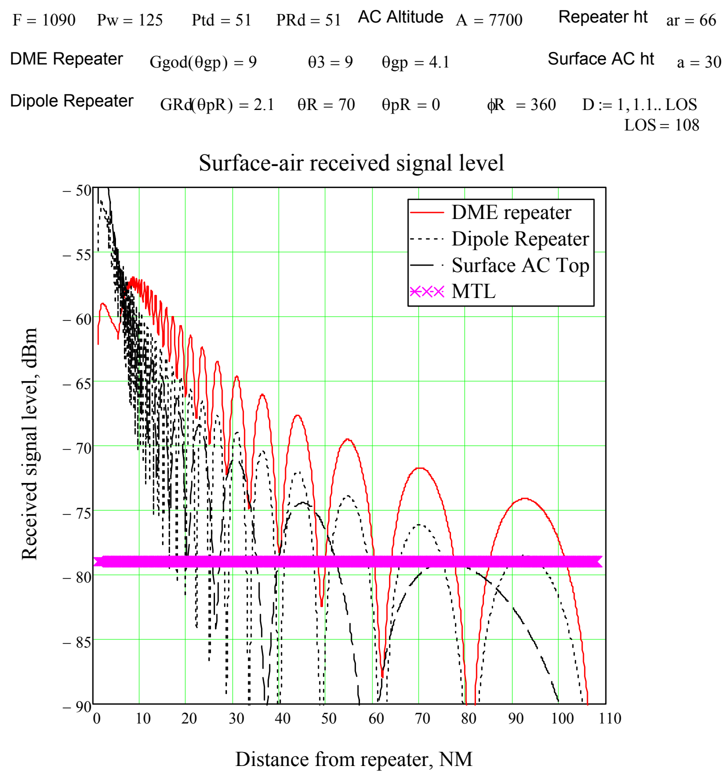

Airborne bottom antenna received signal level from DME and Dipole surface repeater antennas, and from surface aircraft top antenna

Figure 53: Airborne received interference levels from DME repeater, Dipole repeater, and surface aircraft direct. Repeater heights, ar = 66 feet, surface aircraft top antenna height, a = 30 feet, and airborne receiver altitude, A = 7,700 feet.

F = 1090 Pw = 125 Ptd = 51 PRd = 51 AC Altitude A = 50000 Repeater ht ar = 66

DME Repeater Ggod(θgp) = 9 θ3 = 9 θgp = 4.1 Surface AC ht a = 30

Dipole Repeater GRd(θpR) = 2.1 θR = 70 θpR = 0 ϕR = 360 D := 1, 1.1.. LOS
LOS = 275

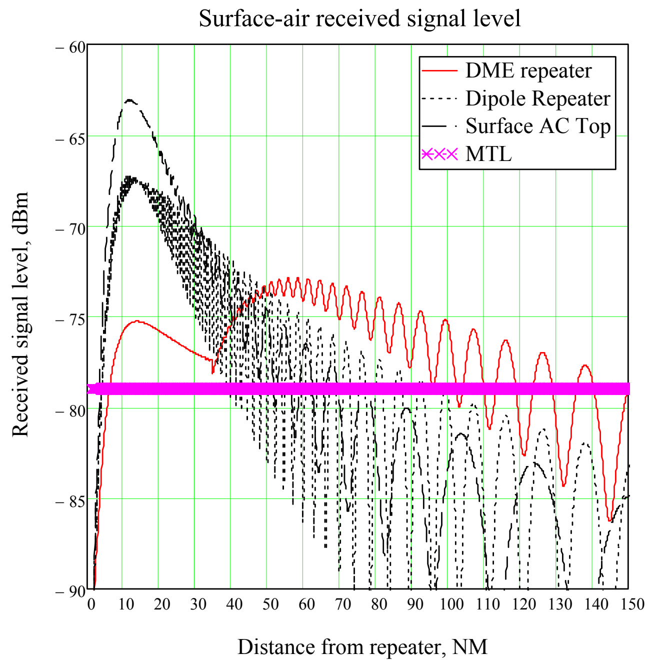

Airborne bottom antenna received signal level from DME and Dipole surface repeater antennas, and from surface aircraft top antenna

Figure 54: Airborne received interference levels from DME repeater, Dipole repeater, and surface aircraft direct. Repeater heights, ar = 66 feet, surface aircraft top antenna height, a = 30 feet, and airborne receiver altitude, A = 50,000 feet.

F = 1090 Pw = 125 Ptd = 51 PRd = 51 AC Altitude A = 10400 Repeater ht ar = 47

DME Repeater Ggod(θgp) = 9 θ3 = 9 θgp = 4.1 Surface AC ht a = 10

Dipole Repeater GRd(θpR) = 2.1 θR = 70 θpR = 0 ϕR = 360 D := 1, 1.1.. LOS

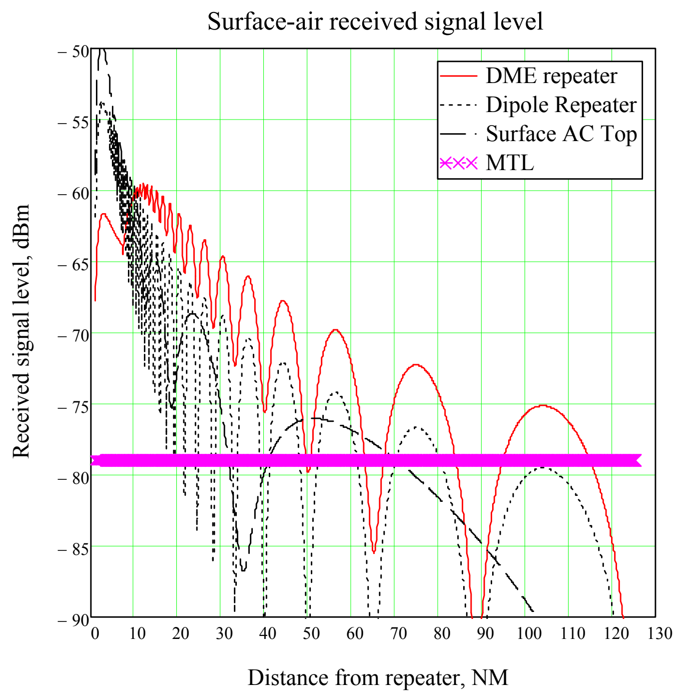

Airborne bottom antenna received signal level from DME and Dipole surface repeater antennas, and from surface aircraft top antenna

Figure 55: Airborne received interference levels from DME repeater, Dipole repeater, and surface aircraft direct. Repeater heights, ar = 47 feet, surface aircraft top antenna height, a = 10 feet, and airborne receiver altitude, A = 10,400 feet.

F = 1090 Pw = 125 Ptd = 51 PRd = 51 AC Altitude A = 7700 Repeater ht ar = 47

DME Repeater Ggod(θgp) = 9 θ3 = 9 θgp = 4.1 Surface AC ht a = 10

Dipole Repeater GRd(θpR) = 2.1 θR = 70 θpR = 0 ϕR = 360 D := 1, 1.1.. LOS
LOS = 108

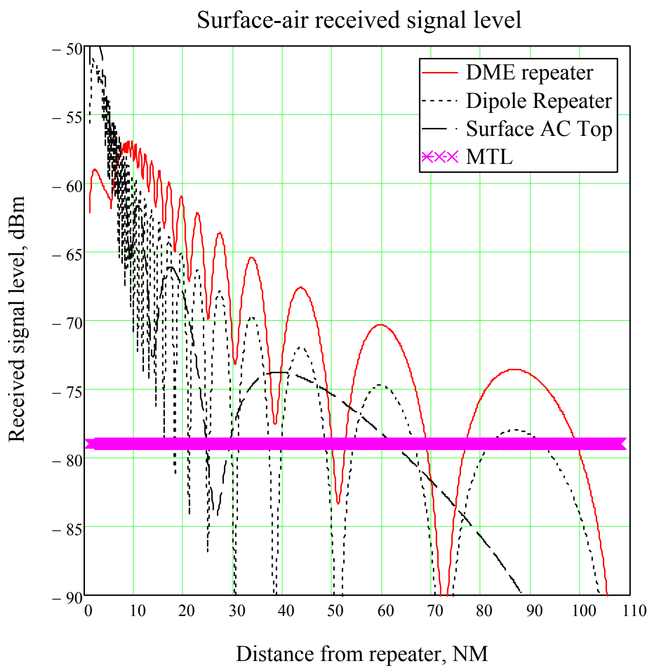

Airborne bottom antenna received signal level from DME and Dipole surface repeater antennas, and from surface aircraft top antenna

Figure 56: Airborne received interference levels from DME repeater, Dipole repeater, and surface aircraft direct. Repeater heights, ar = 47 feet, surface aircraft top antenna height, a = 10 feet, and airborne receiver altitude, A = 7,700 feet.

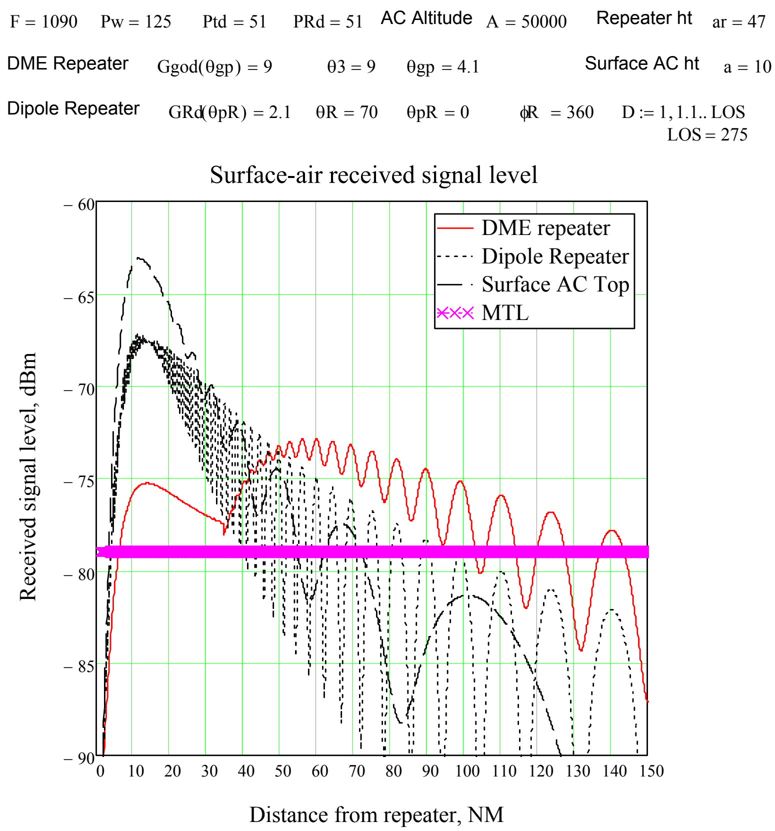

Airborne bottom antenna received signal level from DME and Dipole surface repeater antennas, and from surface aircraft top antenna

Figure 57: Airborne received interference levels from DME repeater, Dipole repeater, and surface aircraft direct. Repeater heights, ar = 47 feet, surface aircraft top antenna height, a = 10 feet, and airborne receiver altitude, A = 50,000 feet.

The final example of SLR impact on co-channel 1090ES interference is Figure 58 showing the effect of rebroadcast of surface vehicle transmissions at the lower power level of 16 watts. This more limited range case is shown for only the median altitude of 10,400 feet and repeater height of 47 feet.

F = 1090 Pw = 16 Ptd = 42 PRd = 42 AC Altitude A = 10400 Repeater ht ar = 47

DME Repeater Ggod(θgp) = 9 θ3 = 9 θgp = 4.1 Surface AC ht a = 8

Dipole Repeater GRd(θpR) = 2.1 θR = 70 θpR = 0 ϕR = 360 D := 1, 1.1.. LOS

LOS = 125

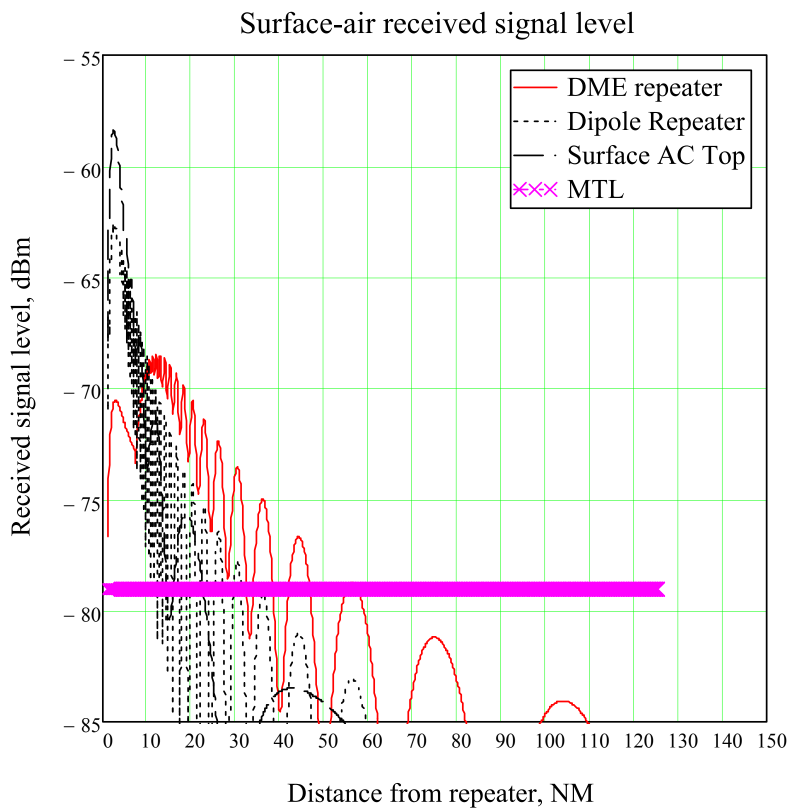

Figure 58: Airborne received interference levels from DME repeater, Dipole repeater, and surface vehicle direct. Repeater heights, ar = 47 feet, surface vehicle antenna height, h = 5 feet, and airborne receiver altitude, A = 10400 feet.

3.2.3 SLR Results Summary

Direct aircraft-aircraft top antenna received signal levels were compared with reception of normalized rebroadcast of these airport surface transmissions. Two repeater heights were assumed and the performance of alternate repeater antenna types was examined. The existing ITT installed DME antenna use as a surface relay was compared with an assumed vertical dipole at the same height. Although the DME antenna gain pattern has a sharp cut-off at elevation angles below the horizon, it still provides a nominal 4 dB higher signal level on the airport surface than the dipole relay. A repeater height of 66 feet typically provided a 3 dB higher relay signal level than a height of 47 feet. The relative level of the DME relayed signal varied from about +13 dB for an assumed large aircraft to large aircraft baseline, to about +22 dB when compared with small aircraft pairs direct links. Although direct aircraft-aircraft transmissions should support most expected coverage requirements, relays can provide coverage in those cases where the direct path is obstructed by buildings or other obstacles.

The impact of the repeated message transmissions on the co-channel interference experienced by an airborne receiver was examined relative to the directly received signal from the aircraft top antenna. This was evaluated at the expected mean altitude for the measured traffic distribution, the median altitude, and the maximum altitude. The airborne received relayed signal is about 5 dB higher for the DME antenna than for the Dipole relay. Elevation plane lobes have a relatively fine structure due to the assumed antenna heights, and the co-channel interference from the DME relay is about 7 dB above that from the direct aircraft top antenna. The MTL limited range for the direct top antenna transmission is on the order of 60 NM, the MTL limit for the DME relay is about the same as the 4/3 earth line of sight.

The SLR option, if implemented through the re-transmission of all ADS-B messages on the same link (including the transmission of two UAT messages per second for each 1090 ES aircraft over ADS-R), would pose spectrum problems for both 1090 ES and UAT, since the transmitter duty cycle would be exceeded for both links, and the spectrum limitation of 1000 messages per second would also be exceeded for 1090 ES. However, with some prudent modifications to the re-transmission protocols, these issues could be mitigated.

3.3 *Rebroadcast All Surface ADS-B on UAT*

3.3.1 Performance Improvement Assessment

3.3.1.1 Rebroadcast on UAT surface assessment

Signal levels achieved with rebroadcast of surface transmissions on UAT are presented in this section. The geometry assumptions and repeater alternative antenna types are the same as for the 1090ES cased already discussed. The assumed UAT transmit power level is 40 watts and the receiver MTL is -93 dBm. Only the limiting height cases are shown for comparison with the previously discussed 1090ES performance. Figure 59 is for a repeater height, ar = 47 feet, and small aircraft antenna heights h = 8 feet and a = 10 feet. Figure 60 shows results for a repeater height of 66 feet and large aircraft heights of 25 and 30 feet.

F = 978 Pw = 40 Ptd = 46 PRd = 46 λ = 1 MTL = −93

DME Antenna Ggod(θgp) = 8.6 θ3 = 10.1 θgp = 4.6 Top AC Antenna Gtd(−θpb) = 4.2

Dipole Antenna GRd(θpR) = 2.1 θR = 70 θpR = 0 ϕR = 360

a = 10 h = 8 ar = 47 δ = 0.1 Ggod(0) = 6.1 GRd(0) = 2.1 Gtd(0) = −0

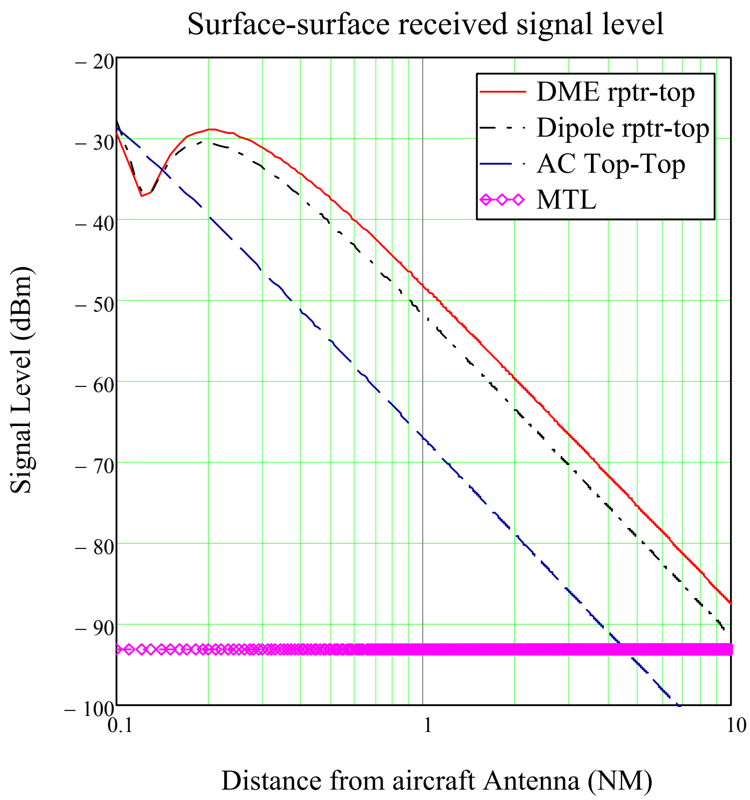

Received signal level (dBm) vs surface distance (NM) for aircraft-aircraft, aircraft to DME repeater, and aircraft to Dipole repeater

Figure 59: UAT Rebroadcast signal levels for DME and Dipole antennas at height, ar = 47 feet to aircraft top antenna height, h = 8 feet. Aircraft-aircraft top antennas at heights, h = 8 feet and a = 10 feet shown for comparison.

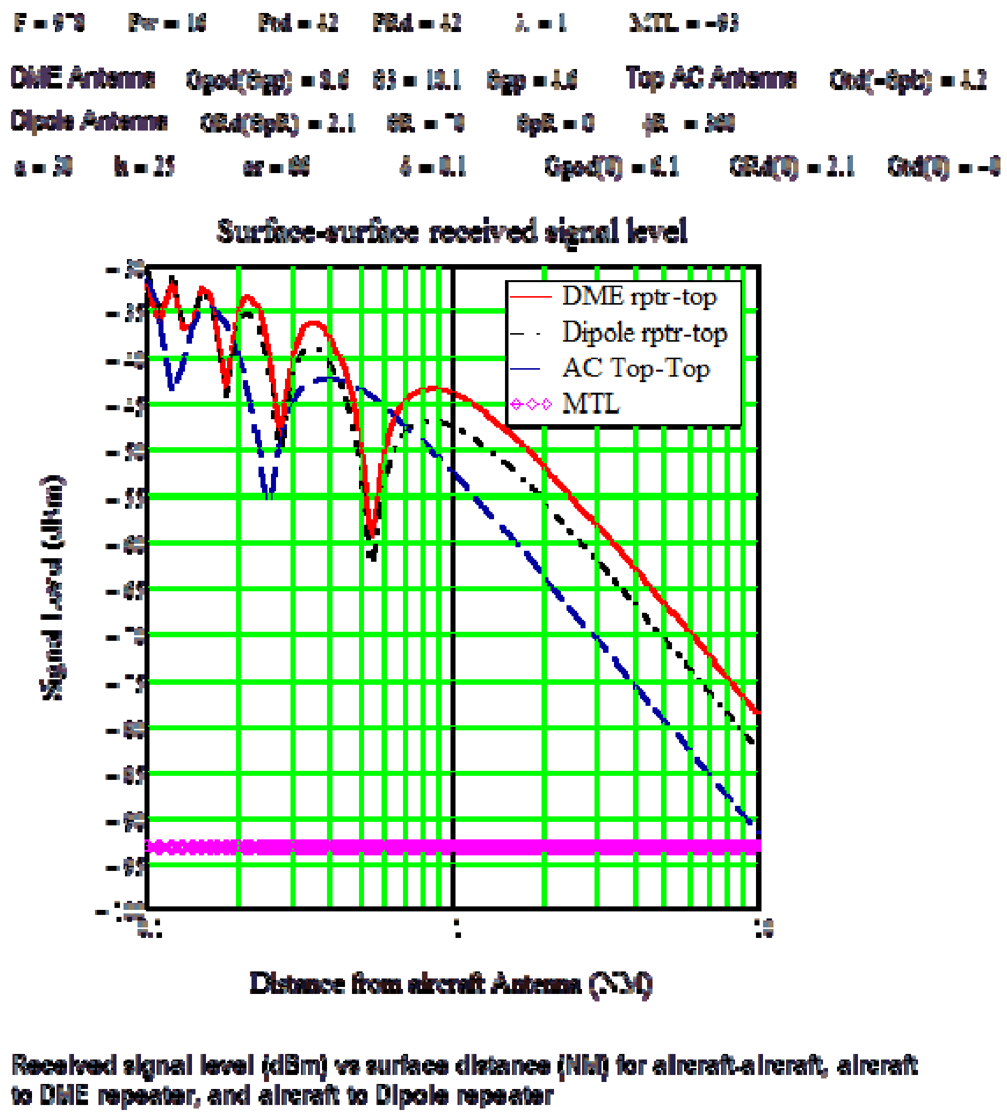

Figure 60: UAT Rebroadcast signal levels for DME and Dipole antennas at height, ar = 66 feet to aircraft top antenna height, h = 25 feet. Aircraft-aircraft top antennas at heights, h = 25 feet and a = 30 feet shown for comparison.

3.3.1.2 Airborne UAT receiver interference level

Potential interference to airborne UAT aircraft to surface rebroadcast on the UAT link is treated just as with 1090ES except for the already mentioned differences in the lower assumed UAT transmit power level and receiver MTL. Results for an airborne victim aircraft at the mean altitude of 10,400 feet are given in Figure 61 and Figure 62. Figure 61 assumes the repeater height is 47 feet and the baseline aircraft antenna height is 10 feet; Figure 62 assumes these values are 66 feet and 30 feet respectively.

F = 978 Pw = 40 Ptd = 46 PRd = 46 AC Altitude A = 10400 Repeater ht ar = 47

DME Repeater Ggod(θgp) = 8.6 θ3 = 10.1 θgp = 4.6 Surface AC ht a = 10

Dipole Repeater GRd(θpR) = 2.1 θR = 70 θpR = 0 ϕR = 360 D := 1, 1.1.. LOS
LOS = 125

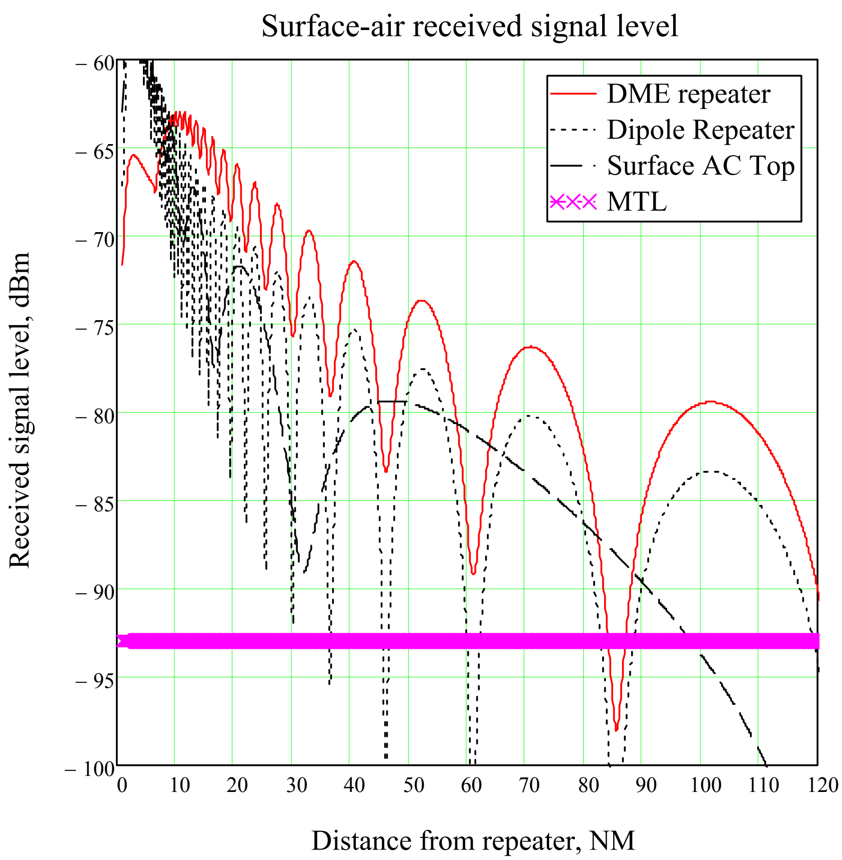

Airborne bottom antenna received signal level from DME and Dipole surface repeater antennas, and from surface aircraft top antenna

Figure 61: Airborne received UAT interference levels from DME repeater, Dipole repeater, and surface aircraft direct. Repeater heights, ar = 47 feet, surface aircraft top antenna height, a = 10 feet, and airborne receiver altitude, A = 10,400 feet.

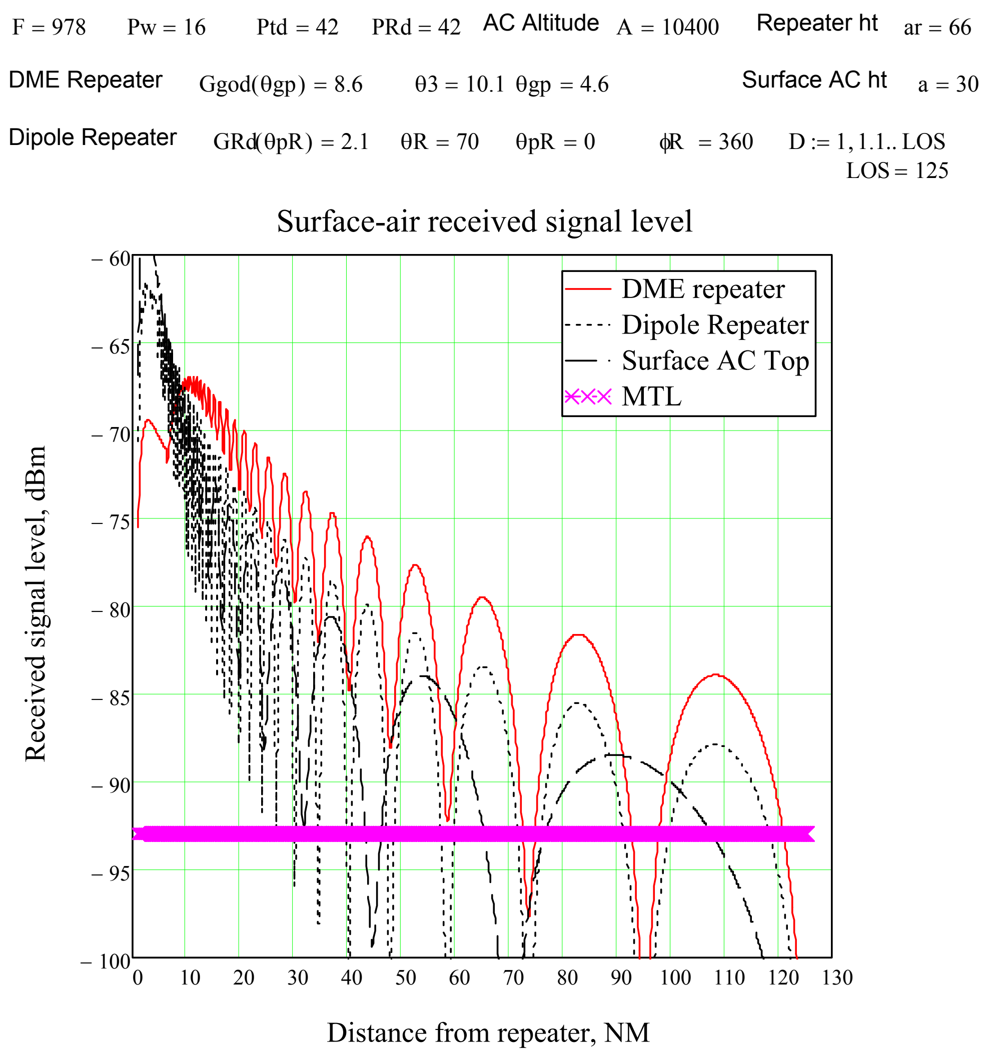

Airborne bottom antenna received signal level from DME and Dipole surface repeater antennas, and from surface aircraft top antenna

Figure 62: Airborne received UAT interference levels from DME repeater, Dipole repeater, and surface aircraft direct. Repeater heights, ar = 66 feet, surface aircraft top antenna height, a = 30 feet, and airborne receiver altitude, A = 10,400 feet.

Rebroadcast produced interference levels for the UAT surface vehicle with transmit power of 8 watts and repeater height of 47 feet is shown for an altitude of 10,400 feet in Figure 63. Both the direct and rebroadcast signal to MTL ratios are higher for the assumed UAT examples than for the comparable 1090ES examples.

F = 978 Pw = 8 Ptd = 39 PRd = 39 AC Altitude A = 10400 Repeater ht ar = 47

DME Repeater Ggod(θgp) = 8.6 θ3 = 10.1 θgp = 4.6 Surface AC ht a = 8

Dipole Repeater GRd(θpR) = 2.1 θR = 70 θpR = 0 ϕR = 360 D := 1, 1.1.. LOS

LOS = 125

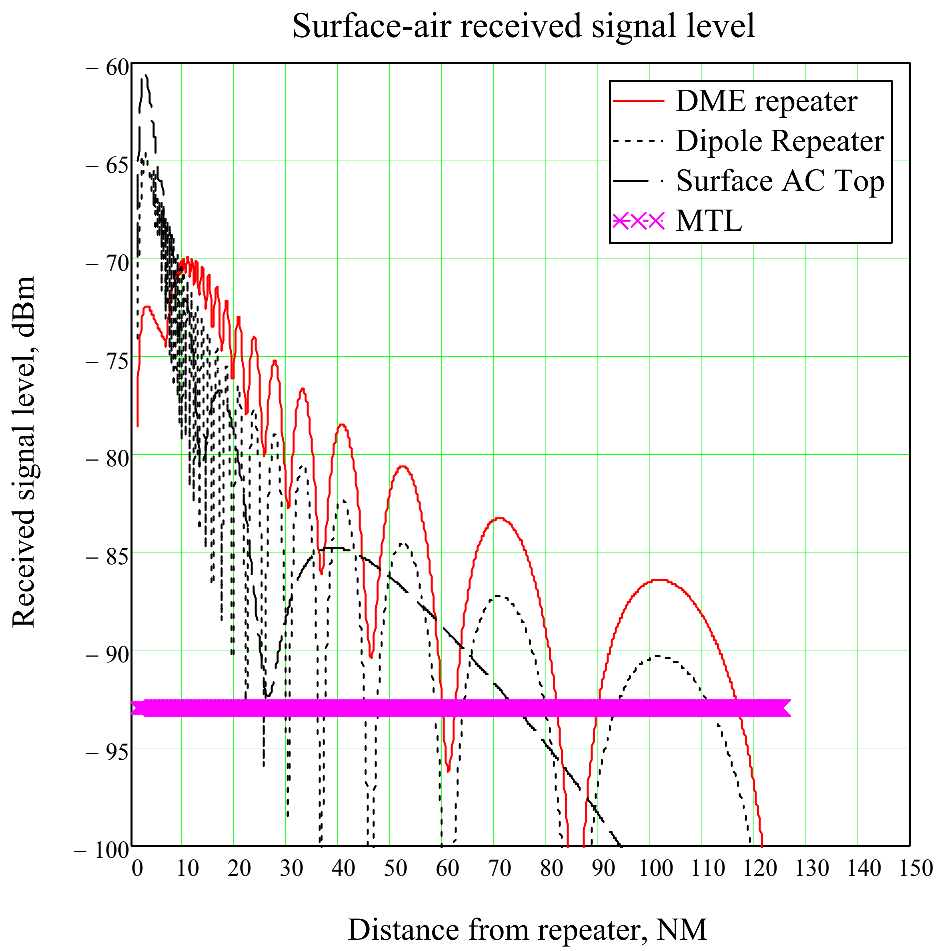

Figure 63: Airborne received UAT interference levels from DME repeater, Dipole repeater, and surface vehicle direct. Repeater heights, ar = 66 feet, surface vehicle antenna height, h = 5 feet, and airborne receiver altitude, A = 10,400 feet.

3.3.2 Spectrum Impact Assessment on UAT

Using the same worst case scenario described in Section 3.2.2.1, the effect on UAT of re-broadcasting all messages transmitted by all aircraft/vehicles is analyzed in this section. Note that the effect on UAT spectrum is expected to be identical to that described in Section 3.2.2.1.2, which summarized the result on UAT spectrum for the SLR option. This analysis is repeated below.

UAT-equipped A/Vs transmit UAT messages at a once per second rate, so the re-broadcast of UAT messages on the surface would amount to 20/s for the twenty UAT aircraft in the Surface SV. This number would be in addition to the ADS-R transmissions over UAT that are currently required for the 1090 ES A/Vs in the SV.

The ADS-R transmission load is two UAT messages per 1090 ES aircraft per second (from the SBS Air Interface Control Document), or 2*180 = 360/s. However, for the option under consideration, ADS-R will be replaced by re-transmission over UAT at a once per second rate, or 180/s, for the 1090 ES aircraft in the scenario. Adding the 20/s for re-broadcast results in a total load of 200/s. This number results in a duty cycle of around 6.5%, well under the 12.5% cited in the SBS Air Interface Control Document. Therefore, this option would result in a reduction in total UAT surface transmissions (replacing ADS-R 2/s with re-transmission 1/s) and would also reduce 1090 ES surface transmissions, since requiring UAT reception would eliminate the need for 1090 ES ADS-R transmissions of UAT aircraft.

3.3.3 UAT Rebroadcast Summary

The rebroadcast signal levels on the surface for both links have similar characteristics except that with typical link transmit power and receiver MTL, the UAT relative signal level is nominally about 9 dB above that for similar assumptions for the 1090ES link. This corresponds to a better signal to noise ratio at maximum airport surface ranges than that available with 1090ES. The behavior of the UAT rebroadcast ground-air potential interference link is also similar to that described for the 1090ES link.

Re-transmitting ADS-B information received from all surface aircraft would reduce the number of surface transmissions on both data links. Therefore, the spectrum impact on both 1090 ES and UAT 978 MHz would be decrease for both. The main negative would be the requirement for aircraft that wish to participate in surface applications to be capable of receiving UAT.

3.4 Diversity / Multi-Channel Reception Evaluation

3.4.1 Activities Conducted for Diversity / Multi-Channel Reception

JHU/APL efforts were focused on an analysis of diversity techniques that can be used to mitigate the effects of multipath in the 1090 MHz band. Messages transmitted in this band use binary PPM modulation at a data rate of 1 Mbps. Therefore, a one is transmitted by inserting a pulse in the first half of the one microsecond time slot, and a zero is transmitted by inserting the pulse in the second half of the one microsecond time slot.

Matlab simulations were developed in order to determine how much performance improvement can be achieved by combining the outputs of the two 1090ES antennas onboard each aircraft. The metric we used to measure the performance improvement is the diversity Eb/No gain, which is the Eb/No required to achieve a target bit error rate (BER) *without* diversity reception minus the Eb/No required *with* diversity reception. We obtained the Eb/No gain for several different diversity combining techniques, including ideal maximal ratio combining, which requires coherent combining of the signals received on the two antennas. After considering the performance vs. complexity of the various diversity combining approaches, JHU/APL recommended a non-coherent post-detection combining method. The results presented in this report are based on the use of this method. We evaluated the performance of this diversity combining technique for a number of simulated channel models as well as for data collected during the Atlantic City and Philadelphia tests.

We started by developing a simulation of a simple two-ray multipath channel model. Figure 64 illustrates the geometry of the two-ray model. The signal received at each antenna is the sum of the direct path (path D in the figure) and a single reflected path (path D_1 and D_2 in the figure).

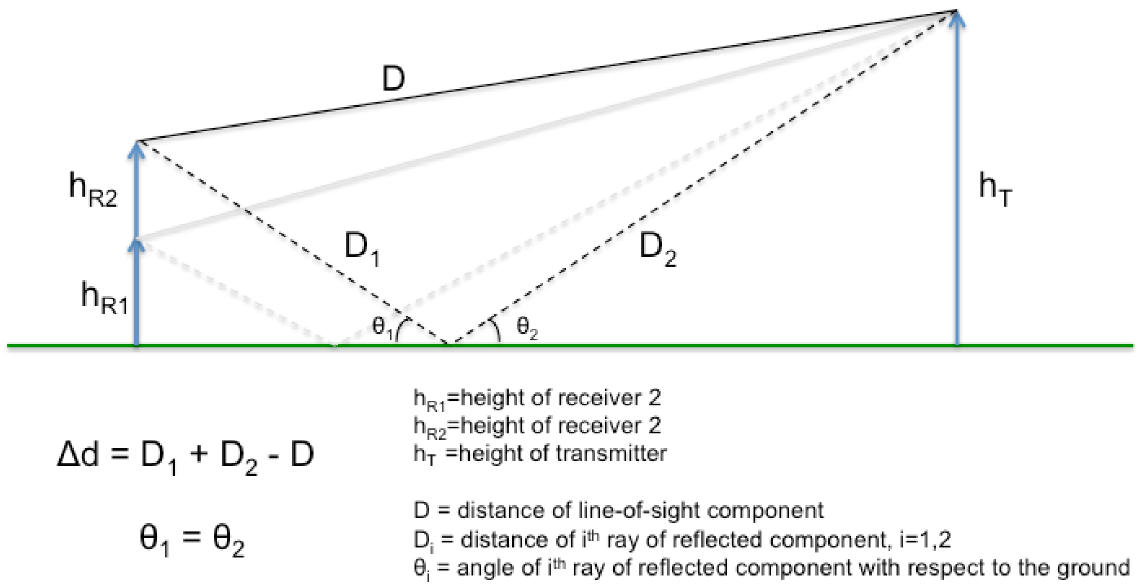

Figure 64: The two ray model used in our preliminary multipath analysis

For the two-ray simulation that we developed, we made the following assumptions:

1. The dominant noise source is thermal noise generated in the two receivers (there is one receiver per antenna using the non-coherent post-detection combining method), so that the noise in the two receivers can be modeled as independent white Gaussian processes
2. The phase shifts of the signals received via the four paths (direct to antenna 1, reflected to antenna 1, direct to antenna 2, and reflected to antenna 2) are uniformly distributed and independent random variables
3. The gross time delay differences between the four paths is small enough that intersymbol interference can be neglected[1]
4. The propagation loss for the direct path from the transmitter to each of the two antennas is the same
5. The antenna gains of the two antennas are the same
6. Interference from other aircraft (fruit) is ignored.

[1] This is a good assumption if the multipath consists entirely of a reflection from the runway surface, as in this case the differential propagation delay between the direct path and the reflected path is a small fraction of the PPM bit interval.

Standard Non-coherent PPM Receiver Architecture

As mentioned above, in order to compute the diversity gain, we need to know the Eb/No required without diversity. The receiver used to evaluate the required Eb/No without diversity is the standard non-coherent PPM receiver, a block diagram of which is shown in Figure 65 below. It is non-coherent because the receiver does not require a coherent phase reference in order to demodulate the signal, thus greatly simplifying the required hardware at a small sacrifice in performance.

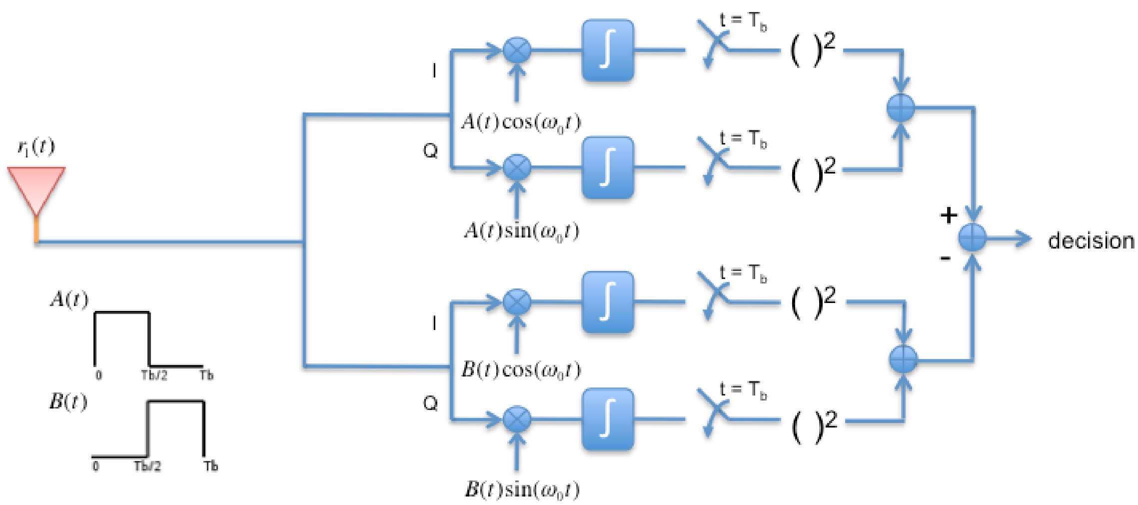

Figure 65: Standard PPM receiver block diagram. The envelopes for the two symbols, A(t) and B(t), are shown.

The receiver performs I and Q correlation on the input signal for each of the two possible symbols (the symbol with the pulse in the left half of the bit period and the symbol with the pulse in the right half of the bit period), then sums the squares of the outputs of the I and Q correlators. If the energy measured by the top half of the receiver is greater than the energy measured by the lower half of the receiver, the bit is declared to be a one and vice versa. When multipath is present on the channel, the signal received on the reflected path can destructively interfere with the signal received on the direct path. If this interference is severe, noise can cause the receiver to make incorrect decisions. By using diversity combining techniques, we can reduce the probability of multipath causing bit errors.

Coherent Pre-detection Combining Diversity Receiver

The first diversity implementation that we considered is the coherent pre-detection combining receiver. It is a single receiver architecture that coherently combines the signals from the two antennas and then feeds the combined signal into the standard PPM demodulator shown in Figure 65 (this process is shown in the block diagram in Figure 66 below). This receiver requires a coherent phase reference, and the receiver must also compensate for any differential time delays between the two antennas (assumed to be negligible for this simulation).

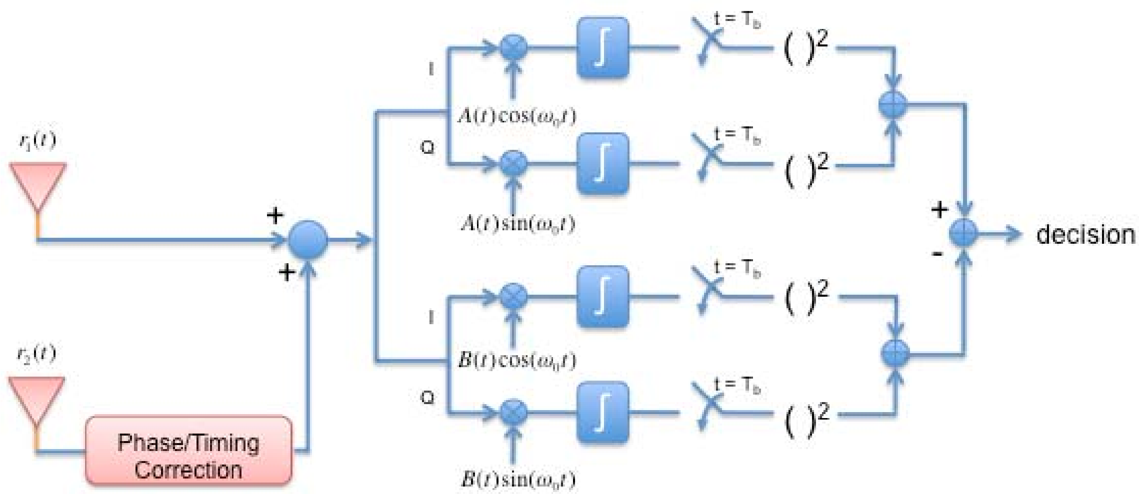

Figure 66: Coherent Pre-detection Combining Receiver block diagram.

If we let $r_1(t)$ denote the signal at antenna 1 and $r_2(t)$ the signal at antenna 2, and assume that their direct path components have the same amplitude (normalized to 1), then

$$r_1(t) = s(t) + \alpha_1 s(t - \tau_1) + n_1(t)$$
$$r_2(t) = s(t - \Delta t) + \alpha_2 s(t - \tau_2) + n_2(t)$$

where $s(t)$ represents the transmitted signal attenuated by the loss experienced on the direct path, Δt is the time of arrival difference of the two direct paths, α_i is the amplitude of the i^{th} reflected component relative to the amplitude of the direct path, τ_i is the time difference for the i^{th} reflected component relative to the direct path, and $n_i(t)$ is the additive white Gaussian noise (i=1,2).

If we can process $r_2(t)$ to achieve phase and time coherence (call this $\hat{r}_2$) , then we can double the amplitude of the direct path component:

$$r_{opt}(t) = r_1(t) + \hat{r}_2(t) = \underbrace{2\cos(\omega_o t)w(t)}_{\text{direct components add coherently}} + \underbrace{\alpha_1 \cos(\omega_o t + \theta_1)w(t)}_{\text{reflected component from antenna 1}} + \underbrace{\alpha_2 \cos(\omega_o t + \theta_2)w(t)}_{\text{reflected component from antenna 2}} + \underbrace{n'(t)}_{\text{noise}}$$

where

$$w(t) = \begin{cases} 1 & during\ pulse \\ 0 & otherwise \end{cases}$$

and

$$n'(t) = n_1(t) + n_2(t) \sim N(0, \sigma_1^2 + \sigma_2^2)$$

That is, $w(t)$ is the envelope sequence for the given symbol sequence (so for each bit period T_b, $w(t)$ is either $A(t)$ or $B(t)$, as shown in Figure 65), and $n'(t)$ is the sum of two independent Gaussian random variables, and is therefore normally distributed with 0 mean and a variance equal to the sum of the variances of $n_1(t)$ and $n_2(t)$.

Non-coherent Post-detection Combining Diversity Receiver

The second receiver that we evaluated used non-coherent, post-detection combining. The block diagram of this receiver is shown in Figure 67 below. In this receiver, the signals from the two antennas are combined *after* non-coherent detection, eliminating the need to establish a coherent phase reference. Note that the receiver shown in Figure 67 essentially consists of two of the receivers shown in Figure 65; however, the outputs of the 1 branches of the two receivers and the outputs of the 0 branches of the two receivers are added together before making a bit decision. Thus, this diversity receiver requires twice as much hardware as a standard single channel receiver.

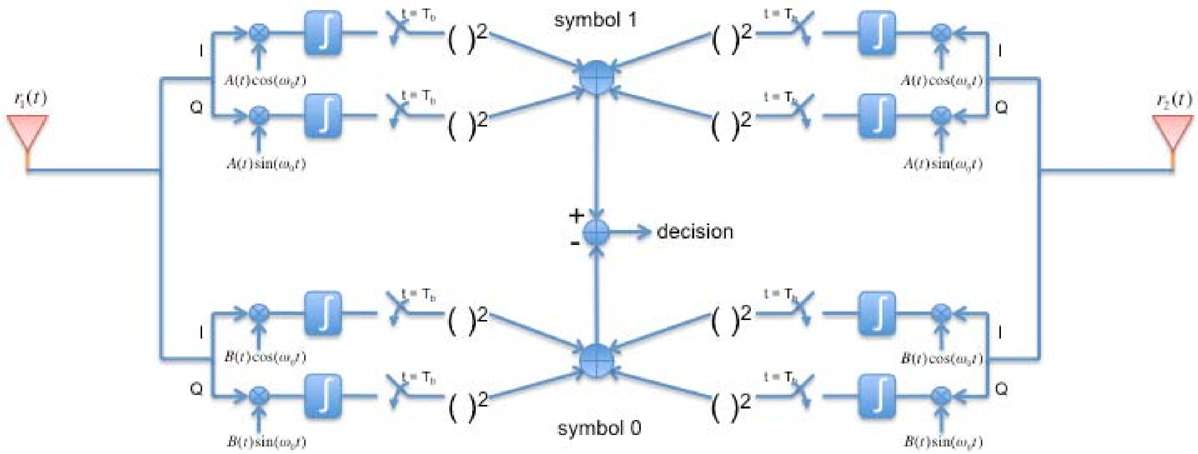

Figure 67: Non-coherent Post-detection combining receiver block diagram

3.4.2 Results for the Two-Path Multipath Model

Monte Carlo simulations were run to measure the performance of each receiver described in Chapter 2 for the case of the simple two-ray multipath channel. The reflection coefficient α represents the amplitude of the reflected signal relative to the amplitude of the direct signal, as measured at the receiver. We varied α from 0.1 to 0.6, representing a reflected component amplitude of 10% to 60% of the amplitude of the direct path. Figure 69 below is an example bit error rate (BER) comparison of the three receivers (no diversity, coherent pre-detection combining, and non-coherent post-detection combining) for an Eb/No range of 0 to 16 dB, and for α=0.6.

We started our simulation effort by developing a Matlab-based RF simulation, meaning that we simulated the waveforms in the time domain as sampled sinusoids and implemented downconversion to baseband. This simulation implemented each of the three receiver concepts defined above for the case of a simple two-ray model with negligible time delay between the direct and reflected paths. The RF simulation allows a clear visualization of the processes at work (see Figure 68), but it has to use a high sampling rate (many samples per carrier cycle) and has to implement computationally intensive downconversion.

Once it was established that this simulation's standard receiver implementation performance (in terms of its BER vs. Eb/No curve) matched the theoretical performance, we developed a second, quasi-analytic simulation with a much faster execution time. The quasi-analytic simulation analytically derives the result of downconverting and integrating the received signal over the pulse interval, both with and without multipath. For the multipath case, the result of this integration is a function of α and the phase difference between the direct and reflected path. The analysis produces an equation that is a function of these two variables.

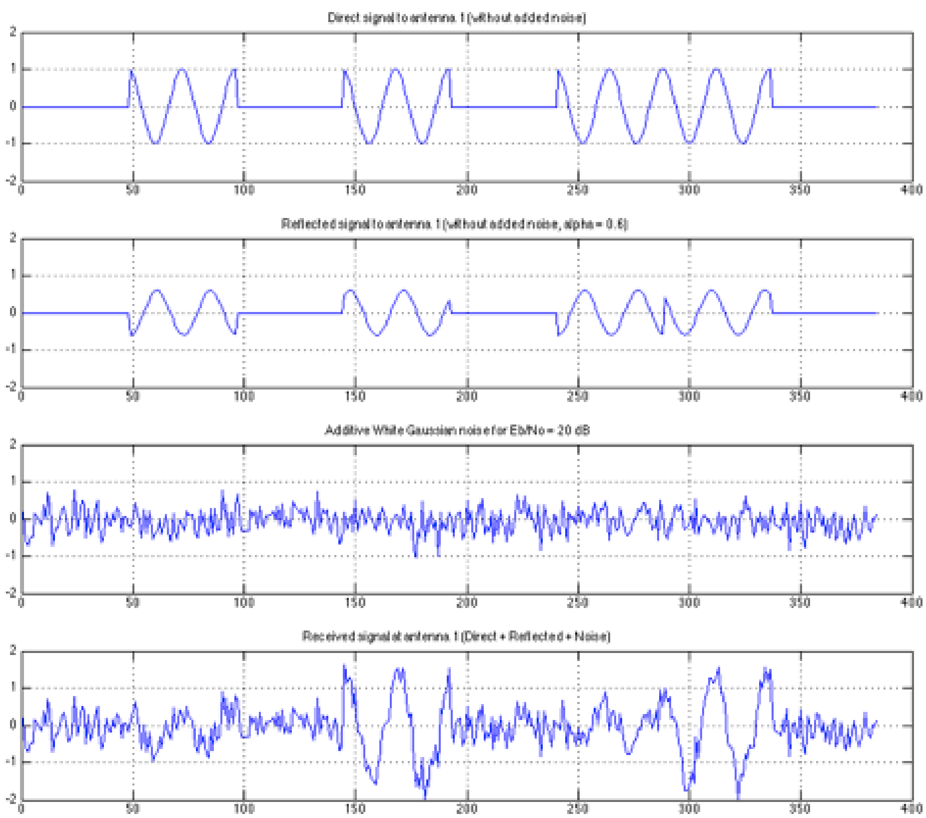

Figure 68: Simulated waveforms from the RF simulation. The signals (in order from top to bottom) are: (1) Direct signal to antenna 1 (without noise), (2) Reflected signal to antenna 1, (3) Gaussian noise for an Eb/No of 20 dB, (4) The composite signal of (1), (2), and (3).

For a given value of α, we can compute the BER for a specified phase difference using Monte Carlo techniques, and then compute the average BER by taking the average BER over all possible phase values. Simulation results from the RF and quasi-analytical simulations were found to agree well over a wide range of simulation parameters (α and Eb/No).

Figure 69 below compares the results of the three receivers for α = 0.6, which is representative of worst-case multipath. We see from the figure that both diversity receivers provide a significant performance improvement with respect to the standard (no diversity) receiver. A good way to quantify the difference in performance between a diversity receiver and the baseline (single channel) receiver is to calculate the difference in Eb/No required to achieve a specified BER. We call this difference in Eb/No the diversity gain of the receiver. A graphical definition of diversity gain is provided in Figure 70. We see from the figure that the diversity gain is a function of the BER at which we evaluate the gain. At a BER of 0.1, we get a diversity gain of 3 dB, while at a BER of 0.01 the diversity gain increases to 5 dB. In general, the lower the required error rate the higher is the diversity gain.

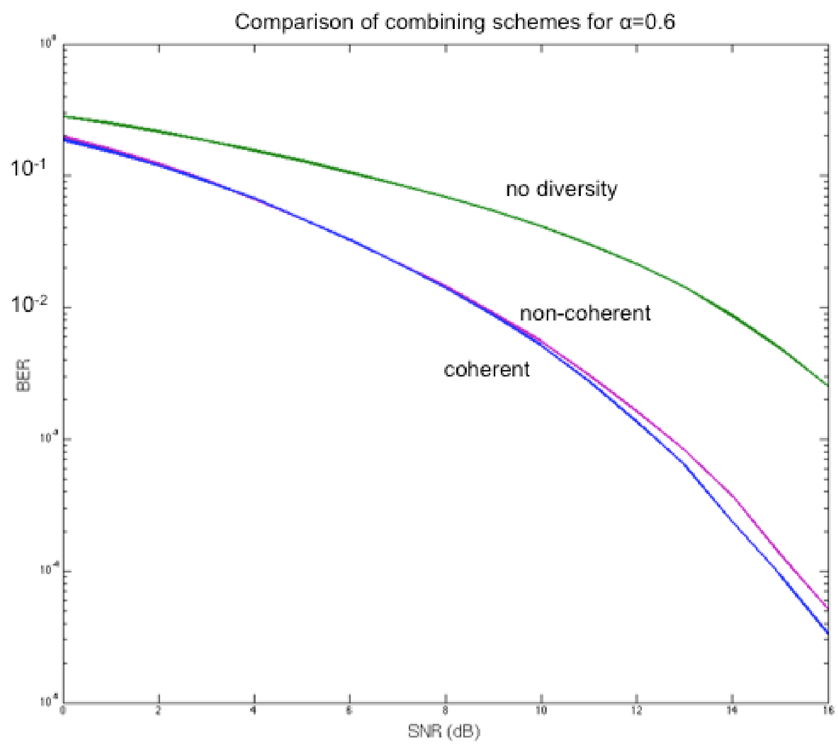

Figure 69: BER comparison of the three receivers (no diversity, coherent, and non-coherent) for the case α=0.6.

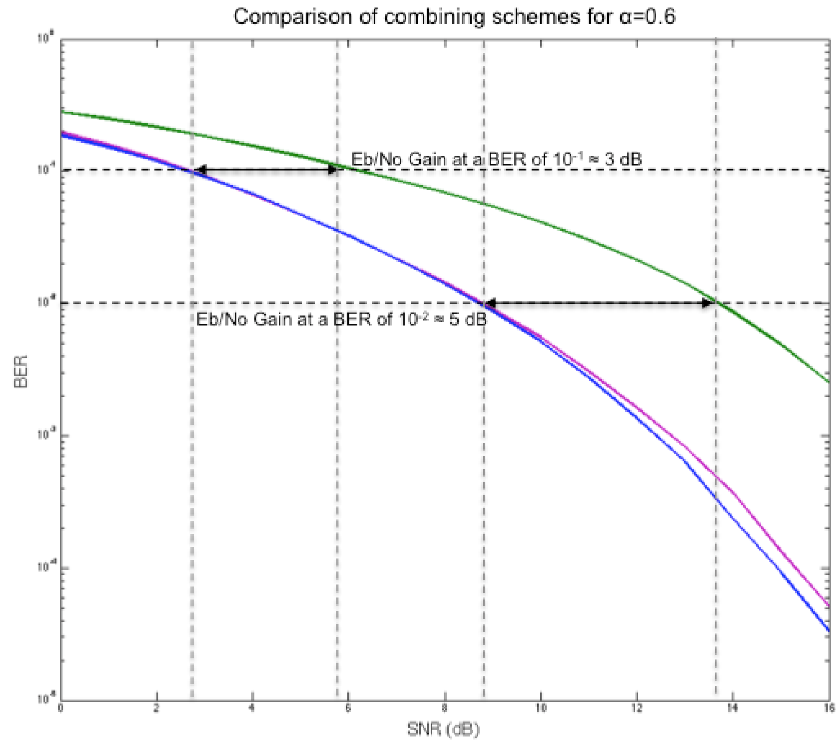

Figure 70: Graphical definition of the Eb/No gain for the results from Figure 69.

In order to evaluate the diversity gain of our candidate receivers, we chose a BER of 10^{-3}. For the standard 112-bit message, a BER of 10^{-3} corresponds roughly to a 90% probability of message detection (i.e., if the BER is 10^{-3}, a message will be demodulated without errors approximately 90% of the time[2]). Figure 71 illustrates how much better the diversity receivers perform on average as compared to the standard single channel receiver, as well as how well the two receivers perform relative to one another. Coherent combining is slightly more effective as it has a higher diversity gain for all α values tested (0.1 to 0.6). The coherent receiver has an advantage over the non-coherent receiver of 0.5 dB at α = 0.1 and 0.2 dB at α = 0.6. Given the significant increase in complexity required to implement the coherent combining receiver and the relatively small performance gain it entails, it seemed clear at this point in the study that it made sense to focus only on the non-coherent post-detection receiver.

[2] This calculation assumes that the bit errors occur independently from one bit to the next and that there is no error detection capability.

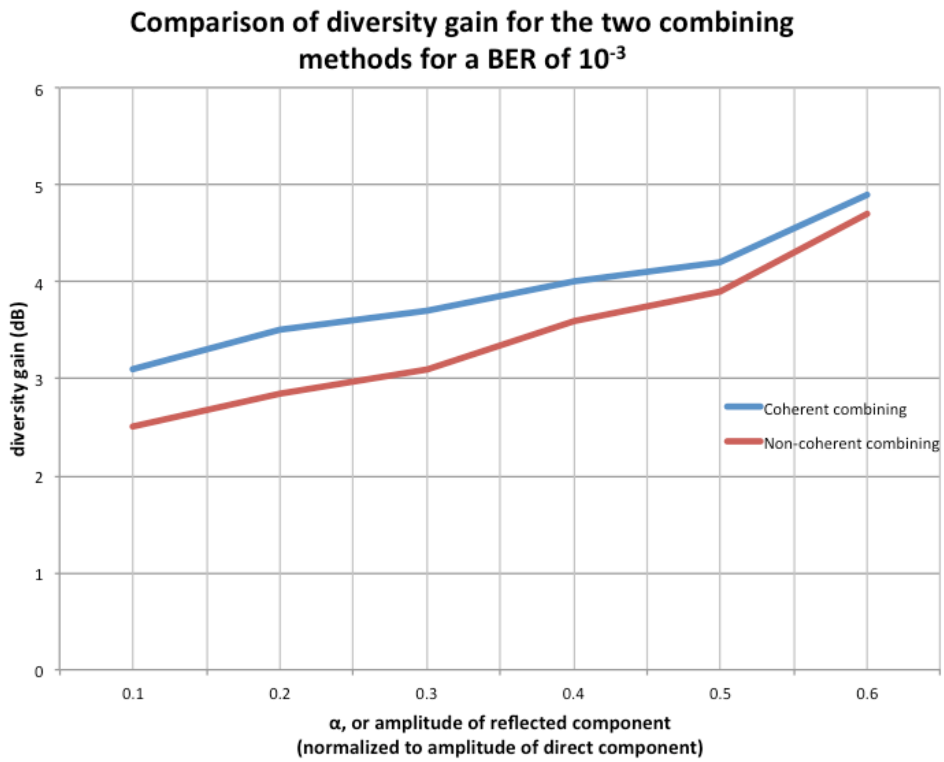

Figure 71: Eb/No gain comparison of the two diversity receiver implementations.

3.4.3 Multipath Simulation Results – Arbitrary path delays

In this section, we describe the generalized JHU/APL multipath simulation tool used to evaluate the performance of diversity combining for multipath channels with arbitrary time delays. The two-ray multipath model described in Section 3.1 assumed that the multipath delays were negligible compared to the pulse duration of 500 ns. The model documented in this section eliminates that constraint, allowing arbitrarily long path delays that could result from reflections from distant buildings, in addition to retaining the capability to model reflections from the runway. The new model also allows an arbitrary number of paths. Each path is defined by a gain (relative to the direct path) and a delay (relative to the direct path). As for the two-ray model, the phase shift associated with each path is assumed to be uniformly distributed from 0 to 2 pi radians.

For the example results that we generated using this model, we assumed that the same gains and path delays apply to the multipath channels experienced by both receivers (the receiver attached to the top antenna and the receiver attached to the bottom antenna). The model allows different channels on the top and bottom antenna; however, allowing the two channels to have different characteristics increases the number of channel parameter combinations to an unmanageable level. Also, the fact that the two antennas are relatively closely spaced (in terms of wavelengths) ensures that the characteristics of the two channel models will be nearly identical. The new model was validated by comparing the results for the following cases:

1. One receiver, no multipath (textbook case)
2. One receiver, two-ray model (no differential delay)
3. Two receivers, two-ray model (no differential delay)

In all cases, excellent agreement was observed between the new model and the available results from theory and the old simulation, which assumed an arbitrary phase shift but negligible differential delay.

The generalized multipath model takes advantage of the ability of Matlab to efficiently process arrays of data. We use a complex baseband representation of the original PPM modulated signal, in order to further reduce the simulation time by eliminating the need to simulate down-conversion to baseband. The simulation processes one message at a time, assuming a fixed message length of 112 bits. The output of the simulation includes the average bit error rate (BER) as well as the probability that the message is correctly decoded (i.e., we successfully demodulate all 112 bits). We did not attempt to model the error correcting capability of the receivers currently in use.

For all of the results presented in the next section, we assume ten samples per bit (five samples per pulse). This parameter can be changed to any desired value, but ten samples per bit is representative of the data that we processed later in this study effort. The simulation can operate in two different modes: either the gains and delays of the multipath channel(s) can be randomly selected between user-specified limits, or specific gains and delays can be specified by the user. The first method was used to evaluate the performance of the diversity combing algorithm over a wide variety of channel conditions. The second method was used to evaluate the performance of the algorithm for specific channels provided to JHU/APL by the FAA.

The simulation's first step is to randomly generate 112 bits. Next, the simulation generates the direct signal based on the resulting sequence of bits and the sampling rate, and the direct signal is given a random phase shift. The next step is to add to the direct signal the reflected signals from each of the indirect paths, as specified in the multipath channel model being used. The signal corresponding to each reflected path is obtained by shifting the direct signal by the integral number of samples closest to the desired delay, multiplying by the gain of the path relative to the direct path, and applying a random phase shift. Each reflected signal is added to the direct signal vector in order to obtain the composite signal consisting of the direct signal plus all of the reflected signals. At that point, noise is added based on the Eb/No specified by the user. For the case of two receivers, the noise on the two channels is assumed to be independent. At this point, we have obtained the output of the multipath channel.

The next step is to demodulate all 112 message bits. For each one-microsecond bit interval, the squared magnitudes of each of the five samples in the first half of the bit interval are added together and added to the same results from the second channel. The process is repeated for the five samples in the second half of the bit interval, and the results for the first half are compared against the results for the second half. If the signal energy in the first half of the bit interval exceeds the signal energy in the second half of the bit interval, the bit is demodulated as a one; otherwise, it is demodulated as a zero. This process is repeated for all 112 bits. The message is determined to be correctly decoded if and only if all 112 bits are correctly demodulated. The simulation repeats this procedure for a user specified number of messages (typically several hundred thousand or more), and the BER as well as the probability of correct message decoding are calculated. We implemented the non-coherent post-detection diversity combining demodulator shown in Figure 67.

Once the new model was validated as discussed above, the first channels we simulated were simple two-path channels consisting of a direct path and a delayed and attenuated reflected path. With only one reflected path, it is possible to consider all possible delays, as the delay is specified by a single parameter. As always, we made the phase of the reflected path relative to the direct path a uniformly distributed random variable, which was changed for each message simulated. The only other parameter that must be specified is the gain of the reflected path relative to the direct path. We chose several values for this parameter covering the range from 0.1 to 0.6. For each specified channel model, we varied the Eb/No until the desired BER was obtained, and repeated this process with and without diversity. The difference (expressed in dB) between the Eb/No required to achieve the target BER without diversity and the Eb/No required with diversity was defined as the "diversity gain." For the initial simulations, we chose a target BER of 0.001, which corresponds to a probability of correct message reception of 90%.

Figure 72 summarizes the results of these two-path simulations. We plot the diversity gain versus the relative path delay for two cases: one in which the amplitude of the reflected path is 40% of the amplitude of the direct path (alpha = 0.4) and one in which the amplitude of the reflected path is 60% of the amplitude of the direct path (alpha = 0.6). Note from the figure that for the alpha = 0.6 case (the red curve), there are regions in which there appears to be no diversity gain; however, this is actually an artifact of the way that we define diversity gain. In these regions there is an irreducible error rate, so that no matter how much the Eb/No is increased, the target BER of 0.001 is never reached. Nevertheless, there is in fact a diversity gain, as the irreducible BER with diversity is less than that without diversity. If the amplitude of the reflected path is reduced to 40% of the amplitude of the direct path (blue curve), we see that the irreducible BER phenomenon goes away, and we always achieve a positive diversity gain ranging from 2.9 to 5.6 dB.

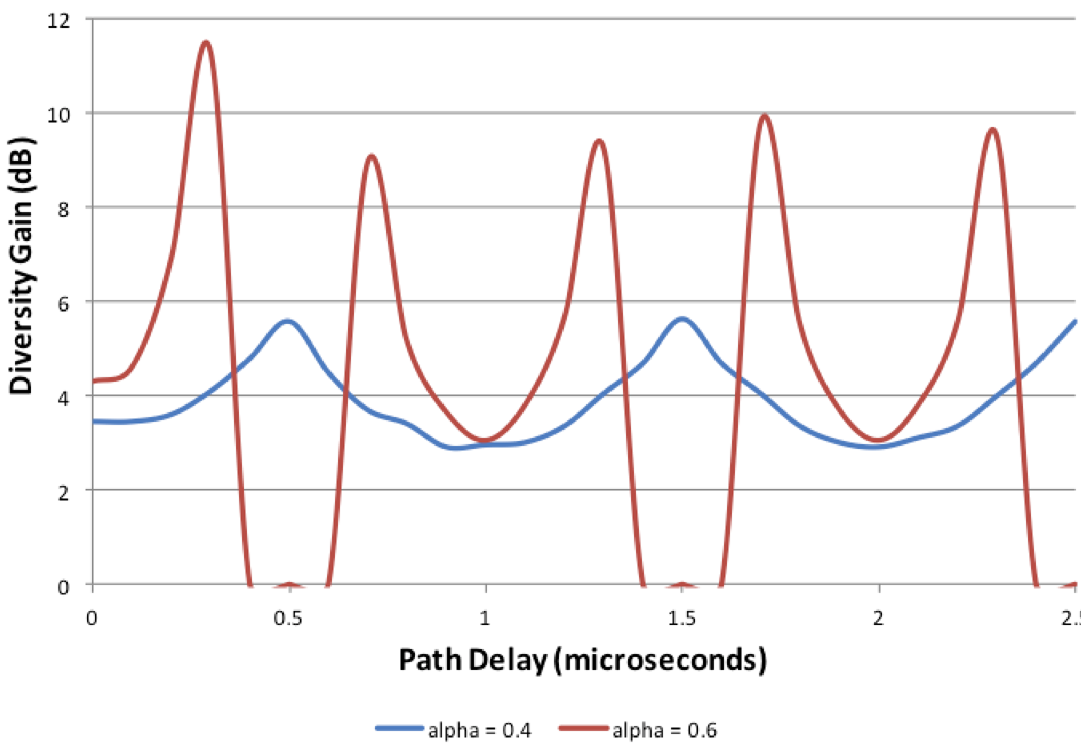

Figure 72: Diversity gain vs. path delay (two path model).

To see why we can observe an irreducible BER for the case where alpha = 0.6, refer to Figure 73. The figure shows a bit sequence of 0, 1, 1, for the case where alpha = 0.6 and the differential path delay is 1.5 us. The left half of the figure shows the transmitted pulses and indicates the location of the reflected pulses with dashed lines. Consider the worst-case phase(the direct and reflected path are 180 degrees out of phase), in which case the reflection of the first pulse reduces the amplitude of the third pulse to 40% of the amplitude of the direct pulse, as shown in the right hand half of the figure. Because the amplitude of the reflected pulse is 60% of the amplitude of the direct pulse, the amplitude of the reflected pulse, which shows up in the second half of the bit interval, will always be greater than the amplitude of the composite signal received during the first half of the bit interval. As a result, the bit will always be incorrectly demodulated as a 0 no matter how small the noise level is. These bit errors will occur with non-zero probability whenever alpha is greater than 0.5. When alpha = 0.6, these errors occur frequently enough to prevent us from ever achieving a BER of 0.001.

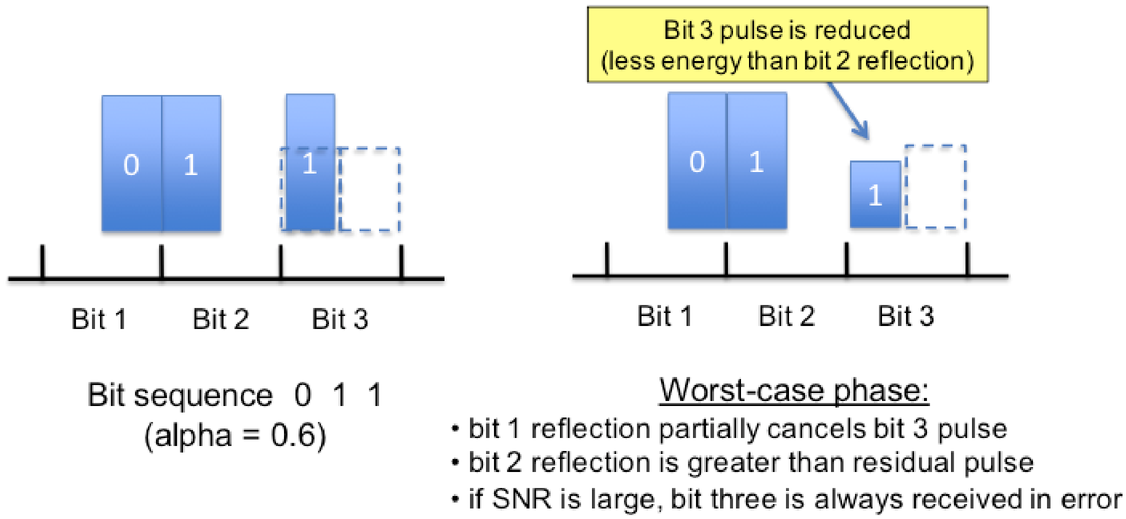

Figure 73: Physical explanation for the presence of an irreducible bit error rate.

When there are more than two paths, the conditions for an irreducible BER are somewhat more complex; however, it is clear that a necessary (but not sufficient) condition for an irreducible BER is that the sum of the gains of the reflected paths must be greater than 0.5. This result can be obtained by considering the pathological case where the paths all have the same delay. It is clear in this case that it is possible (although not likely) that the phases of the signals arriving on the various paths will align in such a way as to produce results identical to the two path case if the sum of the path gains is the same as the gain of the reflected path in the two path case. In practice, it takes "a perfect storm" to get an irreducible BER when the 0.5 limit is exceeded by a small percentage, but this limit provides a good method ensuring that we avoid irreducible BERs.

As the number of paths is increased, the large number of parameters that must be specified makes it impossible to evaluate the diversity gain for every possible channel model. We took two approaches to solve this problem. First, we obtained simulation results for three different examples of fixed path delays and gains for both a three path model and a four path model. The results of these runs are summarized in Table 6. The delays and gains of each reflected path are shown in columns one and two, respectively. It is assumed that the delays and gains are the same for both receivers (but the random phase shifts are independent). Column 3 of the table shows the Eb/No required to achieve a 0.001 BER for one receiver, and column four shows the required Eb/No for diversity reception. The rightmost column shows the diversity gain in dB, which is simply column three minus column four. To ensure that we could evaluate the diversity gain, we intentionally chose path gains that are below or just slightly above the 0.5 limit. For these six test cases, the diversity gain ranged from 2.8 dB up to 3.7 dB. Note that, as a rule, diversity provides the greatest gain for the more stressing channels (where stress can be measured by the Eb/No required in the single receiver case or by the sum of the alphas).

Table 6: Summary of results for multiple reflected paths

Delays (us)	alphas	E_b/N_o (1 Rx)	E_b/N_o (2 Rx)	Gain (dB)
[0.1,2.3]	[0.4,0.1]	13.7	10.1	3.6
[1.2,2.9]	[.3,.1]	12.8	9.8	3.0
[0.5,2.2]	[.2,.1]	12.5	9.5	3.0
[0.8,1.2,2.8]	[0.3,0.2,0.1]	14.0	10.6	3.4
[0.4,1.7,3.5]	[0.2,0.1,.05]	12.1	9.3	2.8
[0.2,1.8,2.1]	[0.4,0.1,.05]	14.0	10.3	3.7

Next, we looked at results for the case where the channel model parameters are selected randomly within user-defined limits. We set the maximum path delay equal to 2.5 us, and the program picked path delays between 0 us and 2.5 us assuming a uniform distribution. The program initially selects path gains that are uniformly distributed between 0 and 1, but then scales these gains by a factor calculated in the program in order to avoid the problem of irreducible BER. Because significant effort is required to find the Eb/No value that produces the target BER, we based the performance on six trials, with random channel parameters for each trial. We ran the first six trials with a four-path channel model (the direct path and three reflected paths) and the next six trials with a six-path channel model (five reflected paths). For all trials, we set the scale factor so that the sum of the alphas is equal to 0.5 (i.e., 100% of the theoretical upper bound). We evaluated the diversity gain at a probability of signal detection equal to 90%.

Table 7 summarizes the results of these two sets of six simulation runs. For each set of runs, we show the minimum diversity gain, the maximum diversity gain, and the diversity gain averaged over all six runs. For the random four-path channel model, the diversity gain ranged from 3.0 to 4.7 dB, with an average value of 3.58 dB. For the random six-path channel model, the diversity gain ranged from 2.8 to 3.1 dB, with an average value of 2.96 dB. Thus, the simulation results show that, while the diversity gain tends to decrease as the multipath energy is spread over more paths, significant diversity gain is obtained over a wide range of multipath channels.

Table 7: Summary of results for randomly selected channel parameters

# of paths*	% of max α	Min gain	Max gain	Avg gain
4	100%	3.0	4.7	3.58
6	100%	2.8	3.1	2.96

* Including direct path

At the Surface Multipath Meeting held on November 21, 2011, JHU/APL took an action to provide results for some additional channels:

1. Two multipath scenarios provided by the MITRE Corporation based on their analysis of the initial FAA multipath tests conducted at Philadelphia International Airport on October 10, 2010.
2. No multipath (to answer the question as to whether there is any diversity gain for the case where there is no multipath)

For each of these scenarios, we were asked to evaluate the impact on diversity gain if one of the two diversity channels has more loss than the other.

We modified the simulation program to be able to accommodate these two scenarios and to allow a relative loss between the primary and secondary diversity channels. MITRE subsequently provided data for two channel models with the following characteristics:

1. Scenario A: One reflected path, delay = 1.25 us, gain = -6 dB (alpha = 0.5).
2. Scenario B: Three reflected paths with the following characteristics:
    - delays = 1.25, 1.5, and 0.75 microseconds
    - gains = -3, -6, and -12 dB (alpha = 0.7, 0.5, and 0.25)

MITRE indicated that the gains of the two aircraft antennas could differ by as much as 10 to 15 dB.

For these simulations, we again used a probability of correct message decoding of 90% as the performance metric for evaluating the diversity gain. The results for the two MITRE scenarios are shown in Table 8 below. For scenario A, we present the results for three cases: antenna 2 having the same gain as antenna 1, antenna 2 having 10 dB less gain than antenna 1, and antenna 2 having 15 dB less gain than antenna 1. The relative gain of the second antenna is shown in column two of the table, which is labeled Rx 2 gain.

When the antenna gains are equal, we achieved a diversity gain of 4.95 dB, which is consistent with the results presented above; however, as the antenna gain for the second receiver is reduced, the diversity gain decreases. If the gain of the second antenna is 10 dB less than the gain of the first antenna, the diversity gain is reduced to 1.15 dB. If the gain of the second antenna is 15 dB lower, the diversity gain shrinks to 0.4 dB.

Unfortunately, the sum of the path gains for Scenario B is almost three times the theoretical maximum to avoid an irreducible BER which, in this case, translates into a maximum achievable probability of detection less than 90%. Furthermore, even for the condition where the gains of the two antennas were assumed to be equal, the use of diversity reception increases the probability of detection by only a small amount (the probability of detection increases from 73.8% to 82.0%). Our conclusion is that it is possible to devise a multipath channel that is so severe that diversity combining will not significantly improve performance.

Table 8: Results for the MITRE scenarios

Scenario	Rx 2 gain	E_b/N_o (1 Rx)	E_b/N_o (2 Rx)	Diversity Gain
A	0 dB	17.25 dB	12.3 dB	4.95 dB
A	-10 dB	17.25 dB	16.1 dB	1.15 dB
A	-15 dB	17.25 dB	16.85 dB	0.4 dB
B	0 dB	∞ (PD = 73.8%)	∞ (PD = 82.0%)	N/A

We performed a similar analysis for the case where there is no multipath. Again, we varied the relative antenna gains from 0 dB to -15 dB. In addition to computing the diversity gain at a probability of detection of 90%, we also evaluated the diversity gain at a probability of detection of 99%. These results are summarized in Table 9. When the antenna gains are equal, the diversity gain is 2.4 dB at a 90% probability of detection and 4.0 dB at a 99% probability of detection. If the antenna gain of the second antenna is reduced by 10 dB, we get a diversity loss of 0.2 dB at 90% probability of detection but a diversity gain of 1.5 dB at a 99% probability of detection. When the differential antenna gain is 15 dB, we see a diversity loss of 0.5 dB at 90% probability of detection but a diversity gain of 1.2 dB at a 99% probability of detection.

Table 9: Results when no multipath is present

Pd	Rx 2 gain	E_b/N_o (1 Rx)	E_b/N_o (2 Rx)	Diversity Gain
90%	0 dB	11.0 dB	8.6 dB	2.4 dB
90%	-10 dB	11.0 dB	11.2 dB	- 0.2 dB
90%	-15 dB	11.0 dB	11.5 dB	-0.5 dB
99%	0 dB	14.0 dB	10.0 dB	4.0 dB
99%	-10 dB	14.0 dB	12.5 dB	1.5 dB
99%	-15 dB	14.0 dB	12.8 dB	1.2 dB

Later in this study, while we were processing test data, we realized that there is no reason that diversity reception should ever result in a loss in performance. The reason is that we can easily demodulate the signal from antenna A, the signal from antenna B, and the diversity combined signal. The CRC check will tell us which of these three demodulations, if any, produced the correct message bits. If any one of the three demodulations produces 112 correct message bits, then we can successfully decode the message regardless of whether the diversity combining was effective. With this implementation of the diversity combining receiver, there can never be a loss relative to demodulation with one antenna and one receiver. This approach was used in processing the multipath corrupted messages collected during the two test events in Atlantic City and Philadelphia.

Figure 74 shows a flowchart that describes the decoding algorithm we used to decode all of the test data. The signal is independently decoded on each standard PPM receiver, and if neither the top nor bottom signal passes the CRC check, the post-detection combining diversity PPM receiver is used.

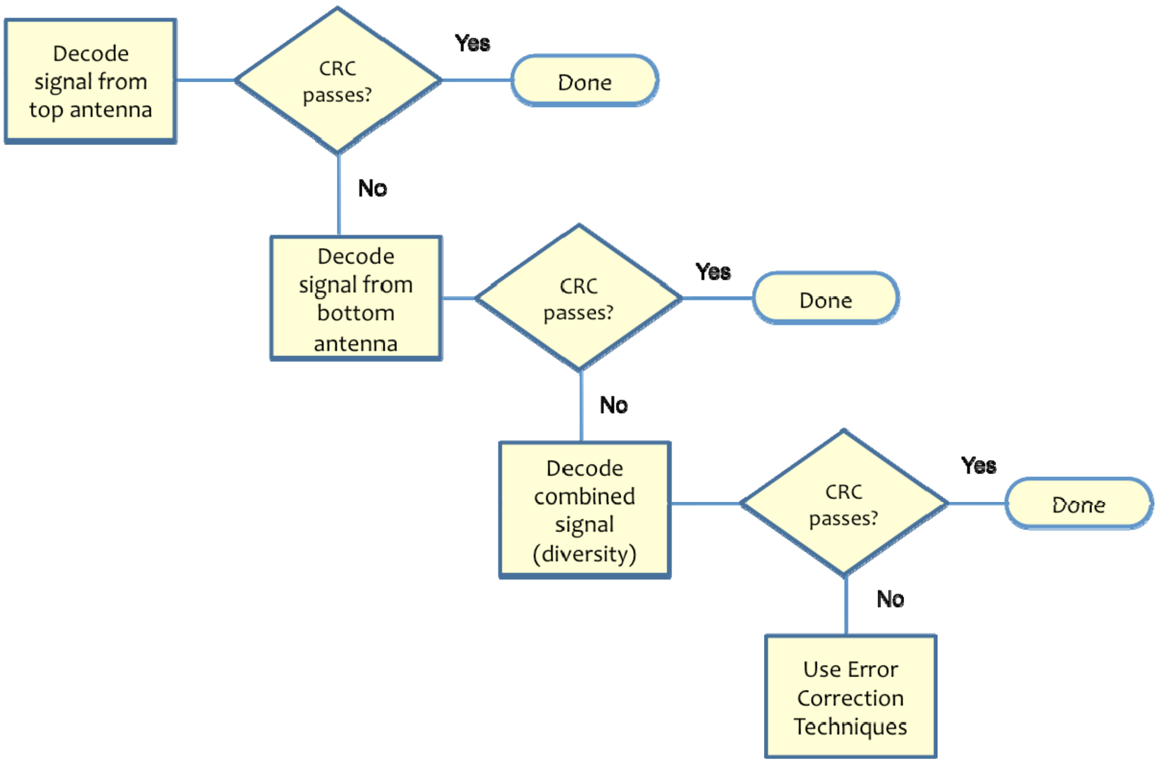

Figure 74: Flowchart describing decoding algorithm used to process the messages from the two test events.

3.4.4 Results from Field Tests

From January to March of 2012, JHU/APL was provided with a series of recordings from field tests in which multipath was present. The recordings were each one message long, and the goal was to attempt to decode the messages using the diversity receiver model implemented in Matlab. The sampling rate was 80 MSps. In November, JHU/APL was provided with a single test message. The message was decoded successfully and a simplified preamble detection algorithm was developed in order to synchronize our diversity receiver algorithm in time with the test message and all subsequent messages in the same format. The preamble correlation, which is at the heart of the preamble detection algorithm, is depicted in Figure 75.

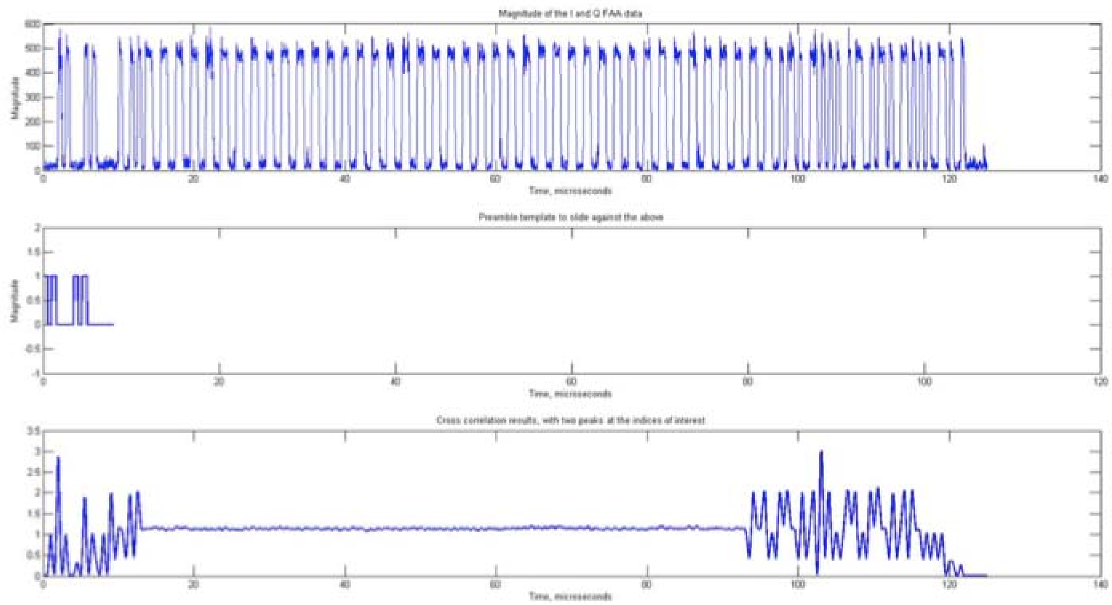

Figure 75: Example of preamble detection algorithm at work: (1) A plot of the received message, an input to the preamble detection algorithm. (2) The preamble for 1090ES messages, set to the correct sequence of pulses and the right durations, was correlated against the input signal in (1). (3) Correlation output, with a peak at the location representing the start of the message.

This preamble detection method was used on all subsequent messages, and helped to successfully decode many of the provided messages by accurately locating the start of the message. At the meeting on January 19, 2012, JHU/APL presented the first set of results from a set of seven messages provided by the Tech Center and recorded in December. The results are summarized in Table 10. The results are given as a fraction of the 7 messages that were successfully decoded, for the top antenna only, bottom antenna only, and diversity cases. Using non-coherent demodulation, a single channel receiver can successfully decode only four or five of the seven messages, depending on whether it is attached to the top or the bottom antenna. The diversity receiver can successfully decode all seven messages.

Table 10: JHU/APL results for the 7 messages from the December tests.

	successful	Avg # of bit errors
top	4/7	13
bottom	5/7	5
diversity	7/7	0

Table 11 shows some additional details. The position on the tarmac at which the results were obtained is shown in column one of the figure. Columns 2 and 3 provides information from the Tech Center regarding which of these messages they were able to decode when their single channel receivers were applied to the signals received by the top and bottom antenna. They were able to successfully decode three out of seven messages using the top antenna's receiver and four out of seven using the bottom antenna's receiver. Columns 4 and 5 show the number of bit errors that we observed when we applied a single channel receiver to the signals from the top and bottom antenna, respectively. The next column shows that we observed no bit errors when we applied the diversity receiver. The actual transmitted bits are shown in the rightmost column of Table 11 (in hexadecimal format). These results are fairly consistent with (and just slightly worse than) the results we obtained using our Matlab-based receiver.

Table 11: Detailed results for the 7 messages from the December tests

Position	FAA top success	FAA bottom success	APL top success (# bit errors)	APL bottom success (# bit errors)	APL diversity success (# bit errors)	decoded message
1	yes	yes	yes (0)	yes (0)	yes (0)	8DA3E2735920024CB4F1CC3EAF59
2	no	yes	yes (0)	yes (0)	yes (0)	8DA3E273592005DC7D5BDBDE4E18
3 (1)	no	no	no (27)	yes (0)	yes (0)	8DA3E2735920024CB6F1CDDAF3D2
3 (2)	no	no	no (20)	yes (0)	yes (0)	8DA3E27399000100200428D86605
6	yes	yes	yes (0)	no (12)	yes (0)	8DA3E2735020024C8CF1CCF7BC0A
7	no	yes	no (46)	yes (0)	yes (0)	8DA3E2735020024C8AF1CD24B185
10	yes	no	yes (0)	no (20)	yes (0)	8DA3E273990001002004272 7C64D
Average bit errors (APL)			13	5	0	

In March, JHU/APL processed a second set of recordings that were provided by the Tech Center. These recordings were made in February 2012 at Philadelphia International Airport. Our results are shown in Table 12. These messages contained much more significant multipath than the previous messages, and even with one-bit error correction, the diversity receiver was only able to decode 9 out of 14 of the messages. However, the results still show that the diversity receiver offers a significant improvement in performance over using the top or bottom antenna alone.

Table 12: JHU/APL results for the 14 messages from the Philadelphia tests

	successful (w/o error correction)	successful (w/ 1-bit error correction)	Avg # of bit errors	Avg # of bit errors (after removing two worst cases)
top	3/14	4/14	15	11
bottom	4/14	4/14	12	7
diversity	8/14	9/14	6	1

Table 13 shows the results from the second set of tests in more detail. Instead of organizing the 14 different messages in terms of their position on the tarmac, which were not available for this set of data, the messages are organized by a capture ID (obtained from the filenames for each message).

Table 13: Detailed results for the 14 messages from the Philadelphia tests

Case	Capture ID	# top errors	# bottom errors	# diversity errors	truth message	Receivers that decoded the message with zero errors
1	33113200	16	24	5	8DA3E27359200293C0C55D371EFD	None
2	4312700	3	0	0	8DA3E273990001002004252 7DA56	Bottom and Diversity
3	37117700	7	0	0	8DA3E2739900010020042527DA56	Bottom and Diversity
4	20394400	31	2	2	8DA3E27359200293BEC55F679903	None
5	41968500	20	5	5	8DA3E27399000100200424D82E5F	None
6	42767300	2	34	1	8DA3E273F8102007005938178D84	None
7	1127800	46	60	46	8DA3E273E1109F000000001A81D9	None
8	20304000	1	0	0	8DA3E27399000400280424B9ADA1	Bottom and Diversity
9	55501000	33	32	31	8DA3E27399000400280424B9ADA1	None
10	12202200	5	3	0	8DA3E27399000100280424B68C57	Diversity
11	50549000	42	0	0	8DA3E27359200622593062E96AEE	Bottom and Diversity
12	32061600	0	2	0	8DA3E2739900010020042527DA56	Top and Diversity
13	64092000	0	2	0	8DA3E2739900010020042527DA56[1]	Top and diversity
14	16253100	0	7	0	8DA3E273592006225B30610D2A7E	Top and Diversity
	Average	15	12	6		
	w/o two worst messages (7, 9)	11	7	1		

3.5 Enhanced ADS-B Reception Evaluation

The 1090 MHz Extended Squitter (1090ES) message signal is based on the transponder reply signal of the Mode Select (Mode S) beacon surveillance system. Mode S was developed to improve the performance of the Air Traffic Control Radar Beacon System (ATCRBS) and to provide a digital datalink. Ground-based ATCRBS beacons interrogate all ATCRBS transponders within the rotating fan beam, which is narrow in azimuth and wide in elevation. ATCRBS performance is degraded when there are too many transponders in the beam because their replies will overlap in time and cause garbling (i.e., corruption) of the 12 Pulse Amplitude Modulated (PAM) data bits, which contain either a digitized altimeter reading or an identity code dialed in by the pilot. Garbling is also caused by replies called fruit elicited by other interrogators. Garbling of both types increased during the 1960's because air traffic increased and the interrogators became more numerous. Mode S solved this by interrogating transponders one at a time using their unique and permanent 24 bit addresses. The interrogations are scheduled so that the replies don't overlap. If no reply is received additional interrogations can be sent. The interrogations and replies can include 32 or 88 data bits in addition to 24 bits of parity/address. In order to make Mode S be forward and backward compatible with ATCRBS, care was used in choosing the modulation techniques. The reply link has a four pulse PAM preamble followed by 56 or 112 data bits, encoded with Pulse Position Modulation (PPM). The bit rate is one bit per us, and a binary 1 is represented by 0.5 us of energy followed by 0.5 us of no signal. A binary 0 has the energy in second half. The preamble pulses are 0.5 us wide and spaced so that it is unlikely that ATCRBS replies will spoof a preamble.

Mode S interrogators use a universal "all-call" interrogation to learn the address of aircraft entering coverage. The sensor instructs the transponder to ignore these interrogations once the aircraft is put into track. The all-call method would not work for the Threat alert and Collision Avoidance System (TCAS) because a narrow beam is required, which TCAS cannot provide due to antenna size limitations. This was solved by having Mode S transponders transmit their address in a spontaneous "squitter" reply once a second, containing 8 control bits, 24 address bits and 24 parity bits. When augmented with 56 bits of position and/or velocity information the squitter becomes the 112 bit 1090 MHz Extended Squitter (1090ES).

Parity

Mode S replies are protected by 24 bits of parity, which is generated as follows. A special table of eighty-eight 24 bit parity words is provided having a word to correspond with each of the possible 32 or 88 message bit positions. The message bits are considered one at a time. If the ith bit is a 1, the ith word is retrieved from the table and retained, and so on for the rest of the bit positions. The retained parity words are exclusively OR'ed together to form the 24 bit parity.

Mode S Transponder

The normal high end Mode S transponder looks similar to Figure 76. It has a top and bottom antenna and includes appropriate diversity switching and signal processing channels to select the best antenna on the basis of the characteristics of the received interrogation signals. The selected antenna is used to receive the rest of the interrogation and, if necessary, to transmit the reply.

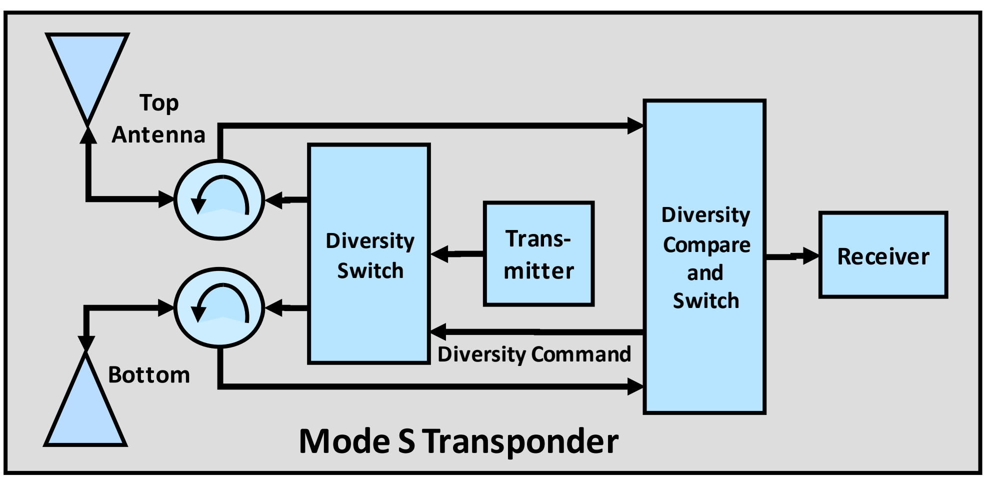

Figure 76: Mode S transponder

Multipath Reflections

In the presence of multipath reflectors the received 1090ES signal is the sum of the direct reception with various reflections, each with a particular delay and amplitude, depending on the location of the reflector, its size, orientation, material, surface roughness, etc. The sum is equivalent to the convolution of the emitted signal with impulses having corresponding delays, amplitudes and phases. The sum of these impulses is the total combined impulse response of the transmission channel. The transform of this impulse response is the sum of complex exponentials.

Measurements of Reflections

Lincoln Laboratory measured reflections in the 1980s at Logan Airport in Boston, MA. In these measurements two vehicles were deployed on the airport surface. One (the large van in Figure 77) contained a transmitter of 1030 MHz ATCRBS P1, P3 Mode A interrogations, a 1090 MHz receiver that was triggered by the interrogations, an A-scope to display the log video of the receptions, and a video camera that recorded the A-scope. The other (the yellow truck) contained an ATCRBS transponder, with an ID code of all zeros (empty brackets). It was observed that the transponder was very good at recognizing interrogations even when they were corrupted by multipath, probably because the interrogation decode circuit simply looks for energy at the prescribed locations of P1 and P3. Even if multipath of 2 us delay occurred the transponder would not interpret this as a P1, P2 suppression pair unless the reflection was very near the amplitude of the directly received P1, an unusual occurrence. The A-scope could be arranged to display the first few 10's of us of reception, which would contain the directly received F1 pulse of the reply and any possible replicas resulting from reflections. Several examples of what was received are shown in Figure 78. Note that the reflections are quite specular, because the F1 pulse shape is preserved. The reflections are generally lower in amplitude than the direct signal, and the delays are on the order of several us. One us, (1000 ns) corresponds to a differential delay on about 1000 ft. The buildings causing reflections 1 and 2 are shown in the right hand picture.

Fig. 6–Experimental test equipment.

Figure 77: Reflection measurement equipment at Logan Airport

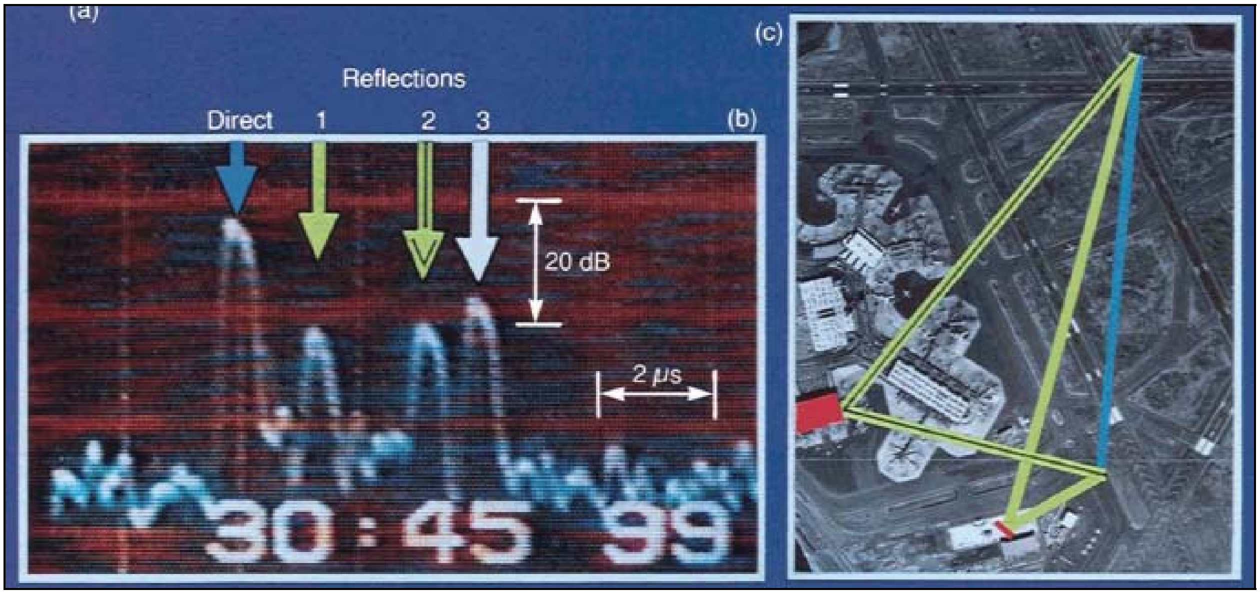

Figure 78: Reflections measured Logan Airport

Deconvolution

These observations lead to the hypothesis that one could combine the preamble portion of the received 1090ES signal with a known generated ideal preamble to infer the reflection environment. This is done by dividing the transform of the preamble reception by the transform of the ideal preamble. This then can be divided into the transform of the complete reception, resulting in a signal in which the reflections have been removed. This process is an application of the well known deconvolution principle in digital signal processing, as shown below

Given transmission $x(t)$ and reception $y(t)$:

$$y(t) = x(t) + \sum_{i=1}^{I} \rho_i x(t-\tau_i) \qquad Y(f) = X(f) + \sum_{i=1}^{I} X(f)\rho_i e^{-j2\pi f\tau}$$

The impulse response is:

$$h(t) = \delta(t) + \sum_{i=1}^{I} \rho_i \delta(t-\tau_i) \qquad H(f) = 1 + \sum_{i=1}^{I} \rho_i e^{-j2\pi f\tau}$$

Such that:

$$y(t) = x(t) \otimes h(t) \qquad Y(f) = X(f) \times H(f)$$

For the known preamble portion, $p_{Transmit}(t)$ and $P_{Transmit}(f)$, of the reception:

$$P_{Received}(f) = P_{Transmit}(f) \times H(f)$$

The $H(f)$ can be estimated as:

$$\hat{H}(f) = \frac{P_{Received}(f)}{P_{Transmit}(f)} \qquad Y_{Received}(f) = X_{Transmit}(f) \times \hat{H}(f)$$

So that $Y_{Transmit}(f)$ and $y_{Transmit}(y)$ can be estimated:

$$\hat{X}_{Transmit}(f) = \frac{Y_{Received}(f)}{\hat{H}(f)} \qquad \hat{x}_{Transmit}(t) = InverseTransform\left(\frac{Y_{Received}(f)}{\hat{H}(f)}\right)$$

Pulse Level Simulation

The Lincoln Laboratory Pulse Level Simulation (PLS) was developed in the 1990s to develop an advanced 1090ES receiver that would work better for air-to-air communications of 1090Es, the range of which is limited not so much by signal to noise, but by the corruption of the weak reception from distant transmitting aircraft by ATCRBS and Mode S fruit from closer aircraft. The decoding method produced by the PLS was in the form of table lookup. The PLS simulated a large number of messages that were combined with ATCRBS and Mode S fruit having statistics like those found in the current environment and predicted future environments. Each 1 us reply bit was sampled in log video 10 times. The samples were quantized into four regions of particular boundaries around the average power seen in the preamble pulses. In this fashion each bit position is described by a single number, which could be used as an index into a table. Tables were generated indicating whether each possible index was associated with a bit value of zero or one. Since the tables were empirically derived under the assumed statistics of ATCRBS and Mode S fruit rates and powers, they are specific to those assumptions. These tables were used in the earlier versions of the deconvolution simulations and tests with real data described in the next paragraphs.

Deconvolution simulation

The feasibility of using deconvolution to process 1090ES messages corrupted by multipath was tested using the Pulse Level Simulation (PLS). The PLS was a convenient way to coherently add reflections onto a direct signal reception, instead of adding fruit. The PLS was also used to detect preambles and decode the message bits, both of which were done using the techniques that were previously developed by the PLS for the air-to-air advanced 1090ES receiver. The simulated corrupted receptions were processed using deconvolution and the correctness of the message decoding was noted as a function of the power and delay of a single reflection. The point of view was that reflections beyond the first traveled a greater distance, and on average would be weaker in power. A feature of PPM decoding is that it is very resistant to corruption that is lower in power than the desired signal by several dB. Thus if deconvolution works against a particular power and delay of a single reflection, the message is likely to be decodable even if there are subsequent reflections. (It is recognized that reflection power is also dependent on characteristics of the reflector, and on the antenna patterns of the transmitting and receiving aircraft.)

It was observed that messages that were initially undecodable were made decodable by deconvolution. It was also noted that the PLS preamble detection method works very well on corrupted signals; it is the message decoding that is degraded by multipath. This is fortuitous, because deconvolution requires first recognizing the presence of a preamble.

Measurement results

The WJH Technical Center made measurements of reflection-corrupted 1090ES replies at the Atlantic City, NJ airport (ACY) and the Philadelphia, PA airport (PHL). The measurement geometry at ACY was such that the reflections were of very short delay and quite high signal power relative to the direct signal; i.e., the signal-to-multipath ratio (SMR) was low. This was because the test van and aircraft could not be placed on the airport surface, but were confined to an area outside a hangar with the van in a nearby parking lot.

Atlantic City

Data were provided for six positions of the van in the parking area. Each had a top and a bottom reply reception at the aircraft totaling 12 replies to work with. Deconvolution gave error-free decoding for nine of them; one reception produced a single bit error in the 112 message bits and the other had 2 bit errors. These errors were corrected with the method described in the next paragraph, resulting in a decoding probability of 0.917 (11/12), for signals which were initially undecodable.

Error Correction. The parity is computed as the exclusive OR'ing of the k 24-bit parity words associated with the k bit positions within the message which are a "1". The transmitting transponder sends the resulting 24 bits as the parity field, which in a 1090ES is sent "in the clear" (i.e., it is not combined with any other information). The 1090ES receiver computes the parity based on the 88 message bits, and compares its result with the received parity. If they are the same, then it is assumed that all 112 bits were received correctly. (The undetected error rate is extremely low.) If one of the 88 bits is received incorrectly, (and the parity bits were received correctly) then the computed parity will differ from the received parity by exactly the parity word associated with the incorrectly received bit. Thus, a single bit error can be corrected by inspection. If two of the 88 are incorrectly received then the parity difference will be the exclusive or of the parity words associated with the incorrect bits, and they can be corrected directly.

Philadelphia.

The PHL measurements were made while both the aircraft and the van were on the airport surface proper. Data for fourteen positions were provided from the PHL measurements, with a top and bottom reply provided for each. Of these 14 positions 11 were decoded without error using deconvolution on either the top or bottom. One position produced 2 bit errors, which were corrected using the method described above resulting is a probability of decode of 0.857. It is possible that refinements in the determination of the impulse from the preamble, or a portion thereof, will enable decoding of the remaining 2 replies.

During the PHL work, it was noticed that the decoding tables generated by the PLS gave a few counter-intuitive bit decoding decisions. As previously discussed, these decoding tables are known to work well with weak replies corrupted by strong fruit. Therefore, two alternate decoding rules were tried. One used the maximum and minimum samples in the two halves of the bit position, and the other compared the average sample in the two halves. The latter method worked better that the former, and better than the table method.

Possible decoding improvements

The decoding performance might be improved by adopting several additional techniques. One is to combine the top and bottom receptions in some fashion. For example, adding the deconvolved log videos might be effective. Or, coherently adding the top and bottom signals before applying deconvolution might work well. The theory would be that, in the case of a single reflection, the four signals all have different phases, due to the different path lengths they travel (recall that the wave length is about one foot). Thus, if the direct receptions can be brought into phase before addition, then the direct signal can be increased in power, while the reflections would not be in phase and therefore the SMR can be improved. These and other methods need to be tried with real data, since it is nearly impossible to simulate complex reflector configurations.

Advanced Multipath Receiver

Figure 79 is a block diagram of the proposed Advanced Multipath Receiver (AMR). The AMR can use the existing Mode S top and bottom antennas. The top and bottom antenna circulators can feed Low Noise Amplifiers, the output of each of which is split, where one path leads to the existing diversity switch and the other feeds the AMP. In this way, the performance of the transponder is not affected, while both antennas are made available to the 1090ES Enhanced Receiver. Manufacturers might suggest other configurations.

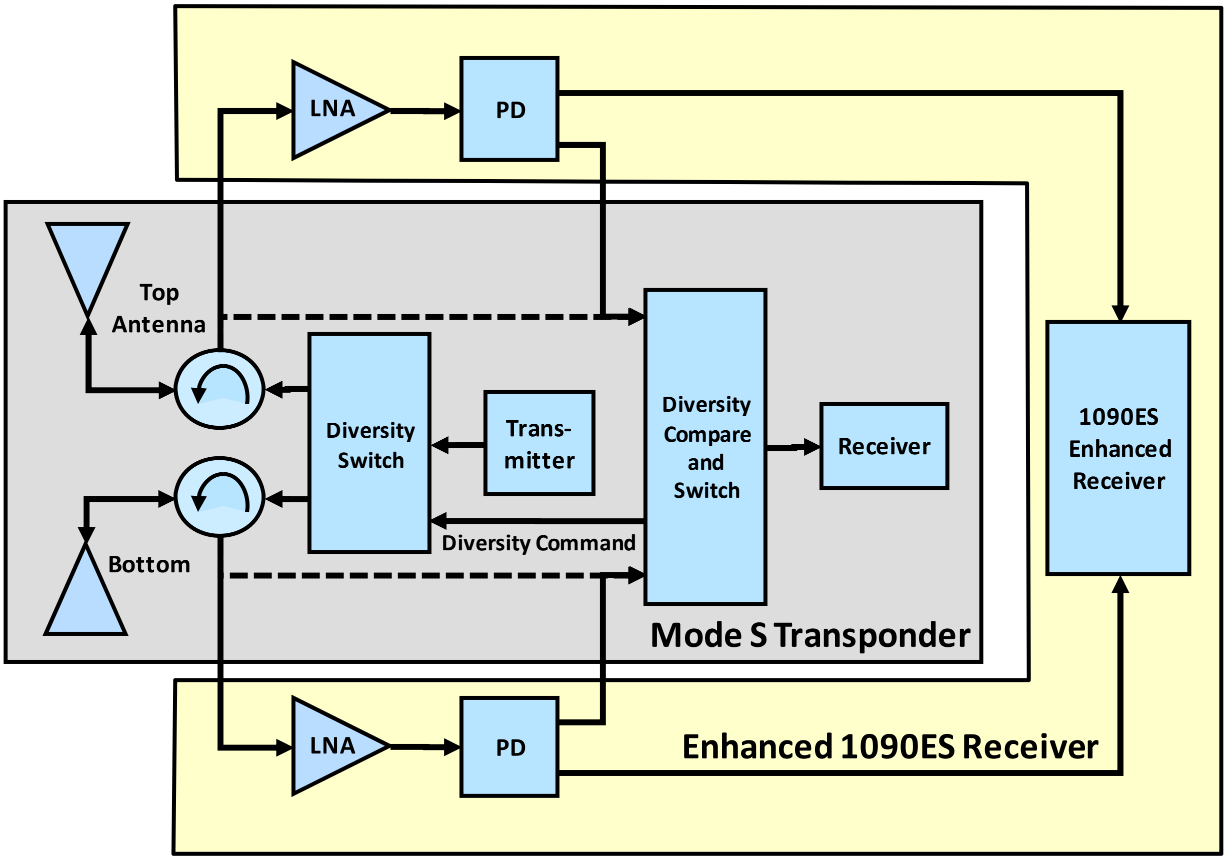

Figure 79: Advanced Multipath Receiver

<u>Advanced Receiver Details</u>

The details of the AMR are shown in the flowchart in Figure 80. The received signal is brought down to digitized baseband I and Q in the usual fashion. The AMR searches for Mode S preambles using the algorithms currently used by the advanced air-to-air 1090ES receiver. When a preamble is seen, the first message bit is decoded. If it is a 1, then the reply is a long one (112 bits) and a candidate 1090ES. If so, then a portion of the preamble is transformed using standard Discrete Fourier Transform (DFT) algorithms. The transform of an ideal such portion is computed, and divided into the former, resulting in the transform of the transmission channel. This is then divided into the transform of the entire reception, and the result inverse-transformed, resulting in the received signal in which the reflections have been removed to a large extent. This is then decoded using methods appropriate to the hypothesis that the residual corruption is related to multipath. The parity of the decoded message bits is computed and compared to the parity decoded from the reception. If they are equal the message is presumed to be correct. If they differ by one of the parity words in the parity table, or by the exclusive or of any of the 7656 (88*87) combinations of two words in the table, then the implicated message bits can be corrected by changing their value from 0 to 1, or 1 to 0 as the case may be.

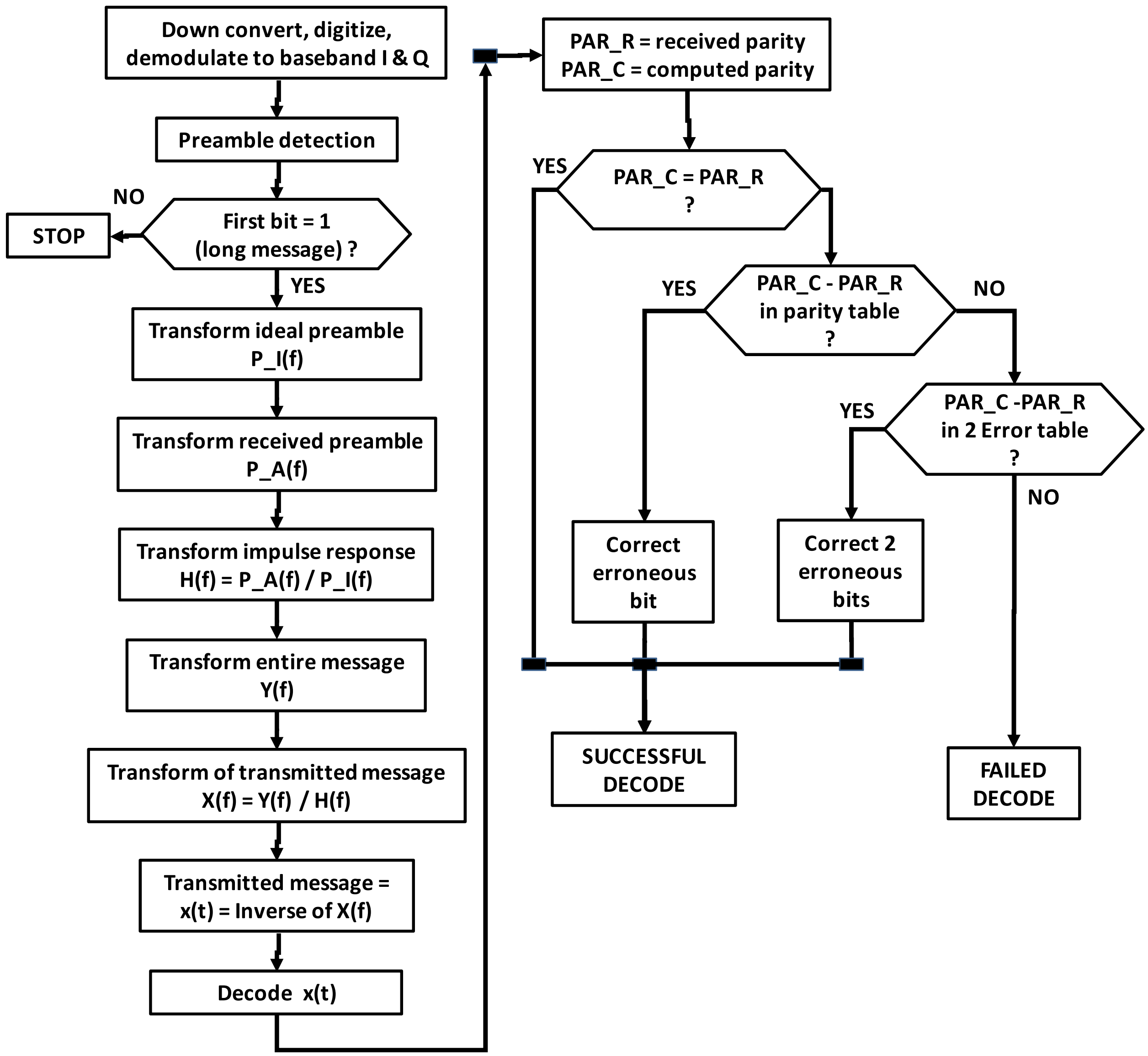

Figure 80: Advanced Multipath Receiver - Flowchart

<u>Reflection Probe</u>

In addition to building a prototype enhanced receiver, it is proposed to also build an experimental adjunct reflection probe, as shown in Figure 81. This consists of a simple transmitter of a single ATCRBS P1, P3 interrogation, and a simple receiver and A-scope and sampling circuitry which displays and records the receiver output for several 10's of us. When used in a low traffic condition, and using low interrogation power, it will interrogate a conventional ATCRBS or Mode S transponder on the surface, and will receive digitize and store the ATCRBS reply signal. The experiment will use two platforms, one with the equipment in the Figure, the other a van or aircraft. This will allow an analysis of the point-to-point impulse response of the transmission channel, i.e., the direct path pulse will be received along with the reflected pulses. The F1 pulse is 0.45 us (450 feet) long so any reflections greater than 450 extra feet will be in the clear. Shorter ones will be noticed by stretching of the pulse if the reflection is in phase, or notching the pulse if out of phase. The absence of code bits means that there is about 19 us of clear channel to capture the reflections.

Ideally, this will be going on simultaneously with communications 1090ES squitters, so that the impulse response of the propagation channel will be measured at the same positions that replies are being received and decoded. When decoding fails, the data will show what the reply signal was composed of.

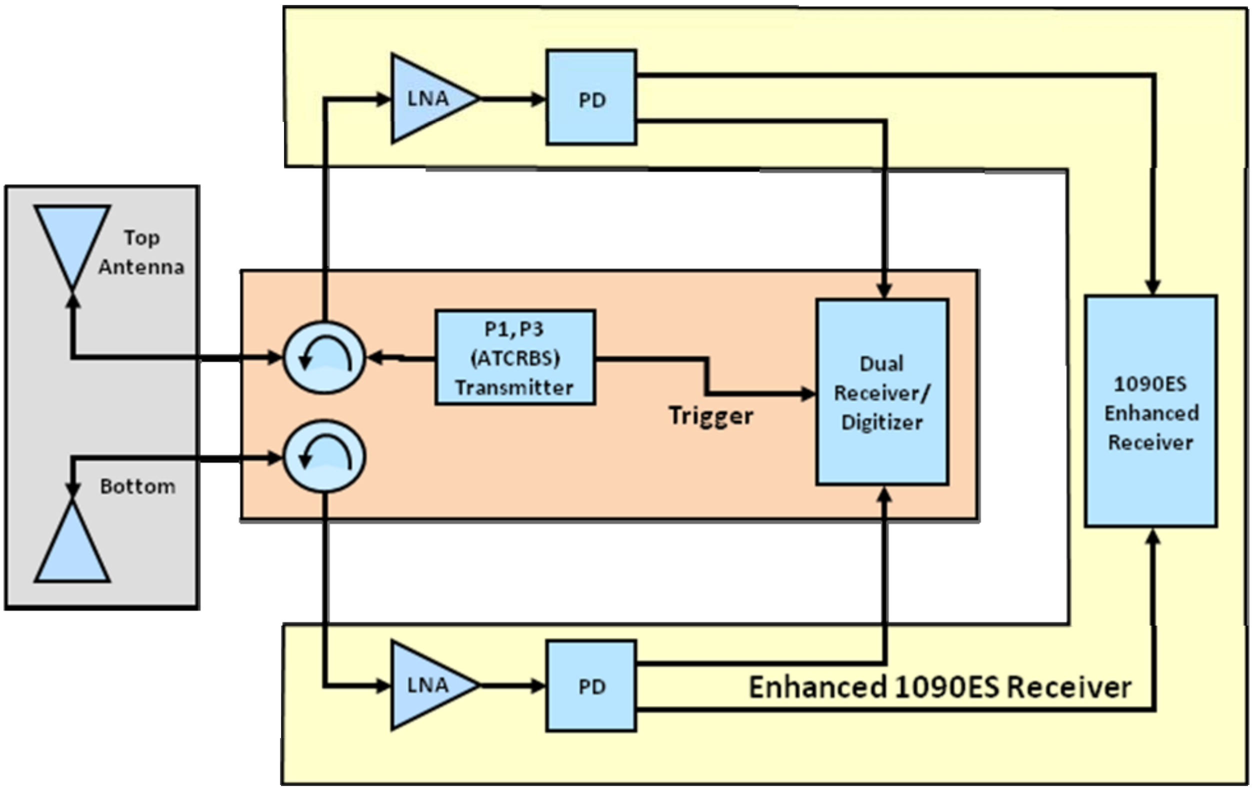

Figure 81: Multipath Reflection Probe

4 Conclusions

Airport surface link performance is dependent upon a complex signal propagation environment. The exact model described herein for the direct aircraft to aircraft path link yields results considerably below levels expected from the usually assumed free space model. Field test measurements are limited, but results obtained by the FAA WJHTC at PHL show very close agreement with the exact model results for the same conditions. These results for top to top antennas are 10 dB below free space levels at 1.4 NM separations, and top to bottom antenna results are 20 dB below the free space reference. Even so, adequate coverage should be obtained for unobstructed direct path links for most airport surface to surface separation distances.

Although surface mode propagation is more susceptible to horizontal multi-path than would be expected with the free space model, a relatively large nearby reflector at the proper orientation is still required to produce a poor signal to multi-path ratio. Since large reflectors tend to be specular, the multi-path affected angular sector would consequently tend to be limited and might in some cases be operationally acceptable. Any direct link fades coupled with geometries including non-obstructed scatters could of course aggravate this circumstance.

Review of the FAA WJHTC field test results indicate that direct link fades did occur due to blocking by terminal gate structures, and possible blocking at certain relative orientations of the aircraft due to aircraft landing gear, engine nacelles, wings, or tail structures. Test van to aircraft antenna signal level variations show a standard deviation of about 2 dB for the aircraft aspect angles associated with their measurements. Shielding due to terminal gate obstruction produced more noticeable signal level drops. Some direct link signal blocking is also associated with geometries that produced horizontal multi-path from nearby buildings. Resulting signal to multi-path interference ratios will result in poor receiver/decoder detection performance.

4.1 Same Link Rebroadcast (SLR) of ADS-B

1. Re-broadcasting all 1090-ES ADS-B messages could result in exceeding the duty cycle limitation of the transmitter as well as exceeding the FAA Spectrum limitation on ADS-B messages at the receiver.
2. If 1090-ES rebroadcast is utilized then judicious reductions in the number and types of messages re-broadcast will be necessary to enable the duty cycle and receiver requirements to be met, although this would still increase the spectrum congestion on 1090MHz.
3. When considering the ADS-R transmission rate of two UAT messages per second for each 1090 ES aircraft results in exceeding the duty cycle limitation of the transmitter, even in the absence of re-broadcasting the UAT ADS-B messages from UAT aircraft.
4. Restricting the ADS-B transmission rate to one UAT message per second would allow the duty cycle requirement to be met, even with the re-broadcast of messages from UAT aircraft.

5. Spectrum impact of SLR on link reception probability has not been evaluated to determine whether there would be an unacceptable degradation in message reception as spectrum use increases.

4.2 Rebroadcast All Surface ADS-B on UAT

1. Rebroadcast signal levels for UAT have behavior similar to that of 1090ES relays except for higher signal to MTL ratios for the implemented transmit powers.
2. Rebroadcasting all ADS-B surface data on the UAT link would eliminate the need for ADS-R over 1090 ES in the surface environment. However, all aircraft desiring to utilize ADS-B IN applications for the surface would need to have dual link receivers.
3. Considering the ADS-R transmission rate of two UAT messages per second for each 1090 ES aircraft results in exceeding the duty cycle limitation of the transmitter, even in the absence of re-broadcasting the UAT ADS-B messages from UAT aircraft.
4. Restricting the ADS-B transmission rate to one UAT message per second would allow the duty cycle requirement to be met, even with the re-broadcast of messages from UAT aircraft.
5. Spectrum impact of re-broadcast of all surface ADS-B over UAT on message reception probability has not been evaluated. However, the proposed solution results in fewer messages transmitted by the ground over both ADS-B links than would be the case for ADS-R transmissions alone, so we can assume that there would be less spectrum congestion with the elimination of ADS-R.

4.3 Enhanced ADS-B Reception Techniques

1. Deconvolution algorithms improve the detectability of 1090ES receptions that were corrupted by multipath at the Atlantic City, NJ, and Philadelphia, PA, airports.
2. These algorithms operate on digitized I and Q signals, and can be implemented with minimal hardware modifications in existing 1090ES receiver designs that have these signals available.
3. No changes are required in existing 1090ES receivers that do not wish to participate in SURF-IA or other ADS-B IN surface applications.
4. Deconvolution does not involve changes in 1090ES messages or protocols, and has no effect on the 1090 MHz spectrum utilization.
5. The results of the enhanced reception technique indicates that substantial improvements in the ability to decode 1090ES messages that are severely impacted by multipath. The improvements provided by this technique can mitigate the previously observed issues with surface multipath that impacted the ability to perform SURF-IA and other surface applications, while providing no affect on spectrum utilization or congestion. Nearly 90% of otherwise failed messages in real data collected at Atlantic City and Philadelphia airports were decoded with these algorithms.

6. Additional gains in decoding multipath affected messages could likely be obtained by combining deconvolution with coherent diversity techniques.

4.4 Diversity or Multi-Channel Reception

1. A diversity receiver based on non-coherent post-detection combining provides significant diversity gain compared to a standard single-channel receiver.
2. Diversity gains typically range from 3 to 5 dB.
3. A diversity receiver provides significant improvement in the probability of message detection in a surface multipath environment compared with a single channel receiver, regardless of whether the single channel receiver uses the top or bottom antenna. Of 21 total multipath cases identified from the field tests, the diversity combining technique successfully decoded 15 messages which provides a message success rate of greater than 70% in a destructive multipath situation. In contrast, a single receiver only decoded 30-40% of these messages.
4. The results of the diversity / multi-channel combining technique for surface ADS-B reception indicate improvements in the ability to decode 1090ES messages that are impacted by multipath. The improvements provided by this technique can mitigate the previously observed issues with surface multipath that impacted the ability to perform SURF-IA and other surface applications, while providing no affect to spectrum utilization or congestion.

5 Recommendations

1. SLR can enhance detection performance of surface ADS-B messages. However, the use of SLR increases congestion on the 1090MHz and 978 MHz frequencies used for 1090-ES and UAT. An intelligent rebroadcast scheme is required for the use of SLR to ensure that any increased spectrum congestion does not affect operational use of ADS-B or other NAS systems.
2. Rebroadcasting all data on the UAT link is a viable solution to mitigating surface multipath performance degradation and mitigates spectrum impacts to 1090MHz. However, this option requires that aircraft equip with UAT receivers. It also requires changes in the ground infrastructure. Considering that other options like SLR and enhanced receivers would only impact one domain (ground infrastructure or avionics), rebroadcasting all data on UAT may be the most costly option.
3. Prudent use of surface rebroadcast for the relay of messages only from aircraft located in regions of the airport surface associated with direct shielding from other active areas of operational interest will improve surface ADS-B detection performance and can be used to help mitigate surface multipath. Such an approach could assure reliable surface to surface operation while limiting the undesired rebroadcast contribution to airborne experienced co-channel interference since only transmissions from aircraft in shielded or multipath affected areas would be rebroadcast.
4. Conduct further field and bench testing of enhanced ADS-B reception and diversity combining techniques to provide statistically significant measures of effectiveness of these options or a hybrid solution.
5. Based on additional testing and analysis of enhanced ADS-B reception techniques define requirements for an ADS-B IN multipath resistant receiver that adequately rejects surface multipath while supporting the performance requirements for surface applications like SURF-IA. This additional work should support the inclusion of a multipath resistant ADS-B IN receiver design in the respective link MOPS for 1090-ES and UAT.
6. Develop an enhanced test facility to evaluate ADS-B avionics such that enhancements in algorithms, receiver designs, and ADS-B avionics processing capabilities can be developed and evaluated to provide additional application support for ADS-B IN equipment.
7. Since only the top 44 airports in the FAA NAS are planned to have ADS-B infrastructure, ADS-B SLR and UAT Rebroadcast will be limited to only these locations. An avionics solution or deployment of ADS-B ground infrastructure is necessary for surface applications, such as SURF-IA, to gain the desired operational and safety benefits at airports beyond these 44 locations.

6 Acknowledgements

This document was developed for the SBS Program office based on an analysis funded by the FAA to identify means of mitigating destructive multipath interference that affects ADS-B performance on the surface movement area. Key contributors in conducting the analysis of the report are identified in Table 14. Those authoring major sections of this report have their names listed in italics.

Table 14: Key Contributors and Authors of this Document

Name	Organization	Contact email
Lawrence Bachman	Regulus Group	lbachman@regulus-group.com
Ryan Hearty	JHU/APL	ryan.hearty@jhuapl.edu
Stan Jones	MITRE	sjones@mitre.org
John Oetting	JHU/APL	john.oetting@jhuapl.edu
Thomas Pagano	FAA WJHTC	thomas.pagano@faa.gov
Robert Pomrink	*Regulus Group*	*rfpomrink@regulus-group.com*
John Van Dongen	FAA WJHTC	john.vandongen@faa.gov
Loren Wood	MIT / Lincoln Laboratories	wood@ll.mit.edu
Doug Arbuckle	FAA SBS	doug.arbuckle@faa.gov
David Gray	FAA SBS	david.e.gray@faa.gov
Alex Rodriguez	FAA AIR	alex.j.rodriguez@faa.gov
Randy Sleight	JHU/APL	randall.sleight@jhuapl.edu
Don Walker	FAA AIR	don.walker@faa.gov